Chalmers University of Technology

Master of Science thesis

Multi-GNSS PPP analysis on SWEPOS reference stations

Erik Jäverbrink

March 1, 2021

Department of Space, Earth and Environment
Chalmers University of Technology
Gothenburg, Sweden, 2021

Master's thesis SEEX30

Multi-GNSS PPP analysis on SWEPOS reference stations

Erik Jäverbrink

Department of Space, Earth and Environment
Chalmers University of Technology
Gothenburg, Sweden 2021

Multi-GNSS PPP analysis on SWEPOS reference stations
Erik Jäverbrink

Examiner: Jan Johansson, Department of Space, Earth and Environment

Master's thesis SEEX30
Department of Space, Earth and Environment
Chalmers university of technology
SE-412 96 Gothenburg

Hereby I certify to be the original author of this report and that it has been designed exclusively by me. In case external information or work has been used, e.g. in form of figures, equations and ideas by other people, this is cited and clearly documented in the text. (Gothenburg, 2021-02-23, Erik Jäverbrink)

Abstract

The Swedish mapping, cadastral and land registration authority, Lantmäteriet, has a permanent network of GNSS stations, SWEPOS, which can be used as reference stations in differencing and RTK. A limiting factor in the RTK service is, or soon will be, related to local, station dependent effects. This study has utilized the carrier phase residuals for GPS and Galileo from the multi-GNSS PPP software GipsyX to analyze the surrounding environment and local effects around 42 SWEPOS stations. 21 of the stations are concrete pillars and 21 are steel grid masts and there exists one of each at each of the locations, which ranges from the southern part of Sweden to the north. The carrier phase residuals were successfully utilized to describe local phenomena such as wooden fences, adjacent houses and multipath from solid bedrock. There was however an effect that was only present for one station, VIS6, that could not be explained. Its residuals at high elevation, $\sim$45° - 90°, followed those of the elevation angle circles instead of the satellites' orbits. It was illustrated and shown with examples that it is useful to analyze stations in pairs. It helps to discredit certain error sources and phenomena that should be affecting both of the stations. It was furthermore illustrated that it is useful to study the monthly mean residuals as a function of elevation angle in parallel with the skyplots. The steel grid mast stations were furthermore analyzed with respect to coordinate repeatability and it was found that the highest performance were achieved with the combination of GPS+GLONASS+Galileo. The achieved repeatabilities (standard deviation) for the latitudinal, longitudinal and vertical components were 1.20 mm, 3.56 mm and 4.00 mm, respectively. The coordinate accuracies for GPS, GPS+Galileo and GPS+GLONASS were within the GPS+GLONASS+Galileo repeatability. Their respective repeatabilities differs to that of GPS+GLONASS+Galileo by sub-millimeter levels, which means that any of the combinations yields comparable results.

Keywords: GNSS, PPP, GipsyX, repeatability, solution offsets, carrier phase residuals, multipath.

Acknowledgements

Thanks to Tong Ning at Lantmäteriet for his support and tutoring in the GipsyX software. His help sped up the learning process of the software, or even made it possible to begin with in the first place.

Thanks to my examiner, Jan Johansson, from the department of Space, Earth and Environment at Chalmers for his help and the keen interest that he put into my work. He made this report possible by giving me a second chance, something that should never be taken lightly and for which I am truly grateful.

Thanks to my opponent, Yin Zeng, who has given me a lot of support in the writing process.

Last but not least, I give thanks to my family and friends who has given me invaluable support throughout my educational years at Chalmers.

Contents

List of Figures

List of Tables

Abbreviations

APC	Antenna Phase Center
CODE	Center for Orbit Determination
DGNSS	Differential GNSS
EOP	Earth Orientation Parameters
ERP	Earth Rotation Parameters
GIPSY	GPS Inferred Positioning System
GLONASS	GLObal'naya NAvigatsionnaya Sputnikovaya Sistema
GNSS	Global Navigation Satellite Systems
GPS	Global Positioning System
ICRF	International Celestial Reference Frame
IERS	International Earth Rotation and Reference Systems Service
IGS	International GNSS Service
ITRF	International Terrestrial Reference Frame
JPL	Jet Propulsion Laboratory
KF	Kalman Filter
N-RTK	Network-RTK
OASIS	Orbit Analysis Simulation Software
PPP	Precise Point Positioning
RINEX	Receiver Independent Exchange Format
RTK	Real Time Kinematic
TAI	International Atomic Time
VMF	Vienna Mapping Function
ZHD	Zenith Hydrostatic Delay
ZTD	Zenith Total Delay
ZWD	Zenith Wet Delay

1 Introduction

GNSS, Global Navigation Satellite System, is used worldwide to provide positioning and navigation and the number of applications that utilizes it is steadily increasing. Historically, only the two GNSS constellations GPS and GLONASS were available. As of recent years, two additional constellations have been launched and are now available, Galileo and BeiDou.

Two common methods of handling error sources in GNSS processing is Precise Point Positioning (PPP) and Real Time Kinematic (RTK) [1]. PPP utilizes precise information about the satellites' orbits and clocks, typically delivered from the International GNSS Service (IGS) [2], while RTK utilizes a reference station to minimize error sources that are common to both receivers [1, 3].

It was shown in both [4] and [5] that the addition of Galileo to the previously used GPS+GLONASS combination improved the PPP performance with respect to several factors. They both showed that the three-dimensional positioning accuracy were increased, both for the kinematic and the static positioning. It was also shown that the convergence time of the PPP processing were reduced with the addition of Galileo. [5] furthermore illustrated that the addition of Galileo helped to remove outliers. The benefits of adding Galileo were larger in [5] since Galileo had 22 active satellites at that time, as compared to 14 active when [4] was performed.

The Swedish mapping, cadastral and land registration authority, Lantmäteriet, has a permanent network of GNSS stations, SWEPOS, which can be used as reference stations in differencing and RTK [6]. It was shown in [3] that the performance of the SWEPOS RTK has been steadily improving to such a level where the limiting factors are now, or soon will be, related to the local, station dependent effects.

The SWEPOS network has permanent GNSS stations located all over Sweden and 21 of those locations are fundamental to the service. Each of the fundamental sites has two different kinds of stations, a concrete pillar station and a steel grid mast station. In order to have as good a control as possible of the local effects, [3] performed site specific antenna calibrations on some of the fundamental sites. To further analyze the local, station dependent effects, [3] left it as further work to study their carrier phase residuals.

This report aims to utilize the PPP software GipsyX to study the surrounding environment and local effects around the 42 fundamental SWEPOS stations (21 concrete pillars and 21 steel grid masts). The stations used are ranging from Hässleholm in the south of Sweden to Kiruna in the north. In [3], the evaluation was based on GPS and GLONASS and this study will have its main focus on GPS and Galileo.

The surrounding environment and local effects will be analyzed with the help of carrier phase residuals. Both in the form of skyplots with color coded carrier phase residuals as well as with a statistical approach where the carrier phase residuals are averaged over both monthly intervals as well as 1° elevation intervals. Any deviations that are found in the residuals will be tried to be explained with the help of photos of the stations [7].

A second part of the study will analyze the coordinate repeatability of the steel grid mast stations. The repeatability will be evaluated for GPS, GLONASS, Galileo and BeiDou separately, as well as in some combinations of them. The repeatabilities will be presented as averages over all stations, to present a national, PPP, performance. This part of the study will furthermore analyze any potential coordinate offset that might be present between the different constellation combinations.

The study performed in [5] used different elevation cutoff angles to analyze the stations' performances. That might also be useful to do for the SWEPOS stations to minimize the local effects at each station but that has not been performed in this study. A constant elevation cutoff angle of 10° has been used.

The report covers a description of Global Navigation Satellite Systems (GNSS) and GPS in particular. It then describes the software used to process the GNSS data, GipsyX, as well as the factors that are taken into account in the PPP processing.

2 Global Navigation Satellite Systems (GNSS)

GNSS is a technique used to determine positions on Earth, or in space, by trilateration and it is a collection name for four different global positioning systems: (i) GPS (USA), (ii) GLONASS (Russia), (iii) Galileo (EU) and (iv) BeiDou (China) [8] [9]. There are moreover two regional systems, IRNSS and QZSS, that are used to enhance the GNSS performance in India and Japan, which will not be described in this report [9]. The four global systems are similar enough so that a modern receiver can use them simultaneously and the theoretic description of the GNSS functionality will primarily focus on the description of the Global Positioning System (GPS).

The basic principle behind the trilateration is that it is assumed that the positions of the satellites are known at every epoch. The satellites continuously broadcasts their positions x_s, y_s and z_s in geocentric coordinates, as well as the time of transmission, T. The different coordinate reference systems will be described in section 2.2.2. When the receiver receives the signal, it compares its own time, t, to that of the satellite's to measure the time difference. That time difference multiplied by the speed of light in vacuum, $c_0 = 2.99792458 \cdot 10^8$ m/s, gives the distance between the two as $R = c_0(t - T)$. In the ideal case, this is the true range to the satellite and it is equal to the length of a vector in a three dimensional space between two points [8]

$$R = \sqrt{(x_s - x)^2 + (y_s - y)^2 + (z_s - z)^2}, \tag{2.1}$$

where x, y and z (without subscripts) is the receiver's coordinates. There are three unknowns in equation 2.1, which means that three satellites are needed in order to solve for the receiver's position. The geometry, in two dimensions, is illustrated in figure 2.1.

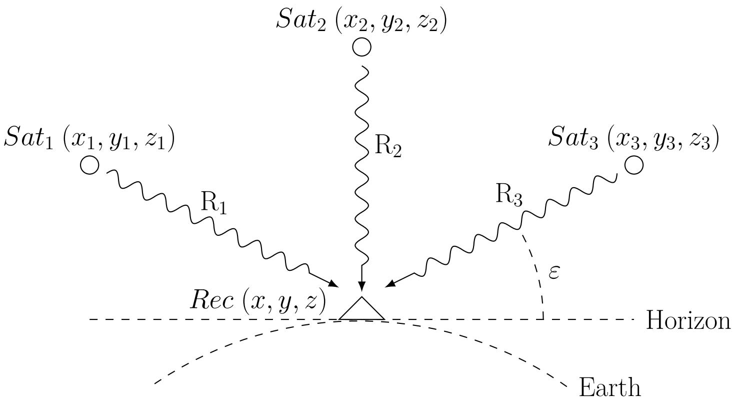

Figure 2.1: Geometry of a GNSS receiver and the transmitting satellites.

In figure 2.1, the elevation angle, ε, from the horizontal plane up to the satellites' positions is also marked, which will be analyzed in section 2.1.1. Note that the model described so far is simplified and that it does not take any error sources into account, it is a description that facilitates the description of the trilateration principle. Equation 2.1 will be iteratively expanded to include several error sources that affects the measurement.

What the receiver actually measures is time, and then that is used to calculate the position. In order to have precise control of the time that the satellites transmits, T, they are equipped with atomic clocks. The receivers are not equipped with atomic clocks, they usually have less expensive crystal clocks, which are synchronized as well as possible to that of the satellites [8]. An example of what inaccurate synchronization leads to is that if the receiver clock has an offset of $\Delta t = 1\,\mu s$ as compared to the satellites' clocks, that yields a positioning error of $\pm 300\,m$.

The atomic clocks on the satellites are also not perfect, they can have an error as compared to the time reference system, denoted ΔT. The different time reference systems will be described in section 2.2.2. Equation 2.1 can then be expanded to include the clock errors for the receiver and satellites, Δt and ΔT, respectively.

$$\rho_0 = \sqrt{(x_s - x)^2 + (y_s - y)^2 + (z_s - z)^2} \tag{2.2}$$

$$P = \rho_0 + c_0(\Delta t - \Delta T) \tag{2.3}$$

ρ_0 has been introduced to represent the true, error free, coordinates of the receiver. Because the distance that the receiver measures is not equal to the true distance, it is henceforth denoted as pseudorange. The advantage with the receiver clock error term, Δt, is that it is common for all observations from the satellites, which means that it can be solved for if measurements to four satellites can be performed. This is the reason why GNSS receivers needs to have four satellites within line of sight to operate, in order to solve for x, y, z and Δt [8]. x_s, y_s, z_s and ΔT in equation 2.3 are known from the navigation message that the satellites broadcasts, which is described in section 2.2.

2.1 Error sources

When it comes to electromagnetic signals, the atmosphere can be divided in two parts, the neutral (troposphere) and the dispersive (ionosphere). The troposphere extends from the ground and up to a height of $\sim 50\,\mathrm{km}$ and it is considered neutral in the sense that it delays electromagnetic signals equally, independent of frequency. The signal is delayed because the speed of light, c, in the troposphere is lower than that of the speed of light in vacuum, c_0. The ionosphere extends from $50\,\mathrm{km}$ to $\sim 1000\,\mathrm{km}$ and it is considered dispersive because it delays electromagnetic signals differently for different frequencies. [8]

2.1.1 Troposphere

The two different speeds are related by $c = c_0/n$, where n is the refractive index of the troposphere. The refractive index is a function of temperature, pressure and water vapor. The tropospheric path delay can thus be divided in two parts, a hydrostatic that relates to the pressure dependence and a wet that relates to the water vapor dependence. A zenith total delay (ZTD) can then be defined as the addition of the zenith hydrostatic delay (ZHD) and the zenith wet delay (ZWD). [8]

$$ZTD = ZHD + ZWD \tag{2.4}$$

Since GNSS receivers are not, in general, equipped with pressure sensors, they can not separate ZHD and ZWD, which is why ZTD is utilized. Typical numbers for ZHD and ZWD are $\sim 2.2\,\mathrm{m}$ and $\sim 0.1\,\mathrm{m}$, which means that the majority of the path delay comes from the hydrostatic part.

The majority of the tropospheric path delay is caused by the reduction in the speed of light, $c = c_0/n$, but the change in the refractive index, n, also creates another phenomena that has to be accounted for in GNSS measurements. When an electromagnetic wave passes from one medium with a refractive index n_1 in to another medium with refractive index n_2, the wave changes its propagation direction. When the satellite is in zenith, the wave is perpendicular to the troposphere and the wave continues without changing direction, but as the elevation angle, ε, gets lower, the additional path length increases [8]. The situation is illustrated in figure 2.2.

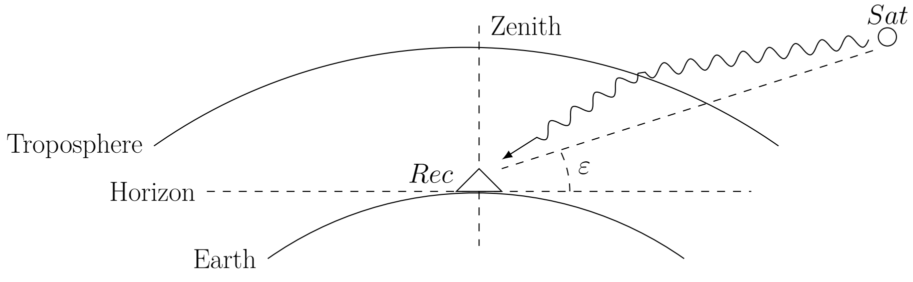

Figure 2.2: Elevation, ε, dependence of the tropospheric path delay.

A common way of how to handle the elevation dependence is to introduce mapping functions that models the additional path lengths at different elevation angles. There exists several different models and one such is the Vienna mapping function (VMF) which calculates mapping coefficients based on latitude and the day of the year.

The VMF divides the mapping coefficients into a hydrostatic and a wet part and it assumes that the troposphere is symmetric around the receiver, i.e. that it does not have any azimuth dependence. [10] A total tropospheric path delay can then be defined as

$$A(\varepsilon) = m(\varepsilon)ZTD, \tag{2.5}$$

where $m(\varepsilon)$ is the elevation dependent mapping function and ZTD is the zenith tropospheric path delay.

2.1.2 Ionosphere

The ionosphere, which is the upper part of the atmosphere, also introduces path delays for the electromagnetic waves. As was the case for the troposphere, it is a result of changes in the refractive index, n. What differs in the ionosphere is that the changes are caused by free electrons, rather than weather effects, varying pressures and water vapor. The refractive index in the ionosphere is furthermore dispersive, i.e. it changes with the frequency of the electromagnetic waves, which was not the case for the troposphere. [11]

The free electrons in the ionosphere is generated by the solar radiation, which ionizes neutral atoms so they release electrons. An important factor when it comes to modeling the refractive index in the ionosphere is the electron density. The density of free electrons varies daily, there is for instance changes every time the sun sets or rises. The solar radiation also has long term variations, it has an 11 year solar cycle where the solar radiation can vary as much as 50%. [11]

The ionospheric path delay can be several tens of meters and methods of how to minimize the error is given in section 2.3.3 [1]. With the introduction of a total ionospheric path delay as I, the pseudorange equation, 2.3, can be expanded to include both of the atmospheric error sources.

$$P = \rho_0 + c_0(\Delta t - \Delta T) + A + I \tag{2.6}$$

2.1.3 Antenna phase center and local variations

When an electromagnetic wave hits an antenna, the receiver perceives the signal to be located at a point outside of the antenna. This point is called the antenna phase center (APC) and it is the electrical phase center where the GPS measurements are referred to. If a physical center point of the antenna is defined as the antenna reference point (ARP), then the APC is different as compared to the ARP. A circular antenna with its ARP and APC is illustrated in figure 2.3.

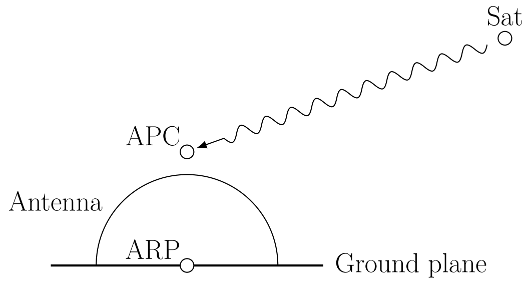

Figure 2.3: Antenna phase center and antenna reference point.

The offset between the ARP and the APC can be calibrated and determined in an electromagnetic compatibility chamber (EMC) or by a robot. Two examples of companies that performs EMC chamber and robot calibrations are Bonn, university of Bonn, and GEO++ in Hannover, respectively [3]. What complicates the matter is that the APC varies with elevation, azimuth and frequency. The azimuth dependence is usually not a problem for geodetic antennas, as is used in this report, since they are symmetric. However, the elevation and frequency dependence means that each received signal has its own APC [8]. The local environment around the antenna, such as water and foliage etc. also affects the APC due to electromagnetic coupling. For stationary, geodetic, GNSS receivers, the APC is calibrated and well documented for different elevations and the frequencies that are used.

Another effect that causes errors in GNSS measurements is the signals that hits the antenna after they have been reflected on a surface, which is called multipath. The satellites transmits electromagnetic waves that are right-hand circularly polarized (RHCP) and the stationary GPS receiver stations have geodetic antennas that are designed to receive RHCP. As an electromagnetic wave is reflected on a surface, the polarization is shifted to left-hand circular polarization (LHCP). What this means is that multipath is usually only a minor problem for geodetic antennas, since they are not tuned to receive LHCP.

The final error term that will be added to the pseudorange equation, 2.6, is denoted v and it includes all of the sources that are not otherwise modeled separately. The errors that are caused by the APC and the multipath effect is also included in v and the pseudorange equation can then be expanded to its final form.

$$P = \rho_0 + c_0(\Delta t - \Delta T) + A + I + v \tag{2.7}$$

2.2 Signals and codes

The GPS satellites are equipped with Cesium atomic clocks which has a fundamental frequency of $f_0 = 10.23\,\text{MHz}$. The satellites transmits signals on two frequencies in the L-band, which are generated by multiplying f_0 by 154 and 120. The reason for why two frequencies are used and for why those specific numbers, 154 and 120, is that it can be used to remove the largest error source, the ionospheric path delay. [8]

$$L1 = 154 \cdot f_0 = 1575\,\text{MHz} \tag{2.8}$$

$$L2 = 120 \cdot f_0 = 1227\,\text{MHz} \tag{2.9}$$

The signal on L_1 is divided into two parts, one in phase component and one quadrature phase component (I and Q). The I component consist of two parts, a C/A code and a navigation message. The Q component only consist of a P code. The signal on L_2 is similarly constructed, except that there is in general no C/A code on it, i.e. it only has the navigation message and the P code as the I and Q components. There exists 37 unique C/A and P codes by the way they are defined today, which defines the upper limit of GPS satellites that can simultaneously broadcast signals. [9]

The C/A code (Coarse/Acquisition) is a civilian code and every satellite has its own unique code. It has a bit rate of $f_0/10 = 1.023$ Mbit/s and an effective wavelength of $\sim 300\,\mathrm{m}$. The C/A code is used by the receivers in order to identify which satellite the code belongs to and to measure the time of propagation, which is needed for the trilateration. How the time measurement is performed is described in section 2.3.1. [8, 9]

The P code (Precise Positioning) is encrypted and is reserved for military and authorized users, such as the stationary GNSS receiver stations used in this report. It has a bit rate of $f_0 = 10.23$ Mbit/s and an effective wavelength of $\sim 30\,\mathrm{m}$. The P code is used in the same way as the C/A code but the effective wavelength, which is lower for the P code, makes the time measurement more precise.

The ground segment for GPS, which is controlled by the US Coast Guard, continuously keeps track of the satellites' orbits and how much their atomic clocks are drifting, ΔT. That information is transmitted up from the Earth to each satellite. The satellites then continuously broadcasts the same navigation message until it is updated, which is approximately every two hours. The message has a bit rate of $f_0/204600 = 50$ bit/s and it takes 12.5 minutes for the satellites to transmit the entire message. [9]

The navigation message does not contain coordinates, it contains orbit information, ephemeris, which the receiver then can use to predict where the satellites are at various time epochs. That prediction yields the x_s, y_s and z_s, as was described in the trilateration principle in the beginning of section 2. [8]

The navigation message also provides information about the satellite's "health", i.e. should the information from that satellite be considered reliable and used in the trilateration or not. The message also contains information about where the other satellites are in the constellation, but it is less precise. [9]

The C/A code, P code and navigation message is modulated with binary phase shift keying (BPSK) on to the carrier frequency $L_1 = 1575\,\mathrm{MHz}$. BPSK means that each time a bit changes from 1 to 0, the phase changes by 180°. The principle of how the complete transmit signal for L_1 is formed is illustrated in figure 2.4.

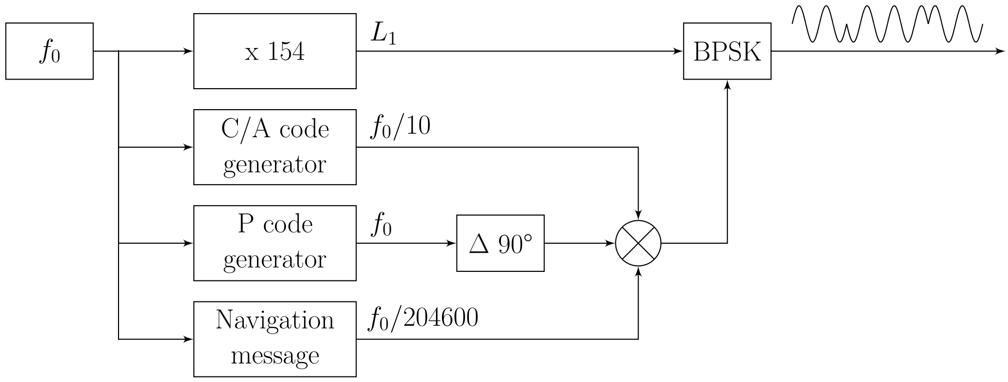

Figure 2.4: Signal configuration of L_1 that consists of the C/A code, P code and the navigation message.

It is similar for L_2 except that there is in general no C/A code on L_2. There is an ongoing effort to upgrade the GPS signals to include the C/A code even on the L_2 frequency. This would help with redundancy and the removal of the ionospheric path delay and some satellites already has it implemented. [9]

The GPS modernisation plan has also included civil signals on a third frequency in the L-band, denoted L_5. Similar to the L_1 signal, the L_5 also has I and Q components and both of them have ranging codes (C/A and P) encoded on them, which is used by a code based receiver to determine the propagation time. Another similarity between the L_1 and L_5 signal is that they only have the navigation message encoded on the I component. Since the Q components, in all three bands, does not have any navigation message encoded on them, they are called data-less signals (or pilot tones). The data-less signals are easier for receivers to track, since they do not download any data from them. [1]

A visual presentation of the frequency band allocation for GPS is given in section 2.5, together with those of GLONASS, Galileo and BeiDou.

2.2.1 Coordinate reference systems

The orbit information, ephemeris, that is provided by the navigation message is given in a celestial coordinate system called the International Celestial Reference Frame (ICRF). The ICRF has its origin at Earth's geocenter, i.e. the Earth's center of mass and it does not rotate with the Earth. The z-axis is oriented as it was positioned from Earth's geocenter to the north pole on the first of January year 2000 (J2000.0). The x-axis is oriented as it was positioned from Earth's geocenter and pointed towards the mean equinox of J2000.0, which is intersection of Earth's equatorial plane and the ecliptic plane. The ecliptic plane is the plane in which the Earth orbits the sun. The y-axis in ICRF comes from the vector product of the x- and z-axis and it is orthogonal to both of them. [9]

The GNSS receiver transforms the ICRF coordinates to a terrestrial coordinate system called the International Terrestrial Reference Frame (ITRF). The ITRF also has its origin at Earth's geocenter but it does rotate with the Earth. The z-axis of the ITRF points from the geocenter to the north pole and the x-axis points from the geocenter and out through the intersection of the equator and the Greenwich meridian. The y-axis in ITRF is orthogonal to both the x- and the z-axis, as was the case for ICRF. [9]

In order for the receiver to perform the transformation between the ICRF and the ITRF, it needs information about the irregularities in the Earth's rotation. Those irregularities are described by the Earth orientation parameters (EOP). The International GNSS Service (IGS) monitors the EOP and makes it available via the internet. [8, 12]

2.2.2 Time reference systems

The trilateration principle described in the beginning of section 2 relies strongly on accurate time measurements. Each GNSS system has its own time reference and GPS time (GPST) is defined using the International Atomic Time (TAI) scale. The TAI scale is based on the definition of the atomic second, which does not take the Earth's rotation in to account. It is maintained by several high-precision atomic clocks that are spread over institutes in several countries. [9]

As the rotation of the Earth is slowing down, it necessary to introduce leap seconds to prevent the Greenwich meridian from drifting eastwards. There has been 19 leap seconds introduced since the GPST was turned on in the year 1980, which means that as of the time of writing, the GPST is defined as GPST=TAI-19 s. [9]

2.3 Range determination

There are two methods by which a GPS receiver can measure the pseudorange. Either by measuring the time difference between the transmit signal and the received signal (code pseudorange), or by comparing the phase difference of the carrier wave (carrier phase pseudorange).

2.3.1 Code pseudorange

The GPS constellation consists of 32 satellites and each of them transmits their own unique C/A code and the different codes are known by every GPS receiver. The first thing a receiver does when it starts the trilateration process is to determine which satellites it is receiving signals from. It does this by creating an internal replica of the C/A code of the first satellite, which it then shifts in time to determine if there is a match (correlation). That time difference between the receiver's clock and the satellite's, $t - T$, multiplied by the speed of light in vacuum, c_0, is the pseudorange to the satellite. If there is not a correlation for the C/A code for the first satellite, it iterates from the beginning with the second satellite's C/A code, and so on. The correlation process is illustrated in figure 2.5, where the carrier wave has been removed for simplification.

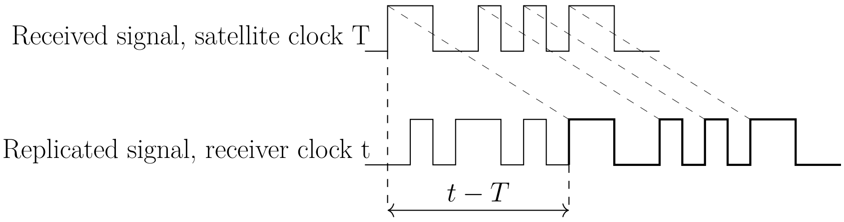

Figure 2.5: Signal correlation to determine which satellite the signal corresponds to and the code pseudorange to it.

The receiver continues the process described above until it has tracked at least four satellites and downloaded the navigation messages of those satellites. With four observations, $i = 1, 2, 3, 4$, the receiver can solve for x, y and z, i.e. its error free coordinates.

$$\rho_0 = \sqrt{(x_{s,i} - x)^2 + (y_{s,i} - y)^2 + (z_{s,i} - z)^2} \tag{2.10}$$

$$P_i = c_0(t_i - T_i) = \rho_0 + c_0(\Delta t - \Delta T_i) + A_i + I_i + v \tag{2.11}$$

The effective uncertainties for the pseudorange measurement, $c_0(t-T)$, for the C/A code for the horizontal and vertical components is ± 10 m and ± 25 m, respectively [8]. For the P code measurements, the effective uncertainties are ± 5 m and ± 10 m for the horizontal and the vertical components, respectively. The reason why the uncertainty is higher in the vertical component is related to the satellite geometry, which is described in section 2.4.

2.3.2 Carrier phase pseudorange

The method of code pseudorange measurement is the conventional way that GNSS (and GPS) use in order to determine positions. However, there is a technique that some receivers can utilize which has a higher accuracy, on the order of ~mm instead of ~m. Instead of comparing a replica of the C/A code as was the previous case, the receiver tracks the phase changes of the electromagnetic wave. [8]

The wavelengths, $\lambda = c_0/f$, for the two different frequencies, for GPS, are $\lambda_{L_1} \approx 0.19$ m and $\lambda_{L_2} \approx 0.24$ m, respectively. The reason why the uncertainties are, potentially, lower for this method is that the carrier phase can be tracked within ~1% of the wavelength [8]. Note that it is custom to denote the carrier phase pseudorange as L, which not should be confused with the two different frequency bands L_1 and L_2.

$$L = \rho_0 + c_0(\Delta t - \Delta T) + A - I + \lambda N + v \tag{2.12}$$

There are one addition and one change to equation 2.12 as compared to equation 2.11. Firstly, the sign on the ionospheric path delay, I, is negative, which has to do with the difference between the phase and the group delay for the electromagnetic wave. Secondly, a phase ambiguity parameter, λN, has been introduced, which comes from the fact that the receiver can not know how many wavelengths it is between it and the satellite when it starts the tracking. [8]

What yields low uncertainties in this method is when N can be determined as an integer number and there exists several methods to achieve that. The software that is used to process the GNSS data from the SWEPOS stations utilizes one such method and the software is described in section 4.2.

2.3.3 Reduction of the ionospheric path delay error

The main reason why the GPS satellites (and the other GNSS systems) transmits signals on, at least, two frequencies is that the combination of the two can be used to reduce the ionospheric path delay [8]. If the receiver is capable of receiving the C/A code and carrier phase on both of the frequencies, f_1 and f_2, then it can form an ionospheric free model, P_3 and L_3 , to remove ∼99.9% of the ionospheric path delay. Instead of presenting the full derivation of P_3 and L_3, which is given in [1] and [8], some assumptions and methods that are used will be described.

$$P_3 = \frac{f_1^2 \cdot P_1 - f_2^2 \cdot P_2}{f_1^2 - f_2^2} \tag{2.13}$$

$$L_3 = \frac{f_1^2 \cdot L_1 - f_2^2 \cdot L_2}{f_1^2 - f_2^2} \tag{2.14}$$

What makes the forming of the equations 2.13 and 2.14 possible is that the ionosphere is dispersive, i.e. that the refractive index, n, depends on the frequency. The derivation is based on expressing the refractive index as a series that is a function of the total electron content. That series is cut after the quadratic term and then integrated along a straight line from the receiver to the satellite. There are two additional simplifications, in addition to the series expression being cut, that contributes to the remaining ∼0.1% ionospheric error. Firstly, the integration path is not modified to account for the additional path length that the bending phenomena introduces, as was illustrated in figure 2.2. Secondly, the change in the refractive index affects the magnetic field differently then it does the electric field, which also has been neglected in the derivation. [1, 8]

Equation 2.13 and 2.14 are said to remove first order ionospheric effects and it is possible to download products from the International GNSS Service (IGS) that estimates the remaining second order effects [2]. With the frequencies used by GPS for L_1 and L_2, equations 2.13 and 2.14 are reduced to the following.

$$P_3 = 2.546 \cdot P_{f_1} - 1.546 \cdot P_{f_2}$$

$$L_3 = 2.546 \cdot L_{f_1} - 1.546 \cdot L_{f_2}$$

One drawback of forming the ionospheric model is that the receiver noise, v, increases by a factor of 3, which comes from the fact that the uncertainties are added as $\sqrt{(2.546 \cdot \sigma_{P_1})^2 + (1.546 \cdot \sigma_{P_2})^2} \approx 3\sigma_{P_1}$ [8, 13]. Another drawback of using the ionospheric model is that the receiver needs to calculate another phase ambiguity term, as was described in section 2.3.2 [8].

If the receiver is only capable of receiving one of the frequencies, it can use a standard model of the ionospheric path delay that is inside the navigation message. In the case of GPS and BeiDou, a model called Klobuchar is used. The Klobuchar model is the same for all satellites and its goal is to remove 50% of the ionospheric path delay, regardless of where on Earth the receiver is. [1]

In the case of Galileo, a model called NeQuick is used, which is the same for all satellites but it differs depending on the receivers' latitudinal location. The model is divided in five equally spaced regions from 90°N to 90°S. The GLONASS satellites do not broadcast an ionospheric model but any of the models from either GPS, Galileo or BeiDou can be used together with a conversion factor that relates to the GLONASS frequencies. [1]

2.4 Dilution of precision and elevation cutoff

The uncertainty in the range measurements (for both code and carrier phase) becomes lower as the spread of the satellites increases, which is called dilution of precision (DOP) [8]. The DOP is the reason why the uncertainty for the vertical component is higher than that of the horizontal, since there are no visible satellites beneath the ground.

It would thus yield lower uncertainties if some of the satellites were located close to the horizontal plane but there is however a tradeoff. When the satellites are at lower elevations, the mapping functions of the atmospheric path delay becomes more complex and can yield larger errors. A compromise is to use an elevation cutoff angle, i.e. to define a minimum angle that the satellites have to be above in order for the receiver to use them.

2.5 Comparison between GPS, GLONASS, Galileo and BeiDou

The four different GNSS systems are quite similar and the description has thus far mainly focused on the functionality of GPS. The space segment parameters for the four different systems are listed in table 2.1: (i) satellites in full operational capability (FOC), (ii) active satellites as of 2020-11-12, (iii) orbital planes, (iv) orbital inclination and (v) orbital height [1]. The GPS, GLONASS and Galileo constellations have all of their satellites placed in medium earth orbits (MEO), while BeiDou also has satellites placed in geostationary (GEO) and inclined geosynchronous orbits (IGSO). The purpose of the GEO and IGSO satellites for BeiDou is to provide enhanced regional performance in China and Asia [14].

Constellation	Satellites in FOC	Active[1] 2020-11-12	Orbital planes	Orbital inclination	Orbital height [km]
GPS	24 MEO	30	6	55°	20200
GLONASS	24 MEO	24	3	64.8°	19140
Galileo	27 MEO	22	3	56°	23222
BeiDou	27 MEO	27	3	55°	21528
	5 GEO	7	-	-	35786
	3 IGSO	10	-	55°	35786

Table 2.1: Space segment parameters for the GNSS constellations

The orbital inclination can be thought of as the maximal latitude, either North or South, where satellites can be seen in zenith. One advantage that GLONASS has compared to the other three systems is that it provides better coverage at higher latitudes. The orbital period is omitted from table 2.1 since it can be calculated with the help of the orbital height [8].

GPS, GLONASS, Galileo and BeiDou are designed to be interoperable and section 2.2 described the signal configuration and frequency selection for GPS within the L_1, L_2 and L_5 frequency bands. Figure 2.6 illustrates where in the frequency spectrum the four different systems are transmitting their respective signals [1].

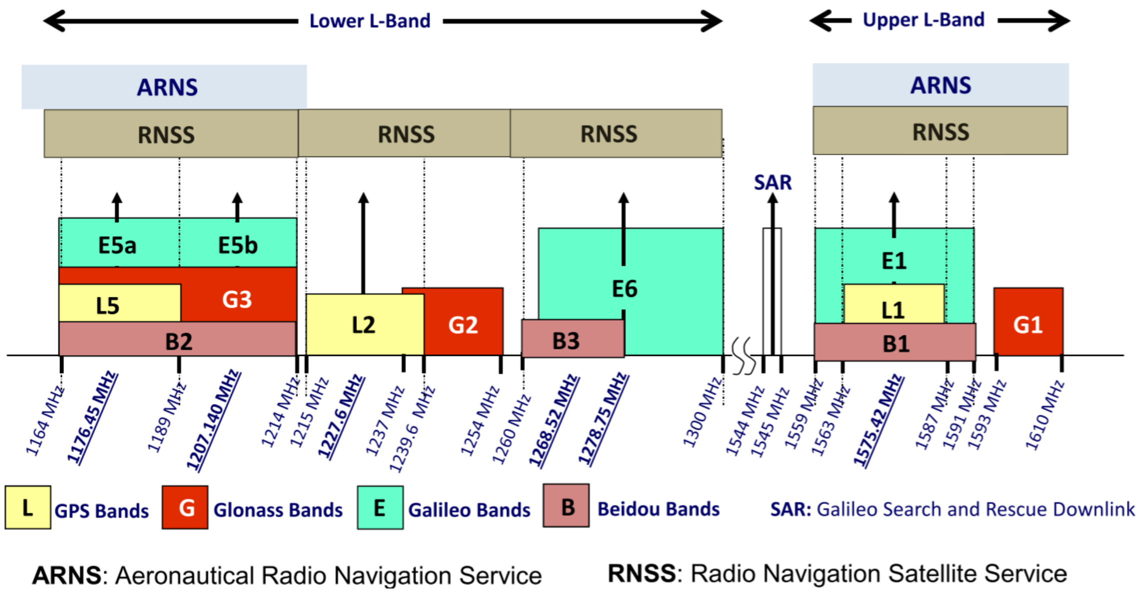

Figure 2.6: Frequency allocation for GPS, GLONASS, Galileo and BeiDou [1]

There are two sub bands in figure 2.6 that are named ARNS which are strictly allocated, worldwide, to GNSS services. That means that no other service or user are allowed to transmit signals there. The signals L_2, G_2, E_6 and B_3 are outside of

[1]Operational status:
GPS: `https://www.navcen.uscg.gov/?Do=constellationStatus`
GLONASS: `https://www.glonass-iac.ru/en/GLONASS/`
Galileo: `https://www.gsc-europa.eu/system-service-status/constellation-information`
BeiDou: `http://www.csno-tarc.cn/en/system/constellation`

the protected ARNS band and are located in a band that used to be shared with ground radars, which make them more vulnerable to interference. [1]

2.6 Receiver Independent Exchange format

There is an international standard called RINEX (Receiver INdependent EXchange format) which is used by GNSS receivers to store measurements in a standardized way [15]. The different frequency bands for the four constellations were illustrated in figure 2.6 and it is determined in the receivers which components of the signals that are stored in the RINEX observation file.

All of the measurements are denoted with a three-letter observation code where the first letter corresponds to one of the four measurement types: C for code pseudorange, L for carrier phase pseudorange, D for doppler and S for signal strength. The second letter is a number that corresponds to the frequency band used by the signal, it can e.g. be 1, 2 or 5 for GPS, see figure 2.6. The third and final letter in the observation code denotes if it is the I or the Q component of the signal. The observation codes are commonly called observables in GNSS terminology and their standards can be found in [15].

2.7 Differencing and real time kinematic

There exists two common methods in GNSS that mitigate error sources, precise point positioning (PPP) and differencing. The software used in this report, GipsyX, is a state of the art PPP software so instead of describing PPP theoretically here, it will be given in section 4.1, together with how it is implemented in GipsyX [16].

The idea behind differencing is to minimize error sources for a GNSS receiver (usually called rover) with the help of a stationary reference station (RS) that has a well known position. The rover can be either stationary or mobile and the technique can be utilized in both real time and in post-processing. By using measurements from both the rover and the RS, difference equations of the pseudoranges can be formed which removes error sources that are common to both receivers, such as the satellite clock errors and potentially the ionospheric and tropospheric path delays. Both of the atmospheric losses can be removed if the RS is close enough to the rover. An example of what *close enough* means is that if the RS is within 20 km, that would be enough to help with the removal of the atmospheric parameters. [8, 9]

If the difference equations are formed for the code measurements, the technique is called differential GNSS (DGNSS) and if they are formed for the carrier phase measurements, it is called real-time kinematic (RTK). The draw back of the method is than when it is performed in real-time, both of the rover and the RS needs to have an internal connection between them, such as Internet or a separate RF link. [9]

If a network of RS are used, they can create an area between them that is basically free of atmospheric path delays, which is called network-RTK (NRTK). The advantage of NRTK is that the receiver can travel in a larger area and still maintain a good control of the error sources. [9]

3 GNSS stations used

The Swedish mapping, cadastral and land registration authority, Lantmäteriet, has a permanent network of GNSS stations, SWEPOS, which can be used as reference stations in differencing and RTK [6]. The stations are located all over the country and 21 of the locations are fundamental to the system and they have two different types of stations at each of those sites: (i) a concrete pillar station and (ii) a steel grid mast station [3]. Both the steel grid mast stations and the concrete pillar stations at the fundamental sites will be analyzed in the study and table 3.1 lists the station ID, location name and latitudinal coordinates for each of the steel grid mast stations.

Station ID[1]	Location	Latitude
HAS6	Hässleholm	56.09°
OSK6	Oskarshamn	57.07°
ONS1	Onsala	57.39°
VIS6	Visby	57.65°
BOR7	Borås	57.71°
JON6	Jönköping	57.74°
NOR7	Norrköping	58.59°
VAN6	Vänersborg	58.69°
LOV6	Lovö	59.34°
KAR6	Karlstad	59.44°
MAR7	Mårtsbo	60.60°
LEK6	Leksand	60.72°
SVE6	Sveg	62.02°
SUN6	Sundsvall	62.23°
OST6	Östersund	63.44°
UME6	Umeå	63.58°
VIL6	Vilhelmina	64.70°
SKE8	Skellefteå	64.88°
OVE6	Överkalix	66.32°
ARJ6	Arjeplog	66.32°
KIR8	Kiruna	67.88°

Table 3.1: Station codes, location names and latitudinal coordinates for the 21 steel grid masts stations in SWEPOS, sorted in ascending latitude.

Each of the steel grid mast stations listed in table 3.1 has a station ID that ends in either 6, 7 or 8 while the station ID for all of the concrete pillar stations ends with a 0. To illustrate the two different kinds of stations, the concrete pillar station ONS0 and the steel grid mast station ONS1 is presented in figure 3.1 [7].

[1] Station photos: https://www.epncb.oma.be/_networkdata/stationlist.php

(a) (b)

Figure 3.1: Sub figure **(a)** and **(b)** illustrates the concrete pillar station ONS0 and the steel grid mast station ONS1, respectively.

4 Method

4.1 Precise point positioning

The information about the satellites' orbits and clocks that are provided through the navigation message by the GPS control segment can have uncertainties of $\sim 3\,\mathrm{m}$ and $<1\,\mathrm{m}$, respectively. Precise point positioning (PPP) is a technique where more reliable data about the satellite orbits and clocks are used [9]. The study will utilize final orbit and clock products from the International GNSS service (IGS), which has uncertainties on the order of ~1-2 cm [2]. The orbit and clock products are calculated at the Center for Orbit Determination (CODE), which is an IGS analysis center [17].

The final products can only be used for post-processing, since they have a latency of approximately 14 days [2]. If a centimeter precision is deemed sufficient for the application, then it is enough to only use the precise orbits and clocks from IGS in the PPP processing [9]. In order to achieve a millimeter precision, GipsyX utilizes several other error correction products as well [16]. The products used can be divided in: (i) atmospheric effects, (ii) antenna offsets, (iii) geophysical displacements and (iv) differential solution biases.

Atmospheric effects

GipsyX utilizes products from two different sources for the tropospheric and the ionospheric path delay. The products that models the second order ionospheric effects, as was described in section 2.3.3, is downloaded from the IGS analysis center CODE [17]. For the tropospheric path delay GipsyX utilizes the Vienna mapping function (VMF), as was described in section 2.1.1, which is downloaded from TU Wien [18].

Antenna offsets

It was described in figure 2.3 and section 2.1.3 that the antenna phase center (APC) has an offset relative to the antenna reference point (ARP). GipsyX utilizes antenna calibration files from IGS that models these offsets for both the receiver and the satellites' and they are named igs14_2114.xyz and igs14_2114.atx, respectively.

There is a second offset that relates to the satellites that GipsyX also accounts for. The precise orbits from IGS refers to the satellites' center of mass and in order to refer the measurements to the ARP, GipsyX utilizes a correction file from IGS, named igs14_2114.pcm, that models the center of mass offset.

Geophysical displacements

There are three different geophysical tidal effects that are taken into account by GipsyX: (i) solid tides, (ii) ocean tides and (iii) polar motion. The station coordinates will be analyzed as constants over 24 hour periods in the study and the geophysical models are needed because the station experiences daily displacements that needs to be accounted for.

The solid tides relates to the movement of Earth's crust that is caused by the gravitational forces of the sun and the moon, primarily [1]. It is compensated in GipsyX with products from the International Earth Rotation and Reference Systems Service (IERS) [19].

The same gravitational forces that causes the solid tides also affects the oceans. When the oceans deforms the underlying sea floor, the adjacent land area is also displaced [1, 9]. Its effect is accounted for in GipsyX with the ocean tide loading model FES2004. The model coefficients depends on the station coordinates so each station has its own specific model and they are downloaded from [20].

The Earth's axis of rotation has an offset as compared to the geophysical axis that varies periodically. This phenomena is what is called polar motion. The polar motion together with the difference in the satellites' time scale, UT1-UTC is monitored by IERS and their combined product is called Earth Orientation Parameters (EOP) [9, 19].

The EOP are used together with the Earth Rotation Parameters (ERP), that are provided by IGS, to transform between the celestial and the terrestrial reference frames, as was described in section 2.2.1 [1].

Differential solution biases

The first order ionospheric effects is removed in PPP, and in GipsyX, with the ionospheric free models P_3 and L_3 for the code and carrier phase pseudoranges, as was described in section 2.3.3. The forming of L_3 introduces a third carrier phase ambiguity that has to be solved for in the PPP processing [1, 21]. GipsyX utilizes products calculated by the IGS analysis center CODE that enables faster convergence times for the new carrier phase ambiguity and they are called wide-lane phase bias (WLPB) products [2].

4.2 GipsyX

GipsyX is a PPP software that is developed by NASA's Jet Propulsion Laboratory and it is a complete redesign of their former version GIPSY-OASIS, where GIPSY stands for GPS Inferred Positioning System and OASIS stands for Orbit Analysis Simulation Software. GIPSY-OASIS could only be used for post-processing and it could only process GPS while GipsyX can process all four GNSS constellations both in real-time and post-processing [16]. A simplified block schematic of the different processing steps in GipsyX is illustrated in figure 4.1.

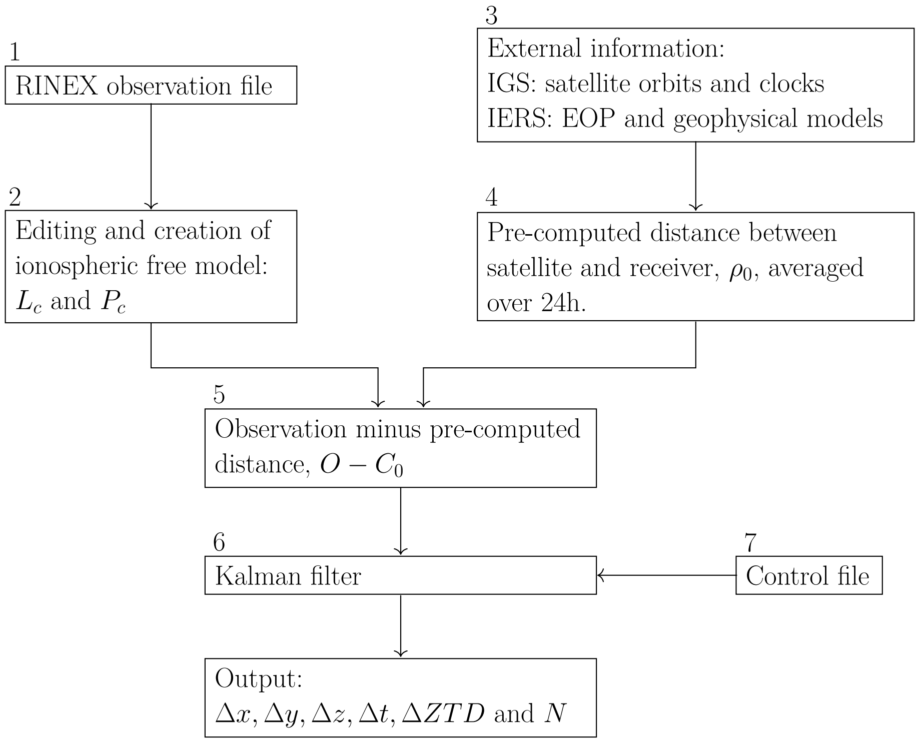

Figure 4.1: Block schematic of the GipsyX processing steps.

The different boxes in figure 4.1 are numbered to simplify the explanation of their functionalities and they will be described by their respective box numbers. In box 1, the GipsyX software utilizes RINEX observation files from the SWEPOS stations as input.

In box 2 of figure 4.1, GipsyX performs editing of the data. It removes data that does not help the solution, i.e. outliers that are above or below a certain threshold. If a receiver looses its track of a satellite and it consequently leads to too small scans, GipsyX removes those scans as well. When the editing is performed, it creates the ionospheric free model, for the code (P_3) and the carrier phase (L_3) measurement, as was described in section 2.3.3.

In box 3 of figure 4.1, information are collected from the external sources, as was described in section 4.1. The precise final products for the satellites' orbits and clocks are downloaded from the IGS, together with the other products needed to reach sub-centimeter precision. The second source of external information comes from IERS which provides information about the solid tides and the EOP.

In box 4, GipsyX performs a pre-computed distance between the satellites and the receiver, ρ_0. In order to do that, GipsyX requires initial values for six parameters, which are listed in table 4.1 (the same six parameters that later is the output of the Kalman filter).

Parameter	Value
x_0, y_0, z_0	Taken from the RINEX header.
Δt_0	The receiver clock error is unknown, so it's set to 0 s.
ZTD_0	The zenith tropospheric delay could e.g. be 2.3 m
N	The phase ambiguity is unknown, so it's set to 0.

Table 4.1: Initial values for the GipsyX software.

In box 5, GipsyX subtracts the pre-computed distance, C_0, from that of the ionospheric free model of the observations, O. This is done for both the code and the carrier phase measurement and the result is used as input to the Kalman filter. The parameters that the Kalman filter is estimates is controlled by the control file. It controls how often each parameter is supposed to be estimated and what kinds of noise parameters there are. Table 4.2 lists the update intervals and the motivations for each of the six parameters.

Parameter	Interval and its motivation
$\Delta x, \Delta y, \Delta z$	Solve as constants over 24 h. This removes the daily variations and it implies that the geophysical models from IERS are reliable.
Δt	Solve every 300 s epoch. Δt is modeled as a white noise parameter, since it varies a lot as compared to the satellites' atomic clocks.
ΔZTD	Solve every 300 s epoch. This is because the ZWD has a relatively fast variation. Modeled as a random walk parameter.
N	Solve as a constant with wide-lane phase bias products from IGS. When the receiver starts tracking, N remains the same until it looses its tracking.

Table 4.2: Parameter estimation intervals in the KF and their motivations.

The Kalman filter can use any of the four GNSS systems separately as well as combining any of them in the solution process and it is also controlled by the control file. The control file furthermore controls the maximum iterations that the Kalman filter can perform before the final output is produced.

4.3 Research questions and analysis method

Section 3 described the 42 GNSS stations (21 steel masts and 21 concrete pillars) within the SWEPOS network that are analysed in the study. The PPP solutions for the steel grid mast stations are analyzed with respect to: (i) repeatability for the four GNSS constellations, (ii) skyplots with color coded post-fit carrier phase residuals for GPS and Galileo and (iii) monthly mean post-fit carrier phase residuals for GPS and Galileo. The PPP solutions for the concrete pillar stations are analyzed with respect to the two latter points.

It is common in GNSS terminology to abbreviate GPS, GLONASS, Galileo and BeiDou as G, R, E and C, respectively. The coordinate repeatability for the 21 steel grid mast stations will be analyzed for the constellation combinations G, R, E, C, GE, GR, GRE and GREC. The coordinate repeatability has not been analyzed for the 21 concrete pillar stations due to the processing time needed to do so. The standard deviation is used as the measure for the repeatability throughout the result presentation.

The solution interval for the receiver clock error as well as the ZTD in the Kalman filter (KF) in GipsyX is set to 300 s. The KF produces one post-fit carrier phase residual per visible satellite per 300 s period and the post-fit carrier phase residual is the difference between the observation, i.e. the actual measurement, and the computed output. The KF also produces post-fit residuals for the code based solutions but those will not be analyzed in the study. The post-fit carrier phase residuals are one of the main analysis methods in the study and they will henceforth be called residuals, for simplicity.

The residuals are used to examine the local environment around the receivers as well as systematic effects that affects all of the stations. The residuals will be presented in the form of skyplots with color residuals as well as with a statistical approach where the residuals are averaged over both monthly intervals as well as 1° elevation intervals.

The skyplots illustrates the residuals as a function of both azimuth and elevation and they are thus a useful tool to examine the local effects around the stations. It is for instance possible to discern if the residuals are higher in any direction which might indicate that there is more multipath in that direction.

The statistical approach where the residuals are averaged over both monthly intervals as well as 1° elevation intervals is useful to study the overall behaviour of the station. But the monthly mean has no azimuth dependence, since it is visualized as a function of elevation angle, which is why it might be useful to analyze it in parallel with the skyplots.

Since there are skyplots and monthly mean residuals for 42 stations, the results will be presented in Appendix A and B and a selection of it will be presented in section 5. In order to explain some of the results that relates to local environments around the stations, descriptions from station photos will be used [7].

In the plots for the monthly mean residuals and the skyplots, it will be listed which two observables that are used in the L3 ionospheric free combination. They are the same throughout the analysis for GPS but some of the receivers for the concrete pillars don't have the same observables stored for Galileo, which means that they will be changed whenever needed.

Some of the receivers at the stations were changed (or updated) 2019-04-02 so the study analyzes the time period 2019-04-03 to 2020-09-30 [2].

5 Result and discussion

5.1 Repeatability and coordinate offsets

It was mentioned in section 4.3 that it is common in GNSS terminology to abbreviate GPS, GLONASS, Galileo and BeiDou as G, R, E and C, respectively. Those abbreviations will be used throughout this section whenever more than two constellations are compared.

Table 5.1 lists the repeatability (mean standard deviation) for the 21 SWEPOS steel grid mast stations for the constellation combinations G, R, E, C, GE, GR, GRE and GREC. The repeatabilities are listed for the latitudinal, longitudinal and vertical coordinate components as well as their combined three dimensional repeatability, which is given by $\sqrt{\sigma_{lat}^2 + \sigma_{lon}^2 + \sigma_{ver}^2}$

	Repeatability [mm]			
Constellation	Latitude	Longitude	Vertical	3D
G	1.48	3.73	4.64	6.14
R	1.39	4.67	4.96	6.95
E	1.71	5.11	5.26	7.53
C[1]	114.8	576.54	134.02	602.94
GE	1.39	3.44	4.21	5.61
GR	1.16	3.67	4.18	5.68
GRE	1.20	3.46	4.00	5.42
GREC	1.26	3.51	4.04	5.50

Table 5.1: Repeatability (mean standard deviation) for the SWEPOS steel grid mast stations in the latitude, longitude and vertical components for the time period 2020-08-01 - 2020-09-30.

A result that stands out in table 5.1 is that the repeatability for C, BeiDou only, is several magnitudes larger than that of any other constellation combination, alone or otherwise. The reason for this is illustrated in figure 5.1 where the mean number of daily carrier phase observations used in the GipsyX processing is presented, together with the number of satellites used.

In table 2.1 it could be seen that the BeiDou constellation is at full operational capability with 27 active medium earth orbit (MEO) satellites as of 2020-11-12. The reason why only 3 BeiDou satellites are used in GipsyX is most likely related to the version of the software that has been used in the processing, the project did not

[1]The reason for the lower performance of BeiDou is not related to its space segment. It is most likely related to the version of GipsyX that was used.

utilize the latest one. It could also be that the SWEPOS stations either don't receive the BeiDou signals or that the observables are not stored in the RINEX observation files.

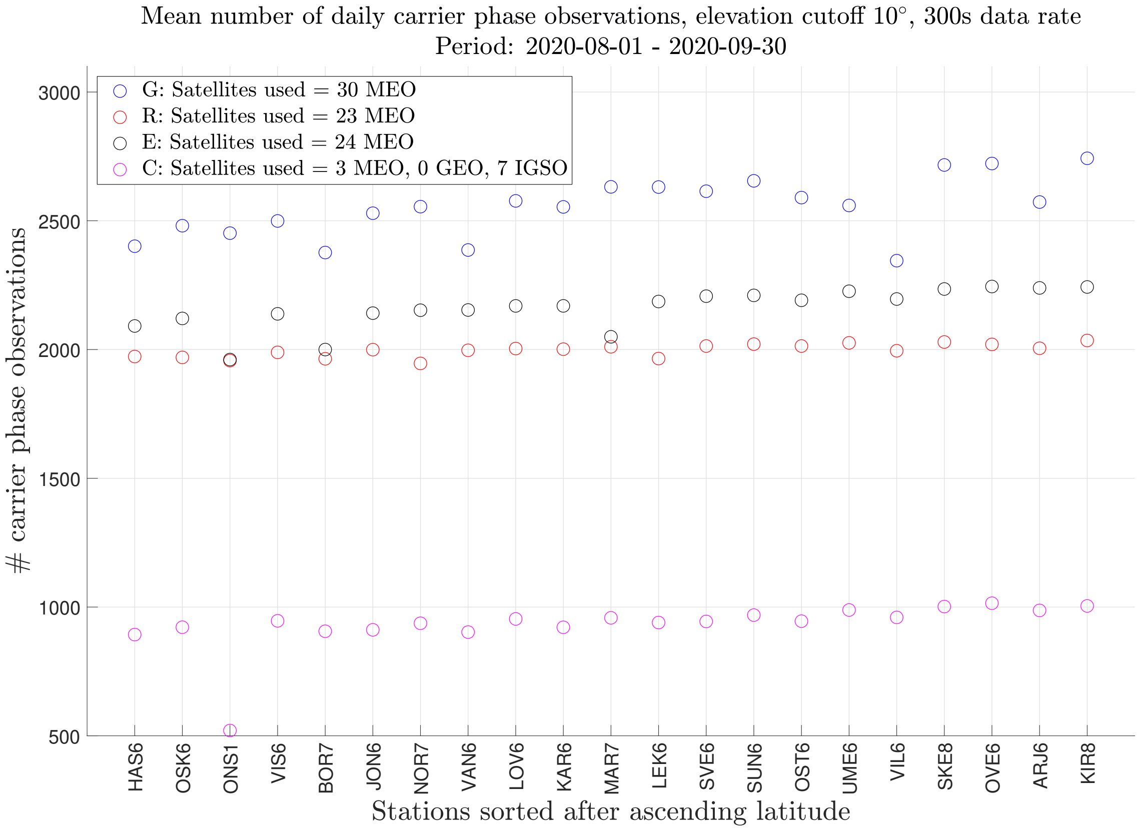

Figure 5.1: Mean amount of daily carrier phase observations for the SWEPOS steel grid mast stations, together with the amount of satellites used in the processing in GipsyX

From table 5.1 it can be seen that the lowest repeatability in the vertical component is achieved through the constellation combination with GPS, GLONASS and Galileo (GRE) at 4.00 mm. With GRE as a benchmark, the coordinate offsets for the latitude, longitude and vertical components for G, E, GE, GR and GREC is presented in figure 5.2, 5.3 and 5.4, respectively.

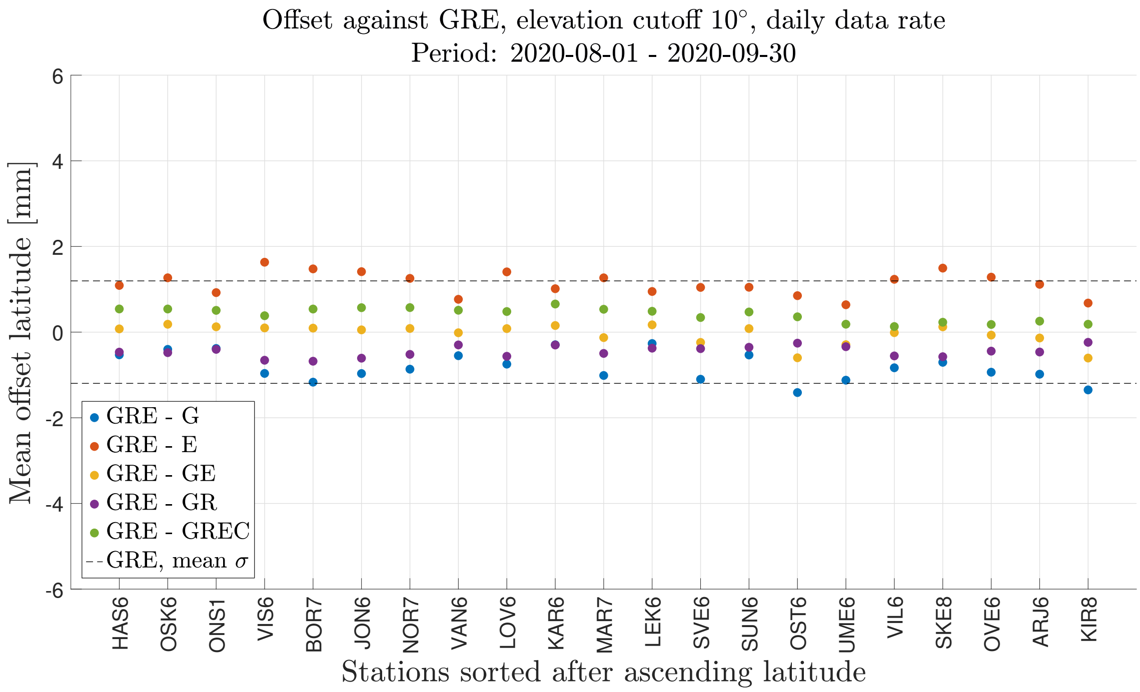

Figure 5.2: Offset against GRE for G,E, GE, GR and GREC for the latitudinal component, together with the 1 σ level for GRE in dashed

The latitudinal offsets for G, GE, GR and GREC, seen in figure 5.2, are within the daily repeatability limit for GRE. Seven of the stations for Galileo alone, E, are outside of the repeatability limit by a sub-millimeter offset.

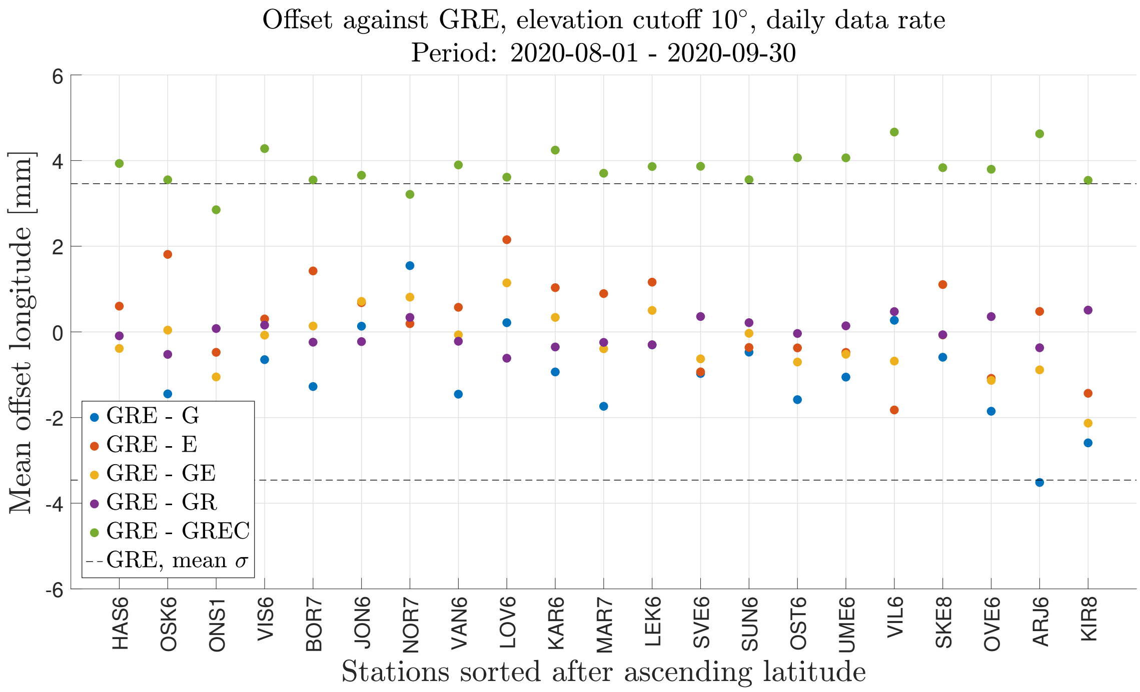

Figure 5.3: Offset against GRE for G,E, GE, GR and GREC for the longitudinal component, together with the 1 σ level for GRE in dashed

For the longitudinal offsets, seen in 5.3, only the constellation combination GREC is outside of the daily repeatability limit for GRE. The reason for this could be related to GipsyX, since only three BeiDou satellites are used, as was shown in figure 5.1. It might be tempting to draw the conclusion that the usage of only three BeiDou satellites degrades the solution of the Kalman filter but it is difficult to make such a claim since that is not the case for the latitudinal and the vertical components. This study have not analyzed the coordinate covariances, which might have helped to explain why the GREC offset is outside of the GRE repeatability by a ~millimeter.

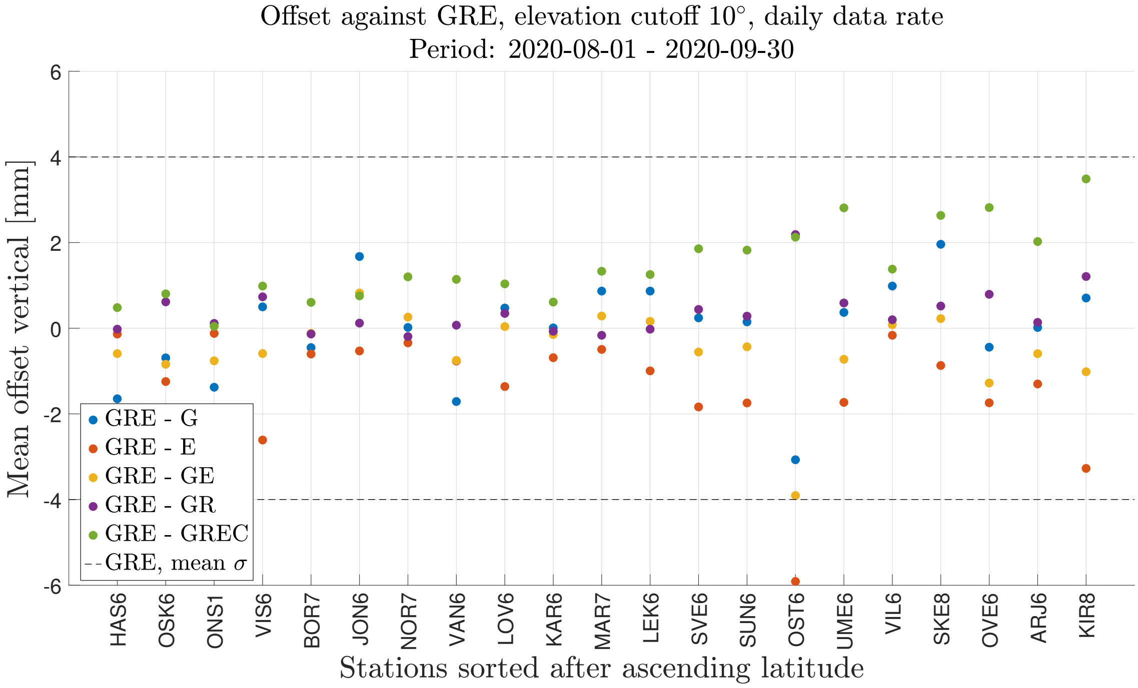

Figure 5.4: Offset against GRE for G,E, GE, GR and GREC for the vertical component, together with the 1 σ level for GRE in dashed

With respect to all three coordinate components, the constellation combinations G, E, GE, and GR have offsets that are within the GRE daily repeatability (with the exception of the sub-millimeter offset for Galileo, E, in the latitudinal component). This means that with respect to the accuracy, any of the constellation combinations produces reliable results. The difference in the repeatability, i.e. the precision, as compared to GRE is presented in table 5.2.

	Repeatability [mm]		
Constellation	Latitude	Longitude	Vertical
GRE	1.20	3.46	4.00
G-GRE	0.28	0.27	0.64
E-GRE	0.51	1.65	1.26
GE-GRE	0.19	−0.02	0.21
GR-GRE	−0.04	0.21	0.18

Table 5.2: Difference in repeatability as compared to the constellation combination GRE for the SWEPOS steel grid mast stations for the time period 2020-08-01 - 2020-09-30.

It can be seen from table 5.2 that the repeatabilities for G, GE and GR differs from that of GRE by sub-millimeter levels. The repeatability for Galileo alone, E, differs by a maximum of 1.65 mm as compared to GRE. The reason for the marginally lower performance of Galileo could be that the constellation is not yet in full operational capability. The constellation is currently, as of 2020-11-12, at 24 out of 27 MEO satellites.

The conclusion that can be drawn from this is that the lowest repeatability for the SWEPOS steel grid mast stations is achieved from the constellation combination GRE with values of 1.20 mm, 3.56 mm and 4.00 mm for the latitudinal, longitudinal and vertical components, respectively. The accuracy for G, GE and GR are within the GRE repeatability limits and their respective repeatabilities differs to that of GRE by sub-millimeter levels. The analysis that has been performed with respect to accuracy and precision for the steel grid masts has not been performed for the concrete pillar stations.

5.2 Skyplots and carrier phase residuals

The skyplots and the monthly mean carrier phase residuals for the 42 SWEPOS stations (21 steel grid masts and 21 concrete pillars) are presented in Appendix A and B, respectively. Both the skyplots and the monthly mean residuals are presented for GPS and Galileo for all of the stations.

It was mentioned in section 2.6 that there exists several types of observables that each receiver can store in the RINEX observation files. Which of the observables that are stored in the RINEX files are set in each specific receiver and most of the stations used in this study have stored the same ones but it can vary between the concrete pillars and the steel grid masts. Because of this, the different observables that are used in each case are listed in the legends of each figure. The definitions for each of them can be found in [15].

In the analysis of the carrier phase residuals that follows, for all of the stations, there is a fact that is important to keep in mind. This study has not analyzed the amount of observations/measurements as a function of elevation angle but there are fewer on higher elevation angles, e.g. above 65°. This has the effect that the residuals at higher elevations are less reliable, just because of the fact that there are fewer observations. If error bars would have been included, they would have been larger at those observations.

It can be discerned by visual analysis of the monthly mean residuals for all of the stations that the concrete pillars and the steel grid masts in general have two distinct curve appearances. To illustrate the two distinct appearances, the monthly mean residuals for the stations UME0 and UME6 is presented in figure 5.5 and 5.6.

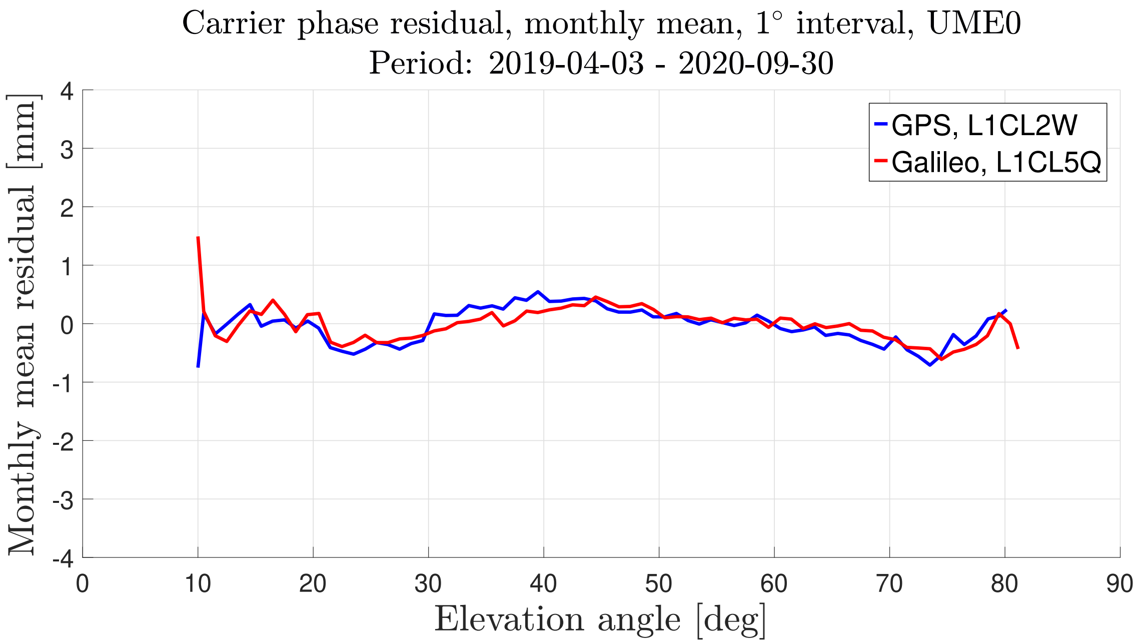

Figure 5.5: Carrier phase residuals, averaged over both 1° elevation angle intervals as well as per month. Station UME0, GPS (L1CL2W) and Galileo (L1CL5Q)

The feature that most of the concrete pillars have in common is that the residual curves for GPS and Galileo closely coincides, similarly to what is presented in figure 5.5. The residuals have different amplitudes depending on local effects and multipath but the residual curves for the concrete pillars are on the whole in agreement.

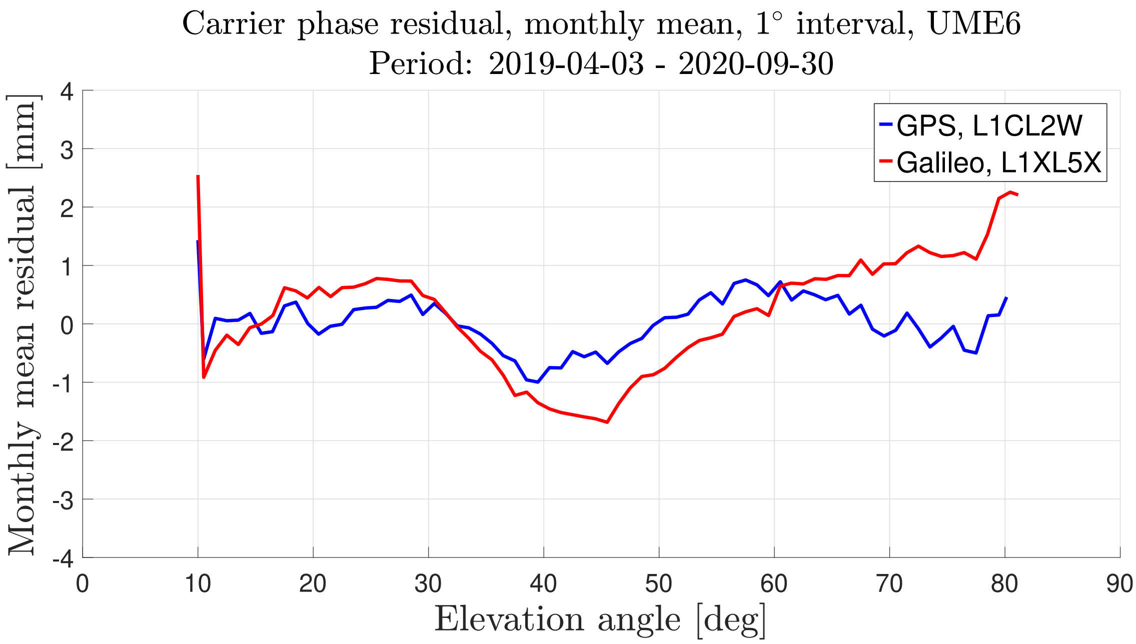

Figure 5.6: Carrier phase residuals, averaged over both 1° elevation angle intervals as well as per month. Station UME6, GPS (L1CL2W) and Galileo (L1XL5X)

The feature that most of the steel grid masts have in common is that the residual curves for GPS and Galileo both have a discernible oscillation. The oscillation can be divided into three approximate elevation intervals: (i) 15° - 30°, (ii) 30° - 60° and 60° - 90°. The amplitude for the Galileo curve inside the oscillating intervals is larger than that of GPS. What is also common for most steel grid masts is that the residual behaviour of GPS and Galileo diverge in the latter elevation interval, 60° - 90°.

One conclusion that can be drawn is that the amplitude difference in the residuals that is shown for Galileo for the steel grid masts can not be related to the space segment, i.e. the satellites, since the difference is not there for the concrete pillars. Neither can the difference be explained by multipath from the stations' local environments, since the appearance is common to most of the steel grid masts.

The study has neither investigated what types of receivers nor what types of antennas and/or antenna covers (radomes) that the two different kinds of stations are equipped with. It has been shown in [3] that the choice of antennas and the foundations themselves has a larger impact on the performance than the receivers. The reason for the difference in the residuals could therefore be accredited to the fact that the steel grid masts could have different antennas or to the steel grid foundation itself.

The monthly mean residuals has thus far been used to describe and analyze the overall, or systematic, behaviour of the steel grid masts and the concrete pillars but they can also be used to analyze local effects. One such example is illustrated in figure 5.7 for the station LOV0. There are two factors that affects the station LOV0, it is located on top of a building instead of being attached to the bedrock as most other stations and it has a rectangular wooden fence around it.

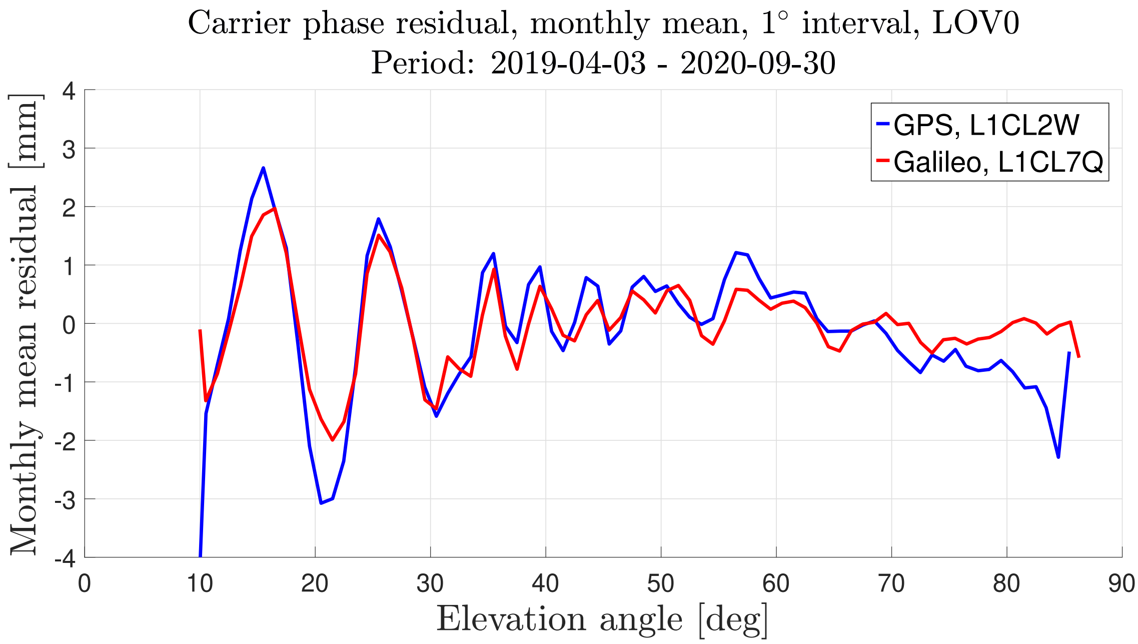

Figure 5.7: Carrier phase residuals, averaged over both 1° elevation angle intervals as well as per month. Station LOV0, GPS (L1CL2W) and Galileo (L1CL7Q)

The multipath from the wooden fence is a contributing factor to the larger residuals at lower elevation angles, below ∼30°, but it is difficult to separate the effect on the residuals that the roof top location has. The effect is there for both GPS and Galileo but it is reduced in magnitude for Galileo. The skyplot for VIS0 is illustrated in figure 5.8.

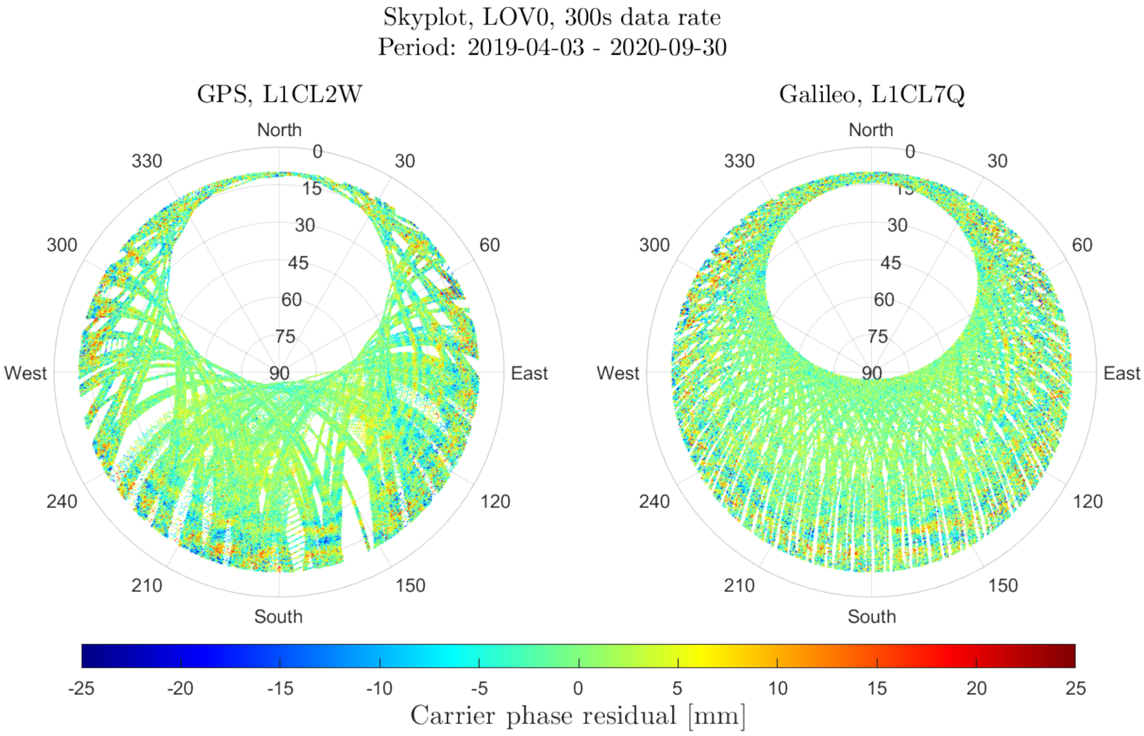

Figure 5.8: Skyplot for station LOV0 for GPS (L1CL2W) and Galileo (L1CL7Q) with color coded carrier phase residuals

The negative residuals in the southern region, figure 5.8, are slightly more pronounced for GPS than they are for Galileo. It is difficult to give a definitive reason for why Galileo has a better performance of handling the low elevation multipath in this case. There are many functionalities of GipsyX that were not described in section 4.2. One of those that could help to explain this effect is that GipsyX uses the code measurements in order to constrain the carrier phase solution. If the multipath has a higher impact on the code measurements for GPS than Galileo, then that might impact the carrier phase solution as well.

If there is an object that is located at a specific azimuth direction, then the large residual variations that was shown in figure 5.7 might be reduced in the averaging over the 1° elevation angle intervals. This is the case for the station SKE0 that is standing adjacent to a building with a typically tilted, v-shaped, roof. The skyplot for SKE0 is illustrated in figure 5.9 where the large residuals in the southeast indicates where the roof is located.

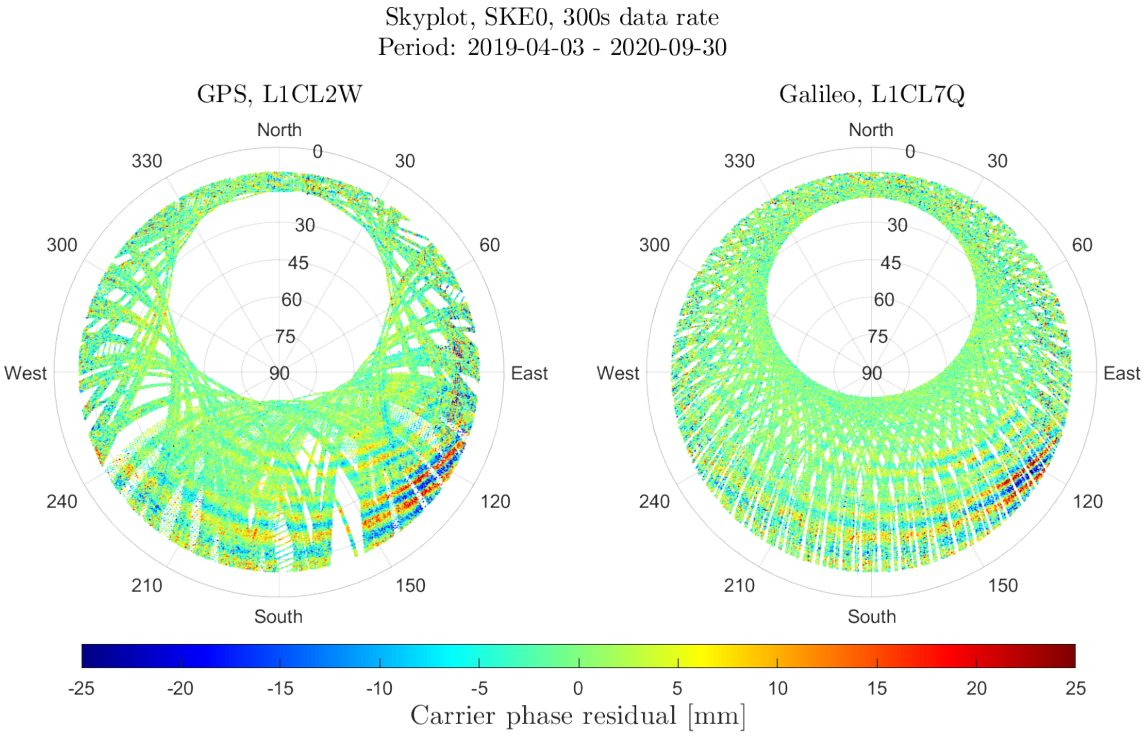

Figure 5.9: Skyplot for station SKE0 for GPS (L1CL2W) and Galileo (L1CL7Q) with color coded carrier phase residuals

The monthly mean residuals for SKE0 is illustrated in figure 5.10. There it can be seen that the large residuals that are present in the southeast in the skyplot in figure 5.9 are reduced, or even hidden, in the 1° elevation angle averaging.

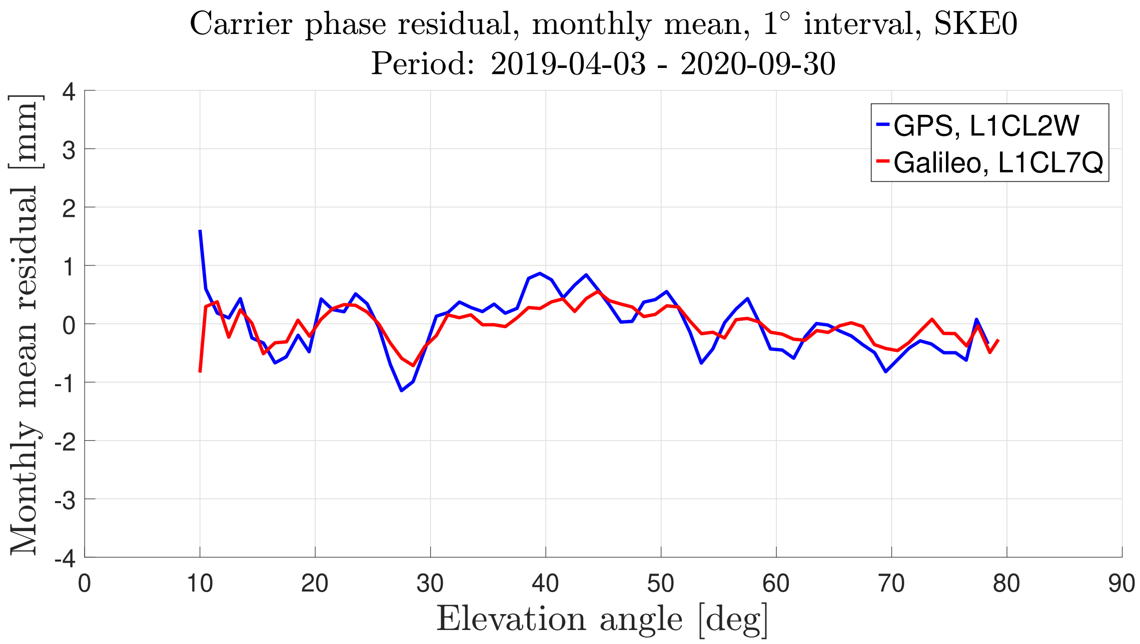

Figure 5.10: Carrier phase residuals, averaged over both 1° elevation angle intervals as well as per month. Station SKE0, GPS (L1CL2W) and Galileo (L1CL7Q)

It was illustrated in [3] that multipath from the ground usually results in a "rapid" oscillation of the residuals at lower elevation angles. Both of the stations VIS0 and VIS6 shows this phenomena, which is illustrated in the figures 5.11 and 5.12, respectively. Neither of the stations have any objects in their vicinities, nor are they standing adjacent to any buildings or are surrounded by any wooden fences. The stations appears to be standing on solid bedrock, limestone, with neither vegetation nor grass in the near environment.

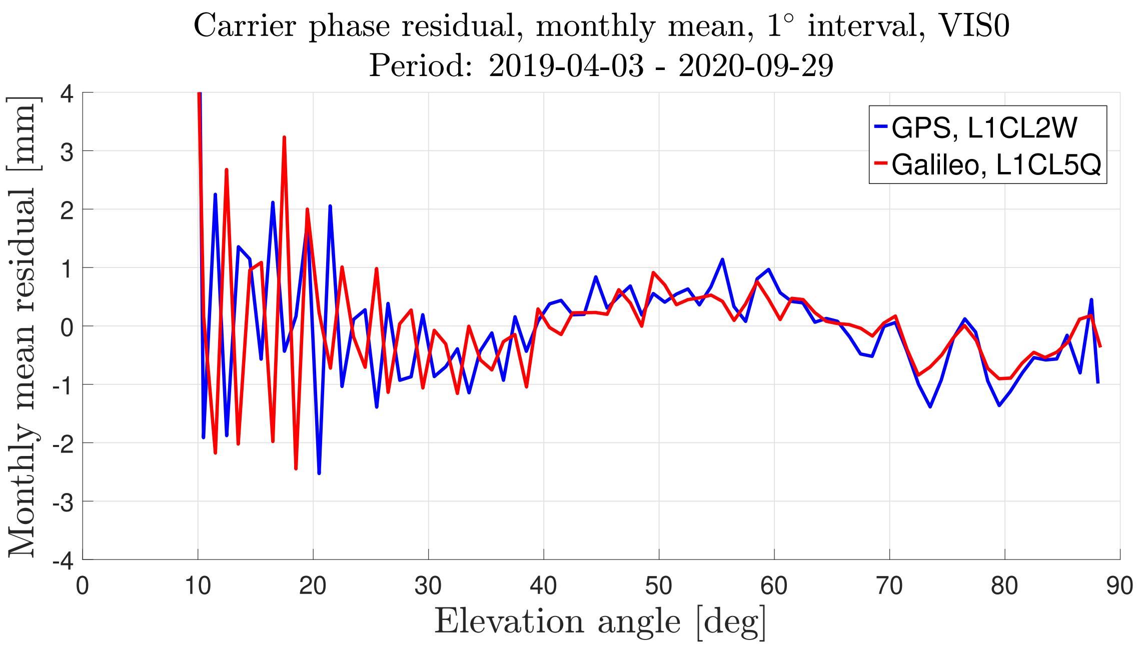

Figure 5.11: Carrier phase residuals, averaged over both 1° elevation angle intervals as well as per month. Station VIS0, GPS (L1CL2W) and Galileo (L1CL5Q)

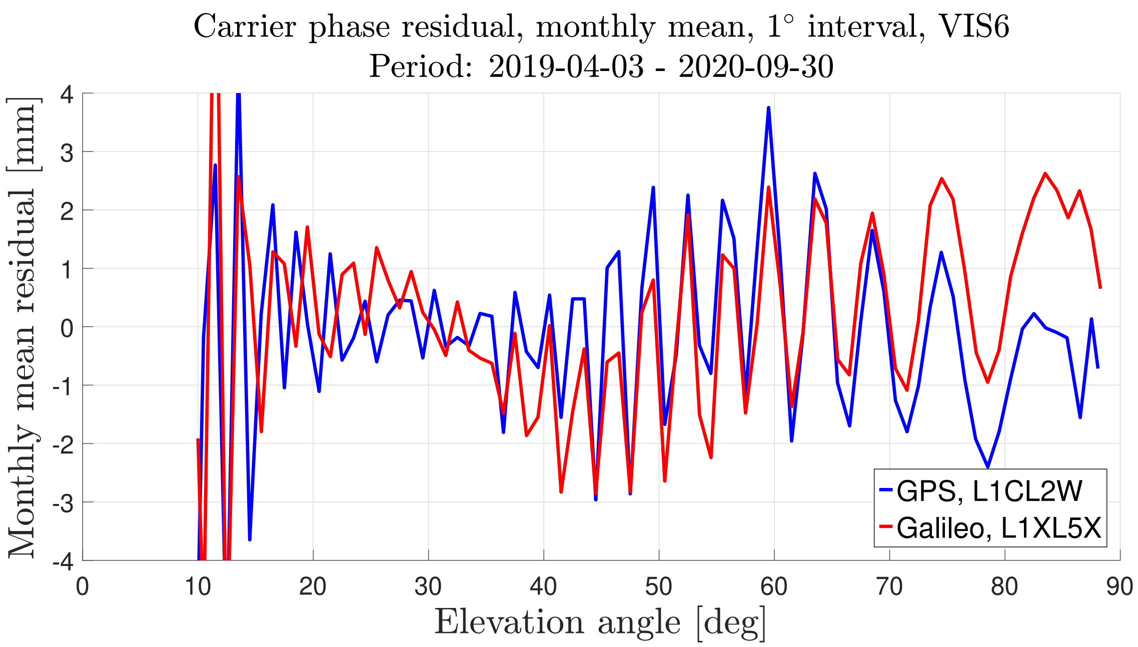

Figure 5.12: Carrier phase residuals, averaged over both 1° elevation angle intervals as well as per month. Station VIS6, GPS (L1CL2W) and Galileo (L1XL5X)

Both of the stations have the high and rapidly oscillating residuals at lower elevation angles, below ~30°, which indicates the multipath effect from the ground. There is however a phenomena that is only present for VIS6, out of all of the 42 stations. The mean residuals of VIS6 are increasing in magnitude after the initial decrease at ~30° elevation angle. In order to analyze this phenomena further, the skyplots for VIS0 and VIS6 are presented in figure 5.13 and 5.14, respectively.

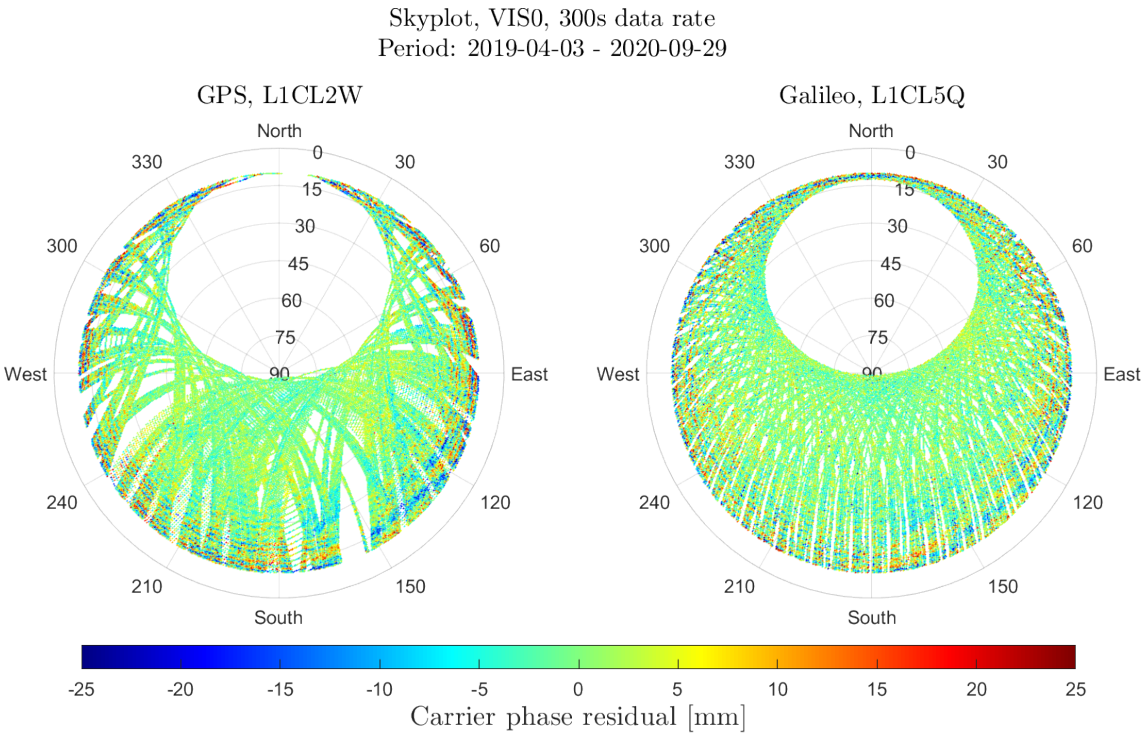

Figure 5.13: Skyplot for station VIS0 for GPS (L1CL2W) and Galileo (L1CL5Q) with color coded carrier phase residuals

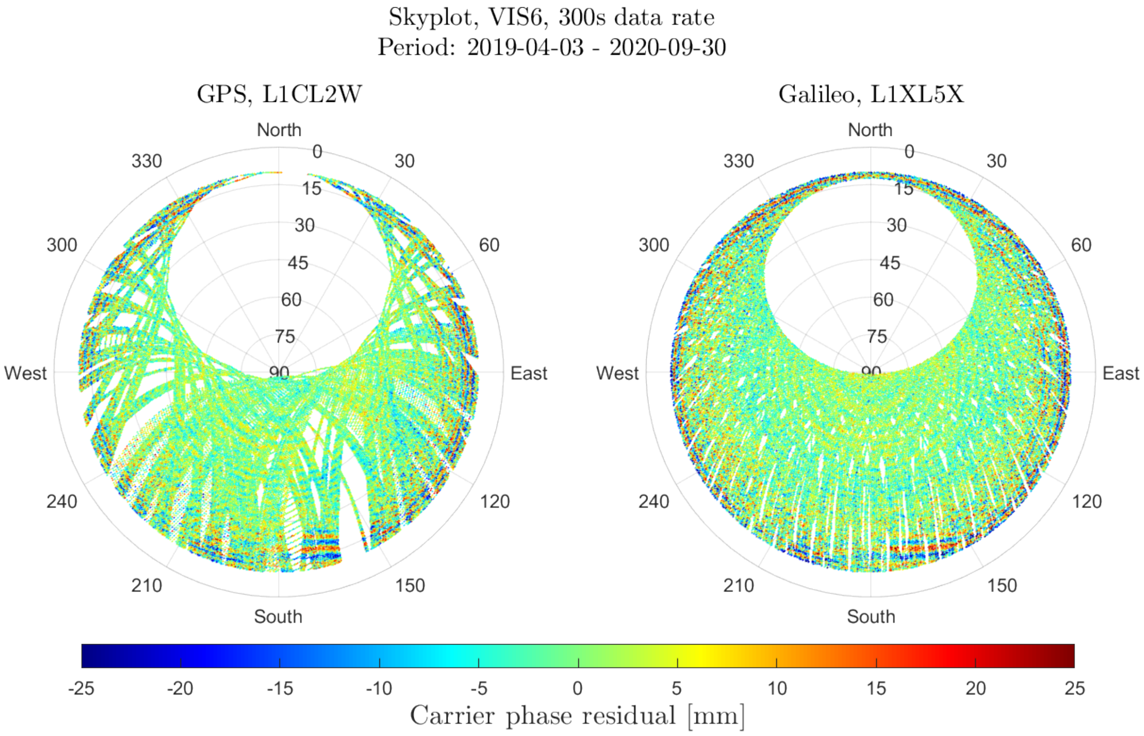

Figure 5.14: Skyplot for station VIS6 for GPS (L1CL2W) and Galileo (L1XL5X) with color coded carrier phase residuals

The multipath effect, for both stations, can be seen as the highly colored, low elevation circles that are present at all azimuth angles. The other phenomena that is present for VIS6 in figure 5.14 might be easy to overlook. In the elevation angle interval ∼45° - 90°, there are residual lines that follows the elevation angle circles. This phenomena, that the residuals follows the elevation angle circles instead of the satellite orbits is only present for one other station, KAR6 (Appendix A), but it is less pronounced in that case and it does not appear in the monthly mean residuals in that case.

The residual circles for VIS6 are present for both GPS and Galileo so it is not related to either of their space segments. One reason for the effect could be related to the fact that the steel grid mast station VIS6 has a different type of antenna as compared to the other mast stations [3]. The higher elevation behaviour for VIS6 could also be accredited to the limestone in its near vicinity, which possibly could affect the multipath for the steel grid mast differently than the concrete pillar, VIS0.

Another reason that also needs to be taken into account is that the station photos are out of date, the most recent ones for VIS6 (and VIS0) are taken 2018-08-15. The measurement period is 2019-04-03 - 2020-09-30 and there might be something present in the station's near vicinity that is not present in the photo.

A concluding remark for the high elevation residual lines for VIS6 is that even though a feasible reason has not been found that can explain the effect, it has helped the analysis to have the station VIS0 in the vicinity. That has helped to discredit several reasons which should have applied the effect to both stations.

5.3 Further work

This study has been based on final, precise products from IGS, meaning that the results here are achieved through post-processing. It would be interesting to study the convergence time as a function of an acceptable repeatability, i.e. to approach real time PPP processing. A step to achieve that could be to utilize predicted products, orbits and clocks, from IGS that have uncertainties of ∼10-20 cm instead of the final products that have uncertainties of ∼1-2 cm. There are also settings in the Kalman filter in GipsyX that could help to facilitate this, such as the reduction of the number of iterations.

The study have not analyzed the Zenith tropospheric delay (ZTD) solutions. It would also be interesting to do a similar analysis that was done for the repeatability in section 5.1 for G, R, E, C, GE, GR, GRE and GREC but for the ZTD instead.

A parameter that has been mentioned in theory but not studied is the carrier phase ambiguity. A study of how well the software can determine those to integers for the different constellation combinations could also be a feature for future work.

6 Conclusion

The repeatability analysis of the SWEPOS steel grid mast stations showed that the highest performance were achieved with the combination of GPS+GLONASS+Galileo. The achieved repeatabilities (standard deviation) for the latitudinal, longitudinal and vertical components were 1.20 mm, 3.56 mm and 4.00 mm, respectively. The coordinate accuracies for GPS, GPS+Galileo and GPS+GLONASS were within the GPS+GLONASS+ Galileo repeatability. Their respective repeatabilities differs to that of GPS+GLONASS+Galileo by sub-millimeter levels, which means that any of the combinations yields comparable results.

The analysis of the monthly mean carrier phase residuals, for all of the stations, showed that the concrete pillar stations and the steel grid mast stations had two distinct curve appearances. The residual curves for GPS and Galileo were on the whole in agreement for the concrete pillar stations. While the residual curves for the steel grid mast stations had a discernible oscillation that could be divided into three elevation angle intervals. Most notably was that the GPS and the Galileo residuals diverged at the upper elevation angle interval, 60° - 90°.

The carrier phase residuals were successfully utilized to describe local phenomena such as wooden fences, adjacent houses and multipath from solid bedrock. There was however an effect that was only present for one station, VIS6, that could not be explained. Its residuals at high elevations, ∼45° - 90°, followed those of the elevation angle circles instead of the satellites' orbits.

It was illustrated and shown with examples that it is useful to analyze stations in pairs. It helps to discredit certain error sources and phenomena that should be affecting both of the stations. It was furthermore illustrated that it is useful to study the monthly mean residuals, as a function of elevation angle, in parallel with the skyplots.

References

[1] J. Sans Subirana et. al., "GNSS DATA PROCESSING, Volume I: Fundamentals and Algorithms", AG Noordwijk, the Netherlands: ESA Communications, 2013. Accessed: Nov. 12, 2020. [Online]. Available: https://gssc.esa.int/navipedia/index.php/GNSS:Tools.

[2] "IGS Products", International GNSS Service. Accessed on: Sep. 30, 2020. [Online]. Available: http://www.igs.org/products.

[3] J. Johansson et. al., "CLOSE-RTK 3: High-performance Real-Time GNSS Services", RISE Report 2019:101, ISBN: 978-91-89049-32-1, Nov. 2019. Accessed: Dec. 18, 2020. [Online]. Available: http://www.diva-portal.org/smash/record.jsf?pid=diva2%3A1368012&dswid=-350.

[4] F. Xia et al., "Assessing the latest performance of Galileo-only PPP and the contribution of Galileo to Multi-GNSS PPP", Advances in Space Research, vol. 63, no. 9, pp. 2784-2795, May 2019, doi: https://doi.org/10.1016/j.asr.2018.06.008. Accessed: Jan. 3, 2021. [Online]. Available: https://www.sciencedirect.com/science/article/abs/pii/S0273117718304745.

[5] Sermet Ogutcu, "Assessing the contribution of Galileo to GPS+GLONASS PPP: Towards full operational capability", Measurement, vol. 151, Feb. 2020, doi: https://doi.org/10.1016/j.measurement.2019.107143. Accessed: Jul. 27, 2020. [Online]. Available: https://www-sciencedirect-com.proxy.lib.chalmers.se/science/article/abs/pii/S0263224119310097?via%3Dihub.

[6] Swepo's Service Portal. Accessed: Dec. 18, 2020. [Online]. Available: https://swepos.lantmateriet.se/.

[7] Royal Observatory of Belgium, "EUREF Permanent GNSS Network". Accessed: Jan. 02, 2021. [Online]. Available: https://www.epncb.oma.be/_networkdata/stationlist.php.

[8] Hofmann-Wellenhof, Lichtenegger and Wasle. *"GNSS Global Navigation Satellite Systems"*. SpringerWienNewYork, 2008.

[9] Navipedia, European Space Agency. Accessed: Oct. 1, 2020. [Online]. Available: https://gssc.esa.int/navipedia/index.php/Main_Page.

[10] J Boehm et al., "Troposphere mapping functions for GPS and very long baseline interferometry from European Centre for Medium-Range Weather Forecasts operational analysis data", Jornal of Geophysical Research, vol. 111, no. B02406, Feb. 2006. Accessed: Dec. 15, 2020, doi: https://doi.org/10.1029/2005JB003629. [Online]. Available: https://agupubs.onlinelibrary.wiley.com/doi/10.1029/2005JB003629.

[11] T. Hobiger and N. Jakowski, "Atmospheric Signal Propagation" in "Springer Handbook of Global Navigation Satellite Systems". Springer Handbooks, Springer, Cham, 2017, ch. 6, pp. 165-193.

[12] S. Byram and C. Hackman, "High-precision GNSS orbit, clock and EOP estimation at the United States Naval Observatory", Proceedings of the 2012 IEEE/ION Position, Location and Navigation Symposium, Myrtle Beach, SC, 2012, pp. 659-663, doi: 10.1109/PLANS.2012.6236940. Accessed: Dec. 16, 2020. [Online]. Available: https://ieeexplore.ieee.org/document/6236940.

[13] Institutionen för rymd och geovetenskap. *"Mätteknik"*. Teknologtryck, Göteborg, 2018.

[14] NovAtel, "An Introduction to GNSS", 2n ed., Calgary, Alberta, Canada: NovAtel Inc., 2015. Accessed: Sep. 30, 2020. [Ebook]. Available: https://novatel.com/an-introduction-to-gnss.

[15] National Aeronautics and Space Administration, "RINEX Version 3 data", Nov. 29, 2018. Accessed: Dec. 22, 2020. [Online]. Avalable: https://cddis.nasa.gov/Data_and_Derived_Products/GNSS/RINEX_Version_3.html.

[16] W. Bertiger et al., "GipsyX/RTGx, A New Tool Set for Space Geodetic Operations and Research", Advances in Space Research, vol. 66, no. 3, pp. 469-489, Aug. 2020. Accessed: Oct. 1, 2020, doi: https://doi.org/10.1016/j.asr.2020.04.015. [Online]. Available: https://www.sciencedirect.com/science/article/pii/S0273117720302532.

[17] O. Montenbruck et al., "The Multi-GNSS Experiment (MGEX) of the International GNSS Service (IGS) – Achievements, Prospects and Challenges", Advances in Space Research, vol. 59, no. 7, pp. 1671-1697, Apr. 2017. Accessed: Sep. 30, 2020, doi: https://doi.org/10.1016/j.asr.2017.01.011. [Online]. Available: https://www.sciencedirect.com/science/article/pii/S0273117717300418.

[18] "Vienna Mapping Functions Open Access Data", TU Wien, Department of Geodesy and Geoinformation. Accessed: Nov. 18, 2020. [Online]. Available: https://vmf.geo.tuwien.ac.at/.

[19] "Earth orientation data", International Earth Rotation and Reference Systems Service. Accessed: Oct. 1, 2020. [Online]. Available: https://www.iers.org/IERS/EN/Home/home_node.html;jsessionid=E3CE684F45CE073E67A6A6F5ECB90BF0.live2.

[20] H.G. Scherneck, "The free ocean tide loading provider". Accessed: Sep. 30, 2020. [Online]. Available: http://holt.oso.chalmers.se/loading/.

[21] G. Nykiel, F. Mariusz, "Precise Point Positioning Method Based on Wide-lane and Narrow-lane Phase Observations and Between Satellites Single Differencing", Proceedings of the 2016 International Technical Meeting of The Institute of Navigation, Jan., 2016, pp. 1055-1066, Monterey, California. Accessed: Oct. 1, 2020, doi: 10.33012/2016.13494. [Online]. Available: https://www.researchgate.net/publication/295919681_Precise_Point_Positioning_Method_Based_on_Wide-lane_and_Narrow-lane_Phase_Observations_and_Between_Satellites_Single_Differencing.

A Skyplots with color coded carrier phase residuals for GPS and Galileo for 42 SWEPOS stations

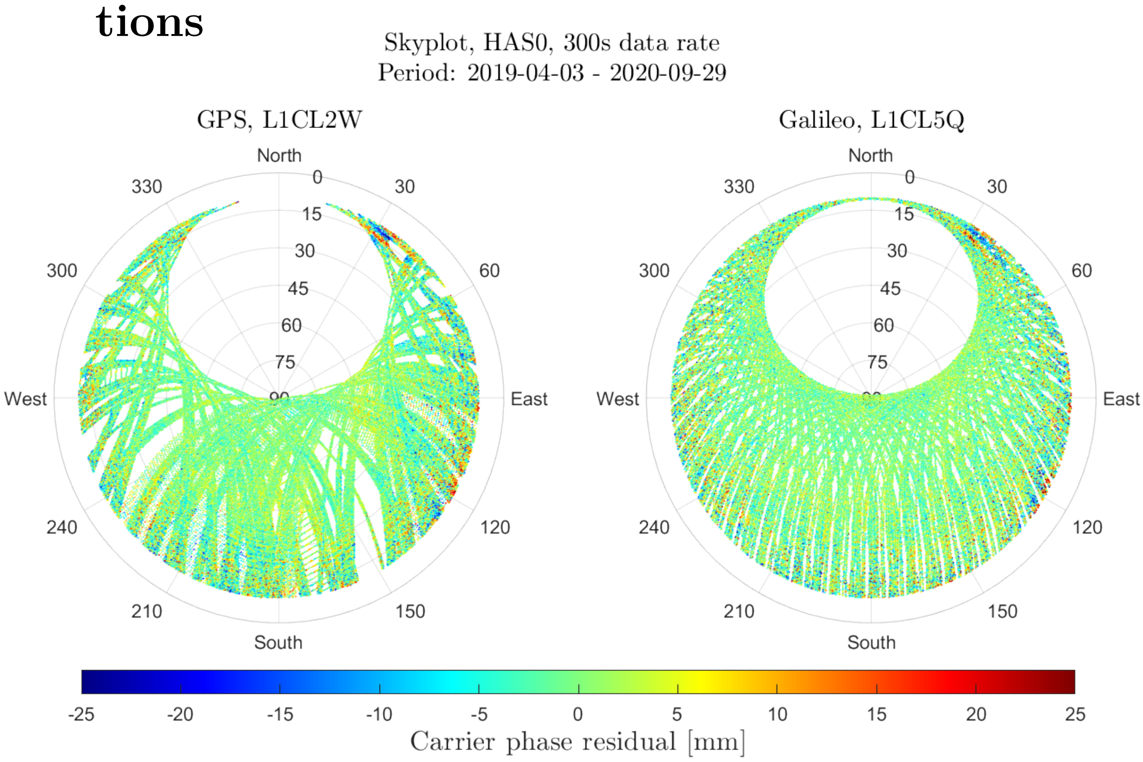

Figure A.1: Skyplot for station HAS0 for GPS (L1CL2W) and Galileo (L1CL5Q) with color coded carrier phase residuals

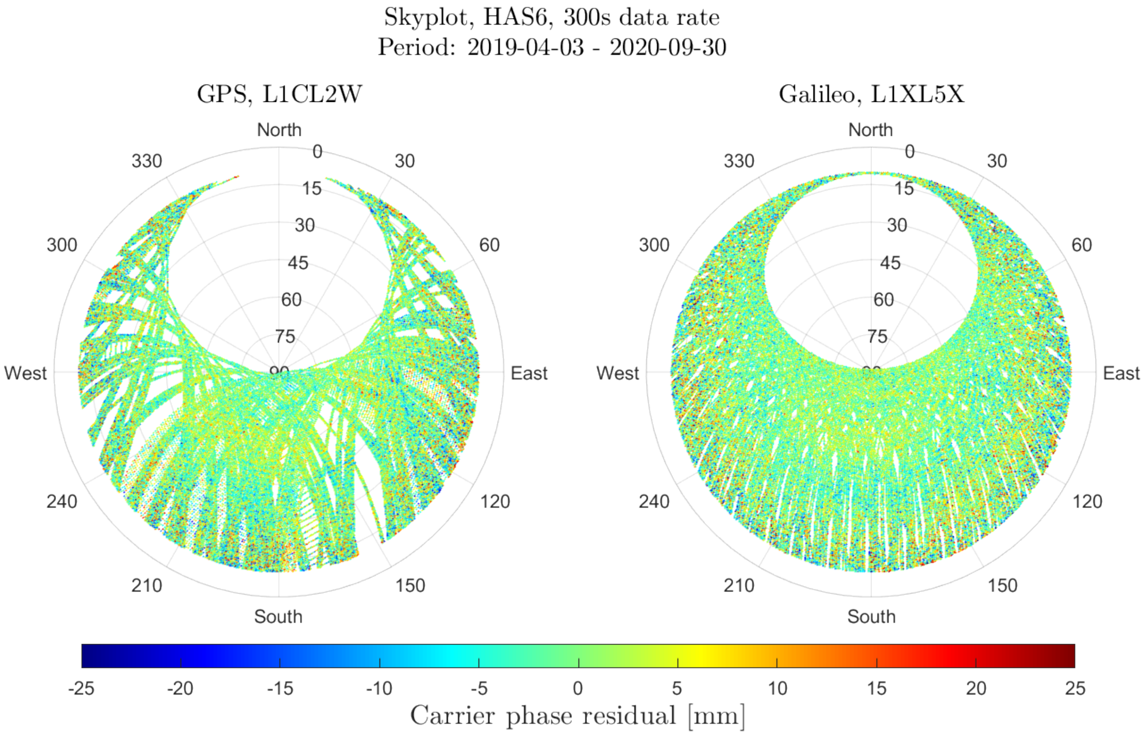

Figure A.2: Skyplot for station HAS6 for GPS (L1CL2W) and Galileo (L1XL5X) with color coded carrier phase residuals

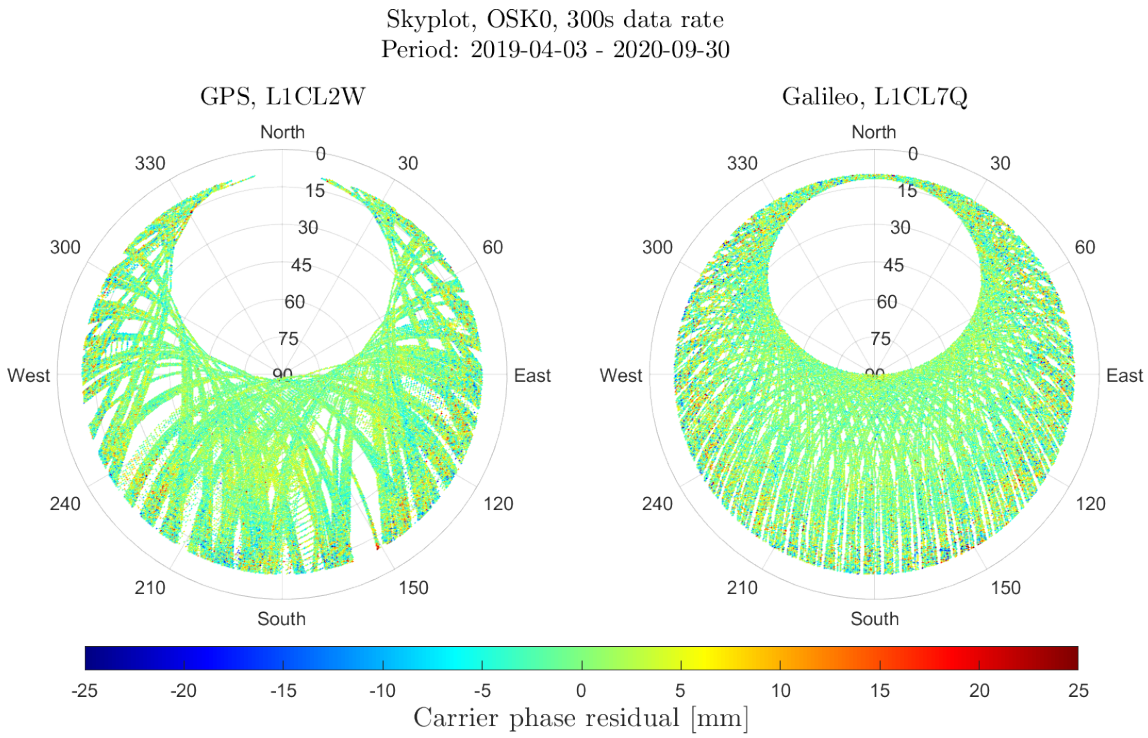

Figure A.3: Skyplot for station OSK0 for GPS (L1CL2W) and Galileo (L1CL7Q) with color coded carrier phase residuals

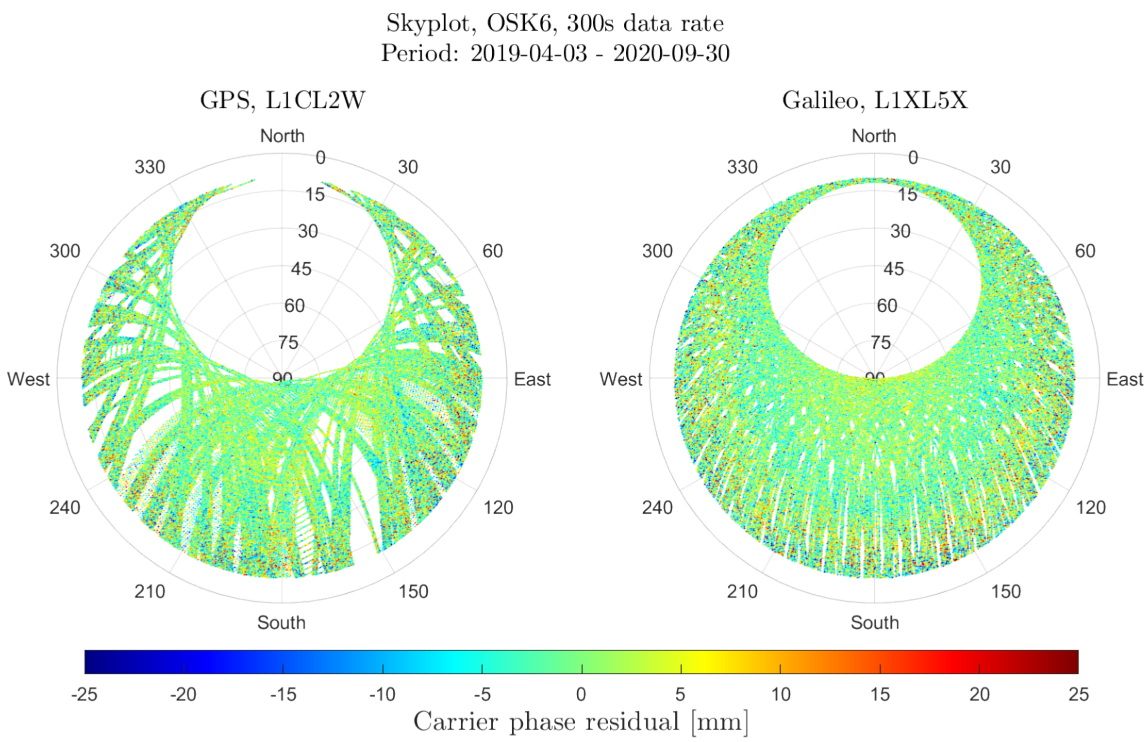

Figure A.4: Skyplot for station OSK6 for GPS (L1CL2W) and Galileo (L1XL5X) with color coded carrier phase residuals

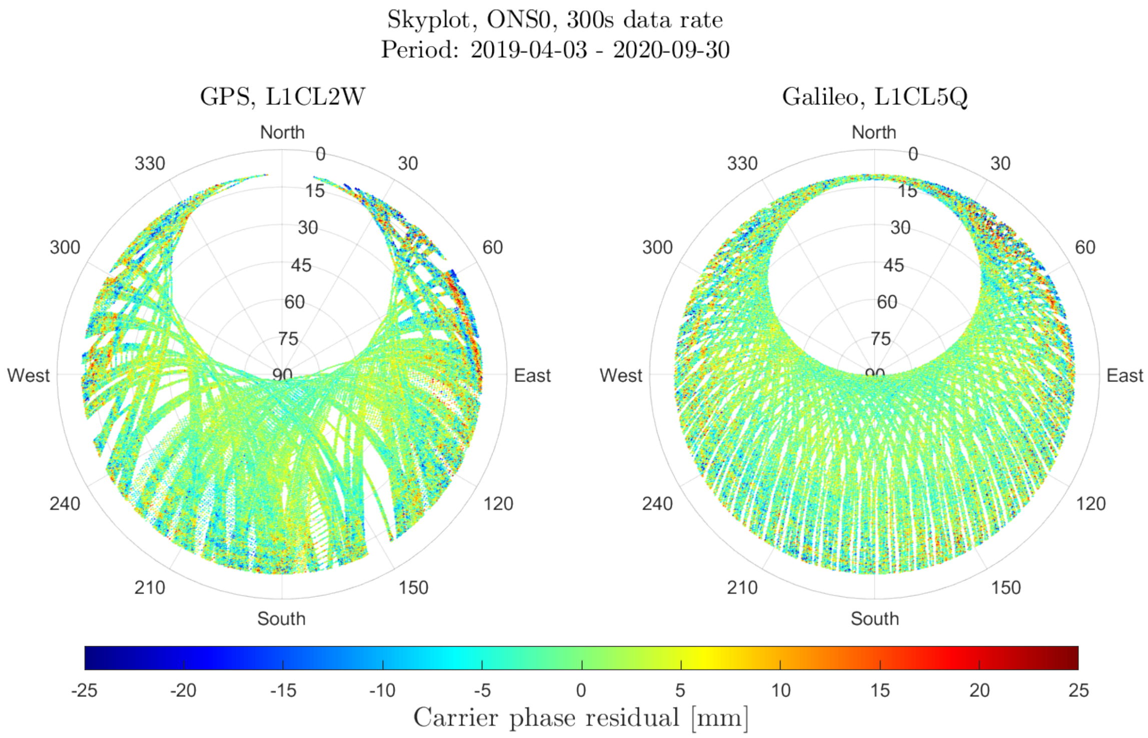

Figure A.5: Skyplot for station ONS0 for GPS (L1CL2W) and Galileo (L1CL5Q) with color coded carrier phase residuals

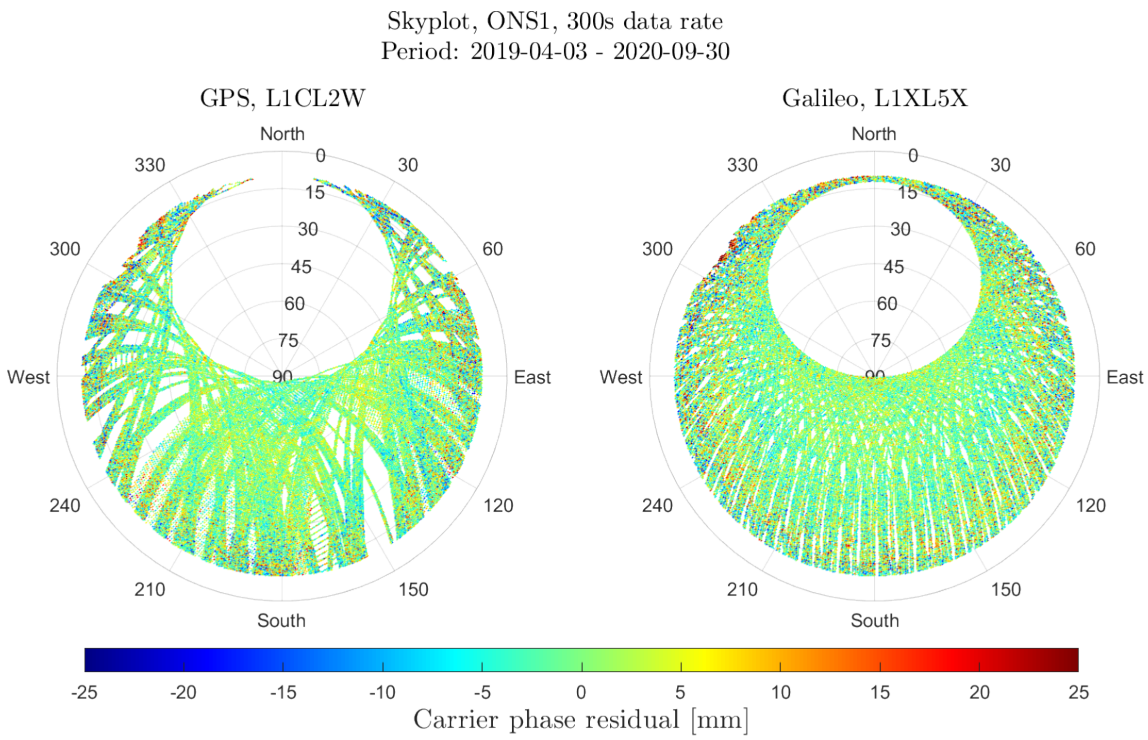

Figure A.6: Skyplot for station ONS1 for GPS (L1CL2W) and Galileo (L1XL5X) with color coded carrier phase residuals

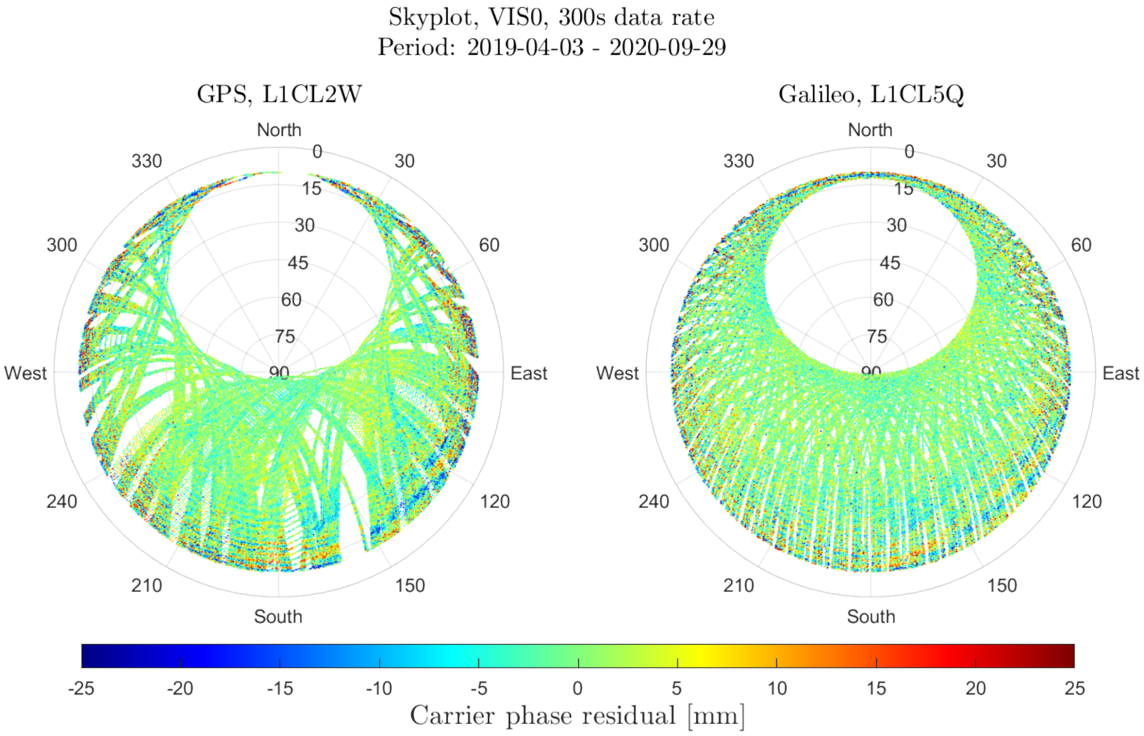

Figure A.7: Skyplot for station VIS0 for GPS (L1CL2W) and Galileo (L1CL5Q) with color coded carrier phase residuals

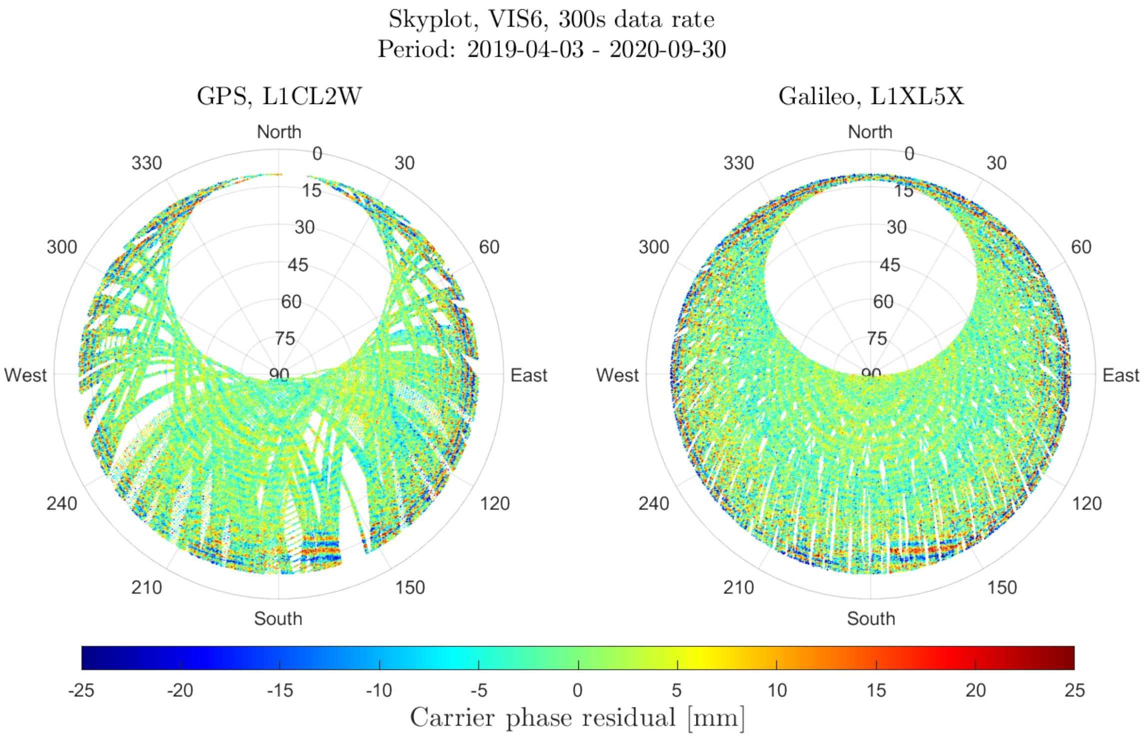

Figure A.8: Skyplot for station VIS6 for GPS (L1CL2W) and Galileo (L1XL5X) with color coded carrier phase residuals

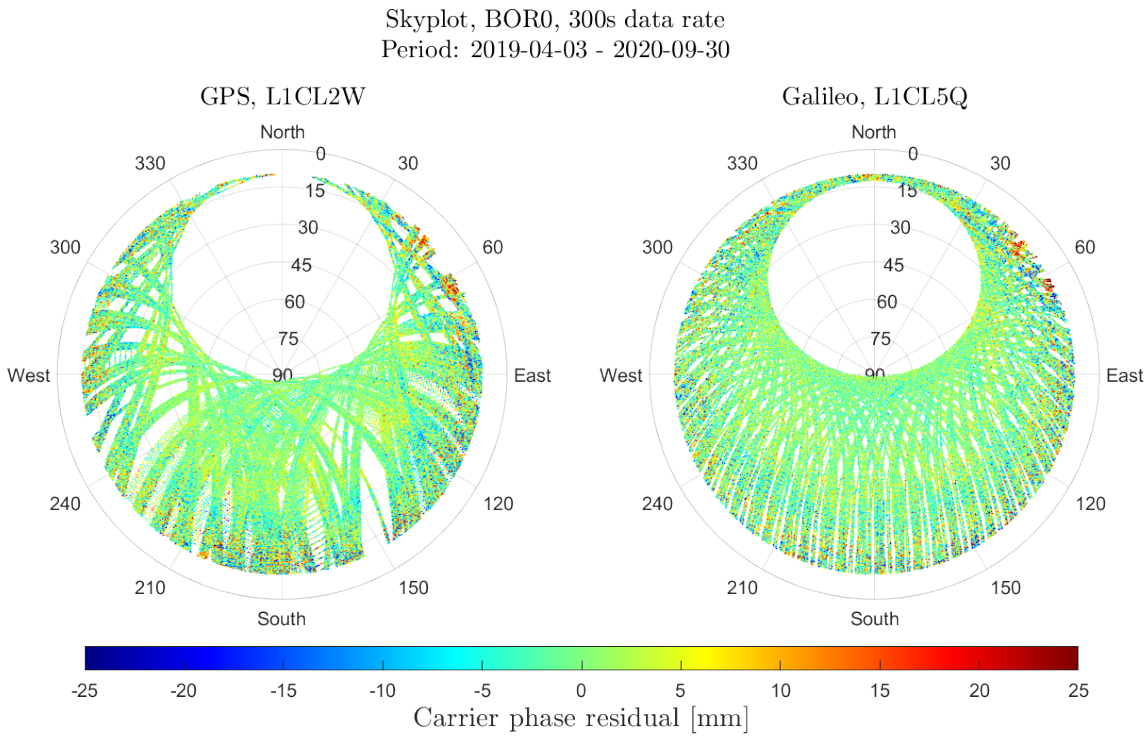

Figure A.9: Skyplot for station BOR0 for GPS (L1CL2W) and Galileo (L1CL5Q) with color coded carrier phase residuals

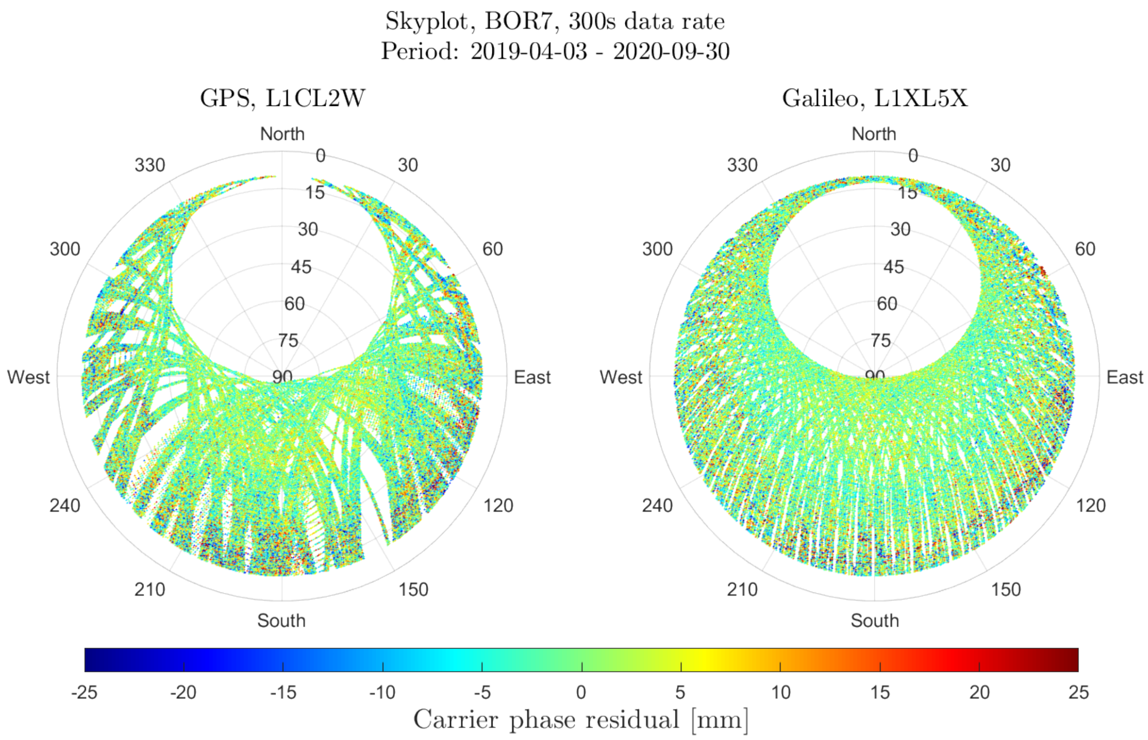

Figure A.10: Skyplot for station BOR7 for GPS (L1CL2W) and Galileo (L1XL5X) with color coded carrier phase residuals

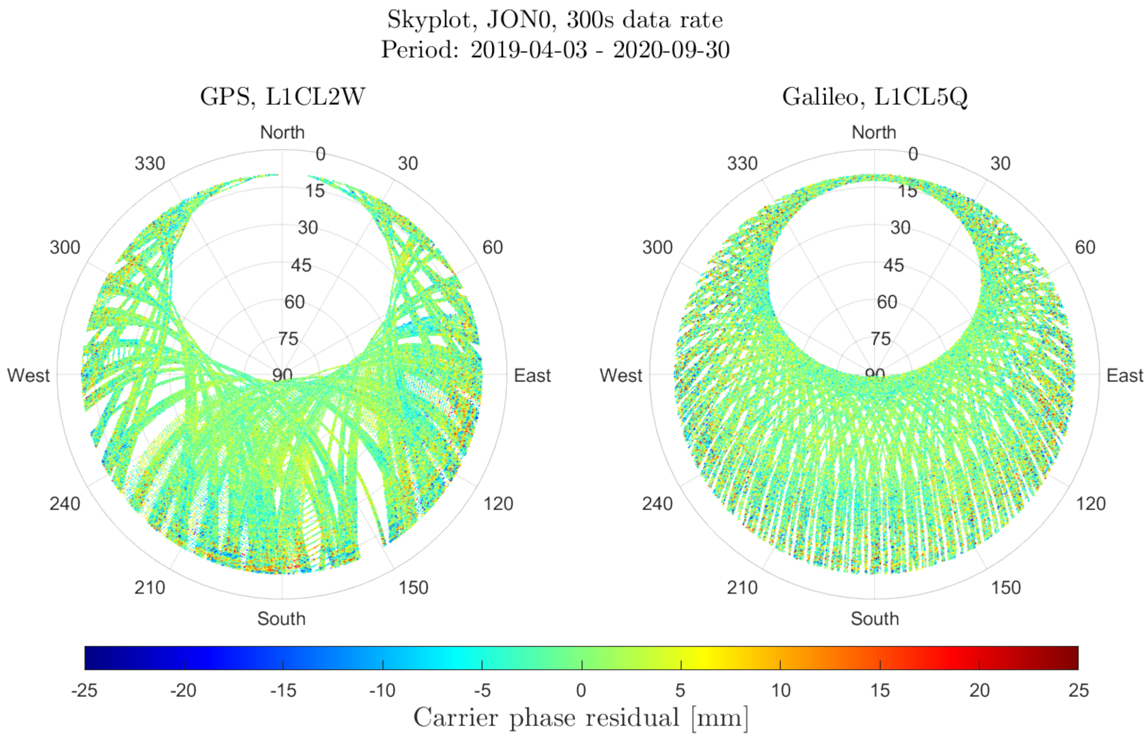

Figure A.11: Skyplot for station JON0 for GPS (L1CL2W) and Galileo (L1CL5Q) with color coded carrier phase residuals

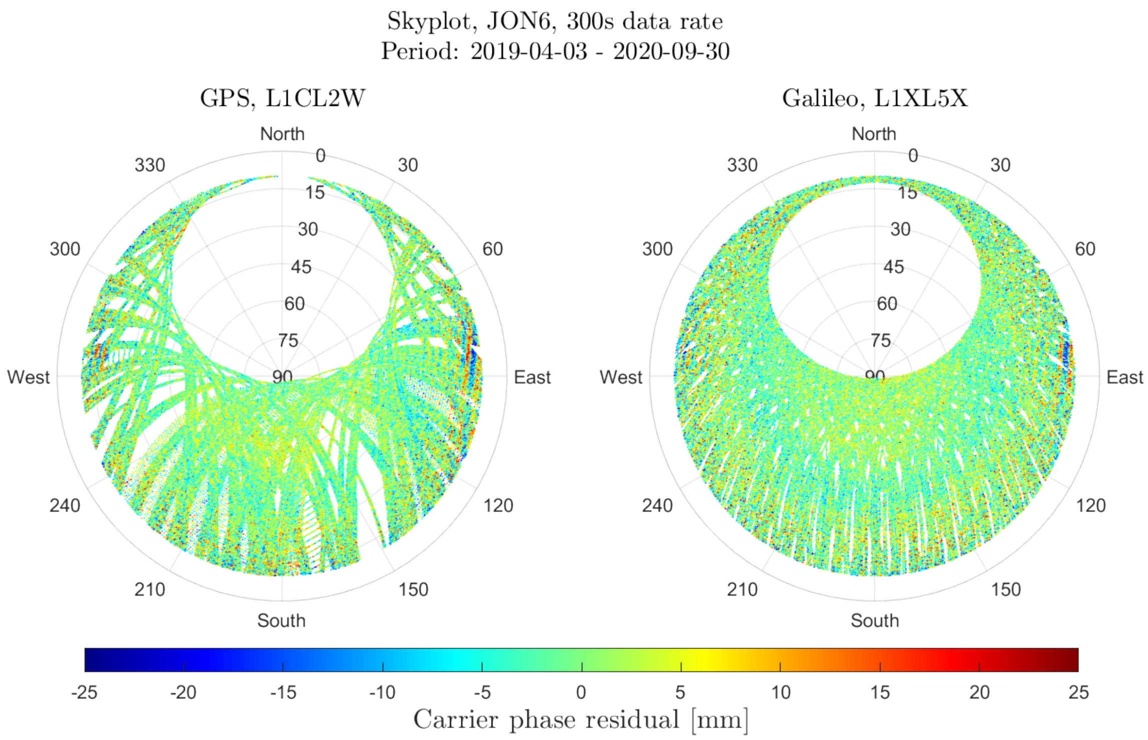

Figure A.12: Skyplot for station JON6 for GPS (L1CL2W) and Galileo (L1XL5X) with color coded carrier phase residuals

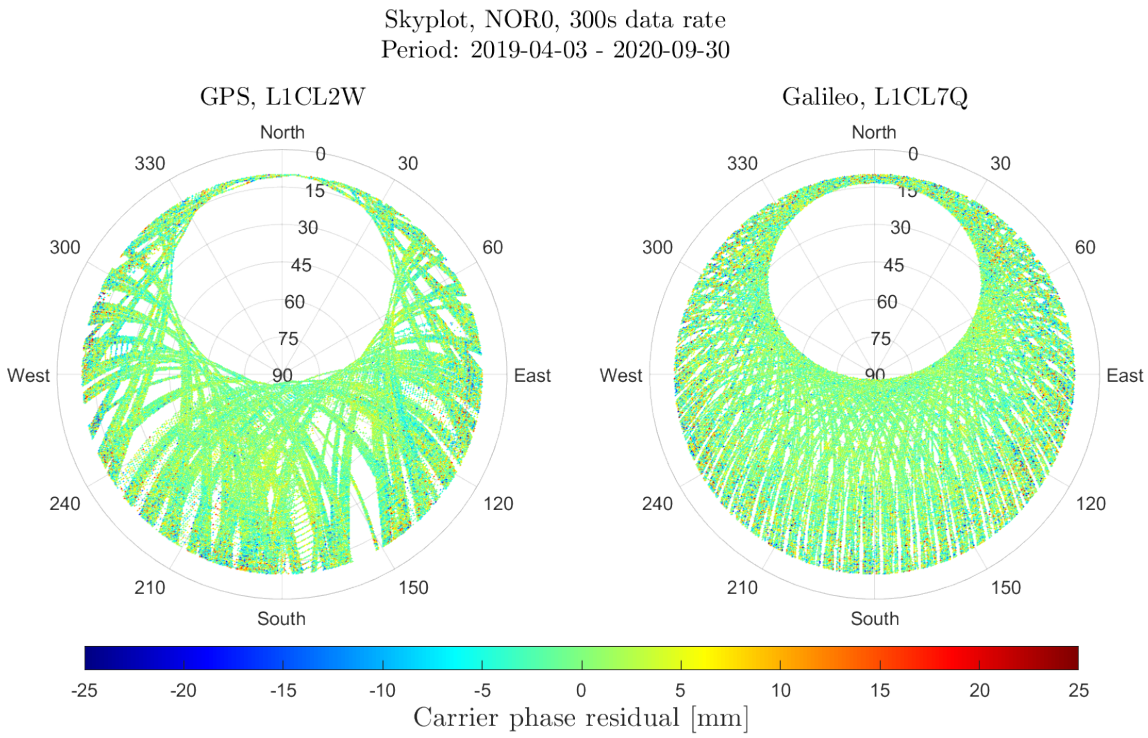

Figure A.13: Skyplot for station NOR0 for GPS (L1CL2W) and Galileo (L1CL7Q) with color coded carrier phase residuals

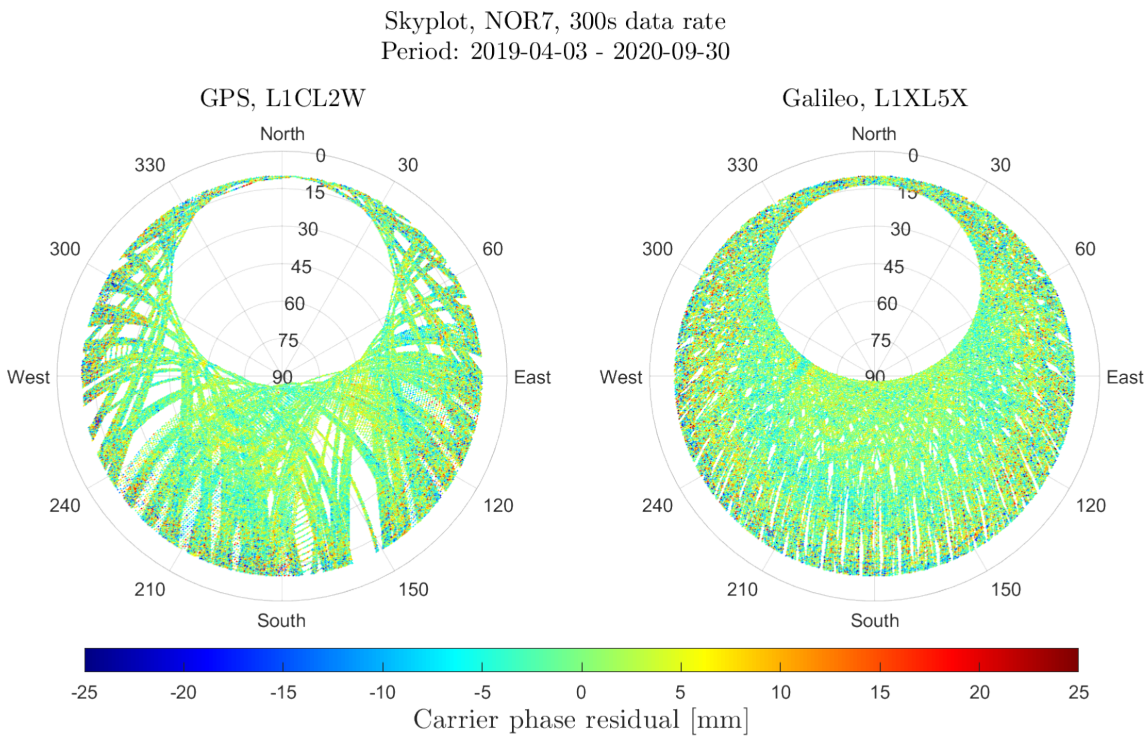

Figure A.14: Skyplot for station NOR7 for GPS (L1CL2W) and Galileo (L1XL5X) with color coded carrier phase residuals

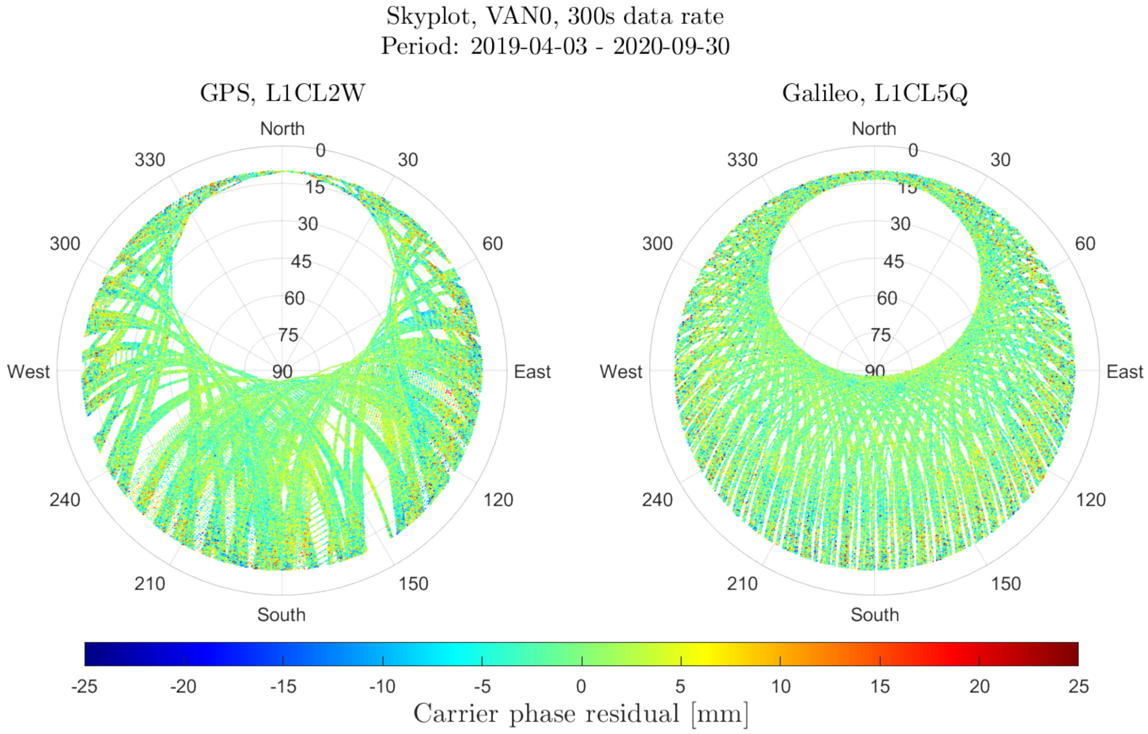

Figure A.15: Skyplot for station VAN0 for GPS (L1CL2W) and Galileo (L1CL5Q) with color coded carrier phase residuals

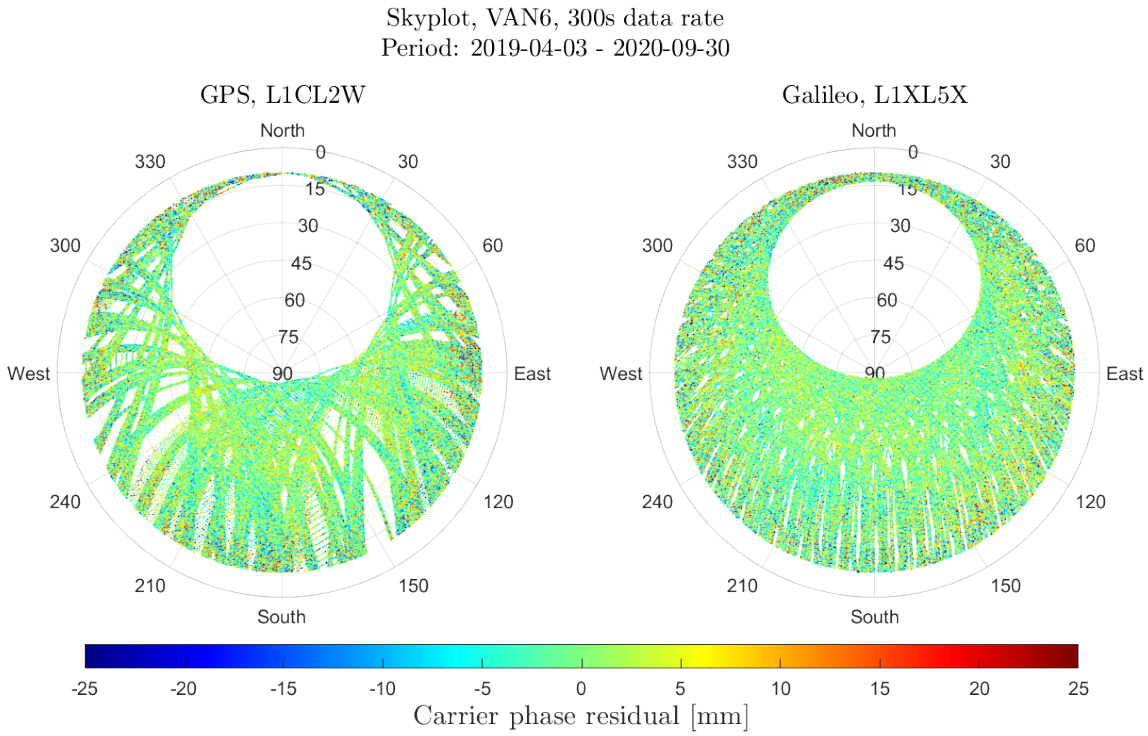

Figure A.16: Skyplot for station VAN6 for GPS (L1CL2W) and Galileo (L1XL5X) with color coded carrier phase residuals

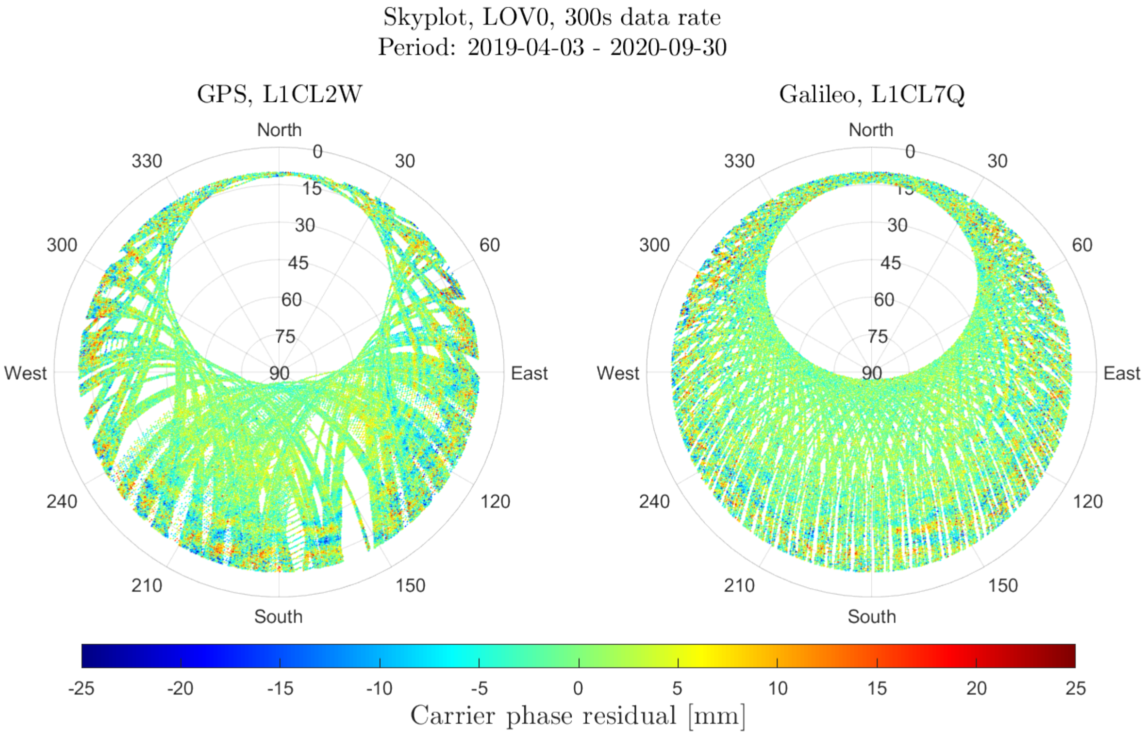

Figure A.17: Skyplot for station LOV0 for GPS (L1CL2W) and Galileo (L1CL7Q) with color coded carrier phase residuals

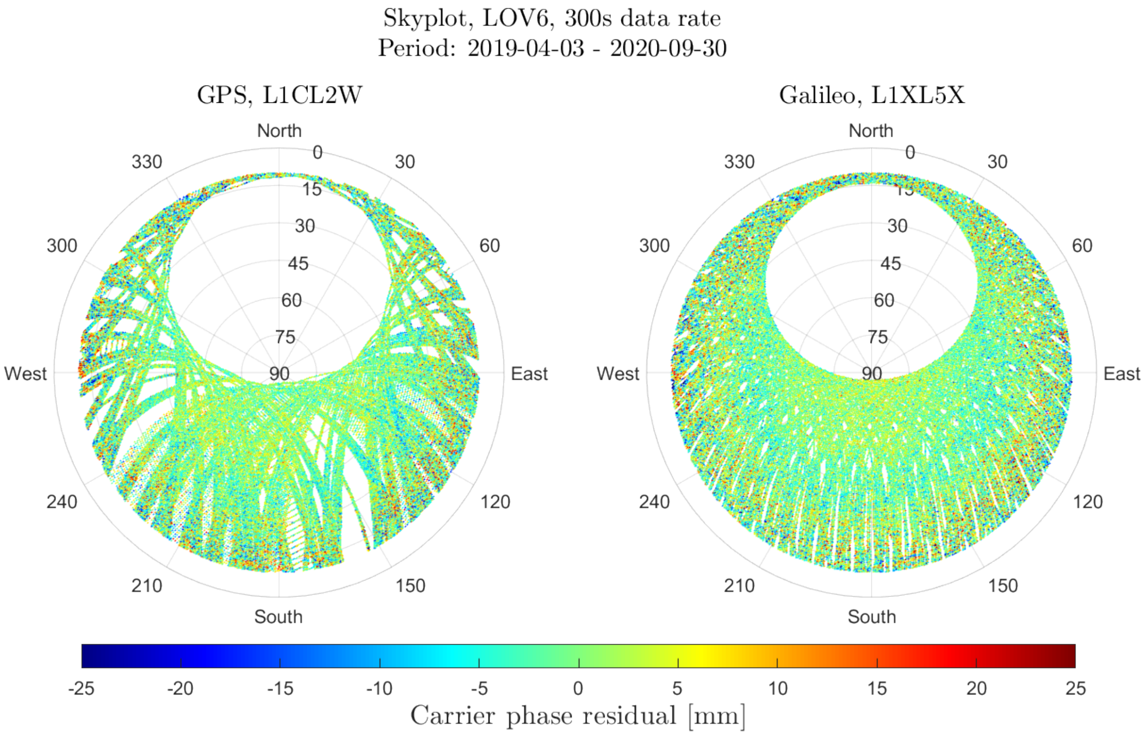

Figure A.18: Skyplot for station LOV6 for GPS (L1CL2W) and Galileo (L1XL5X) with color coded carrier phase residuals

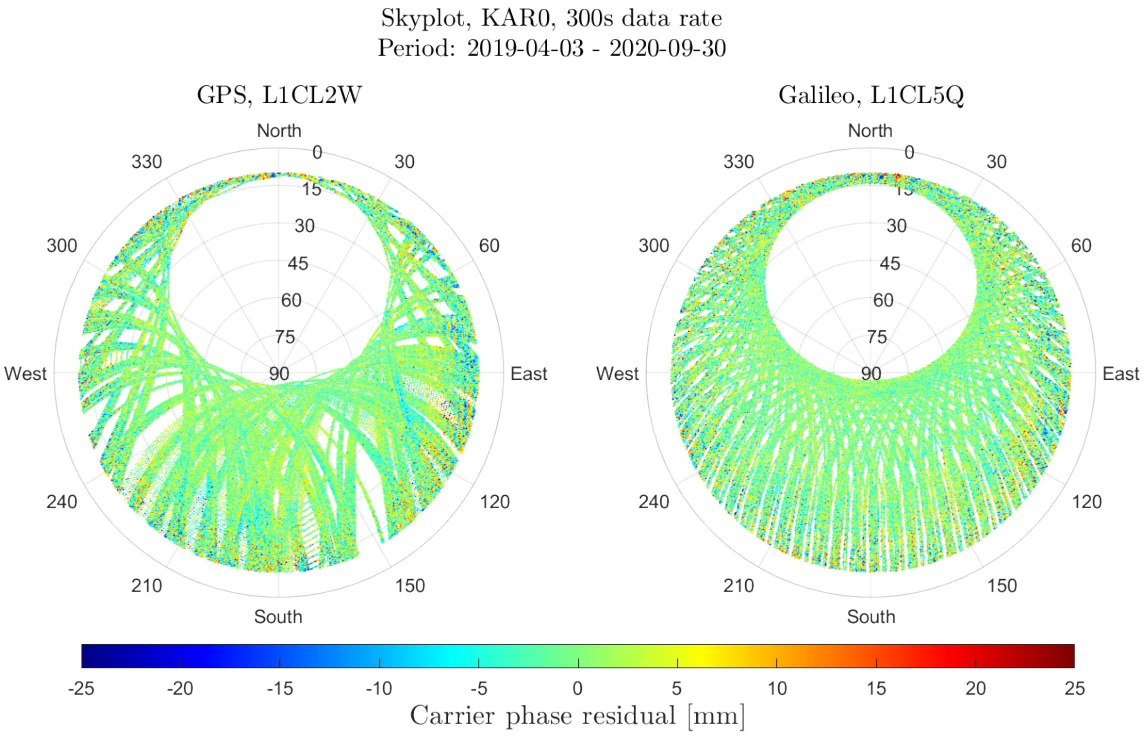

Figure A.19: Skyplot for station KAR0 for GPS (L1CL2W) and Galileo (L1CL5Q) with color coded carrier phase residuals

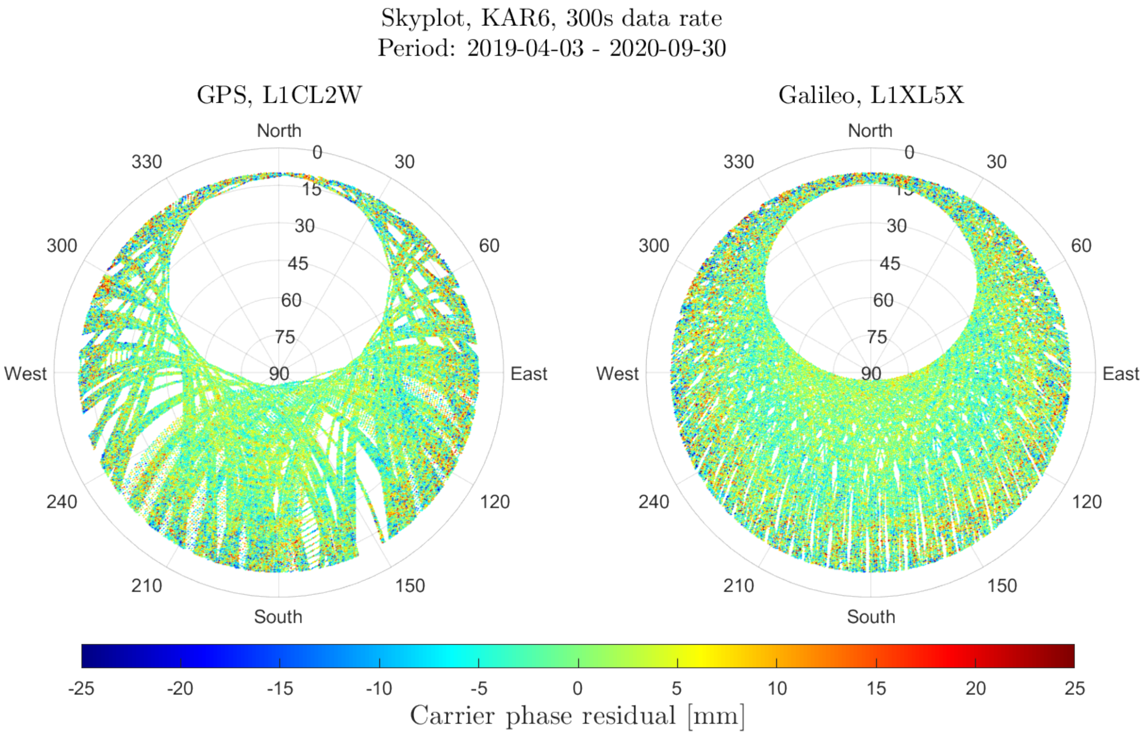

Figure A.20: Skyplot for station KAR6 for GPS (L1CL2W) and Galileo (L1XL5X) with color coded carrier phase residuals

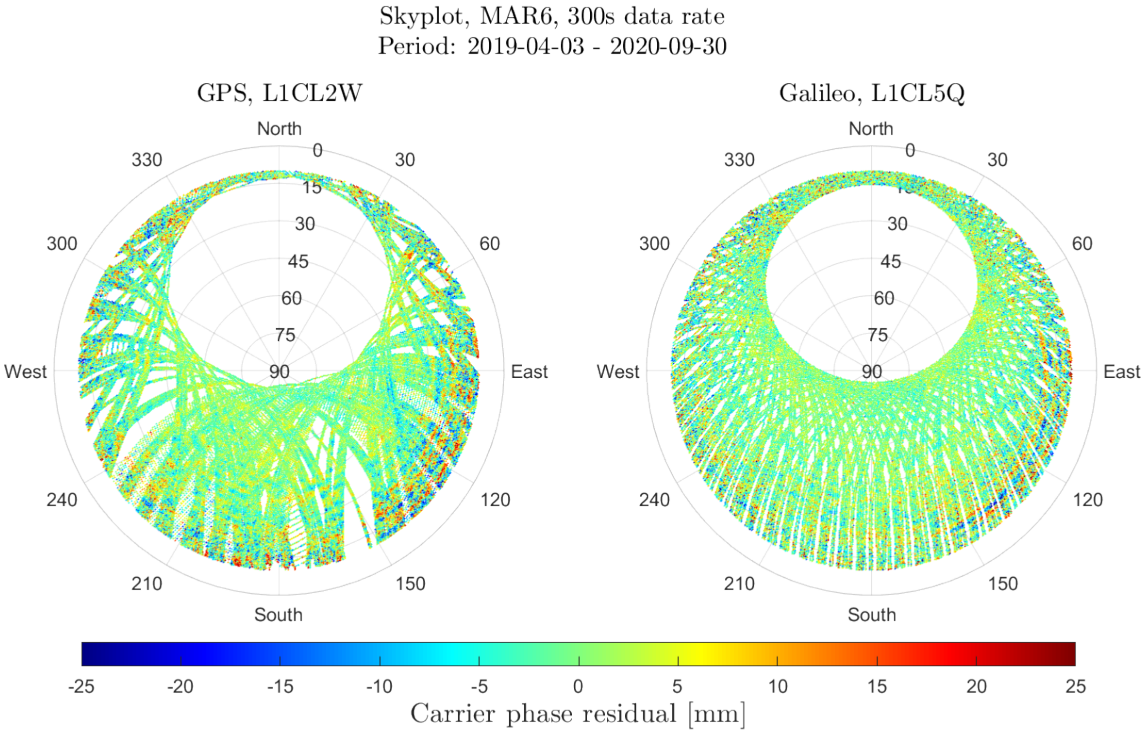

Figure A.21: Skyplot for station MAR6 for GPS (L1CL2W) and Galileo (L1CL5Q) with color coded carrier phase residuals

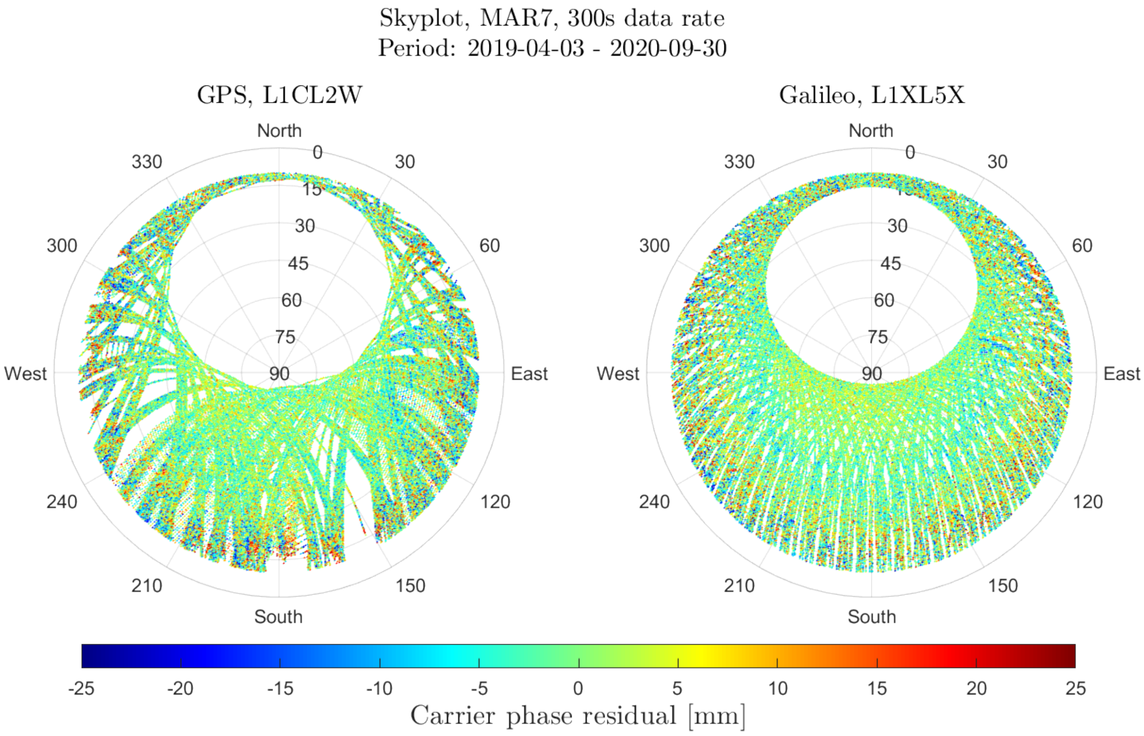

Figure A.22: Skyplot for station MAR7 for GPS (L1CL2W) and Galileo (L1XL5X) with color coded carrier phase residuals

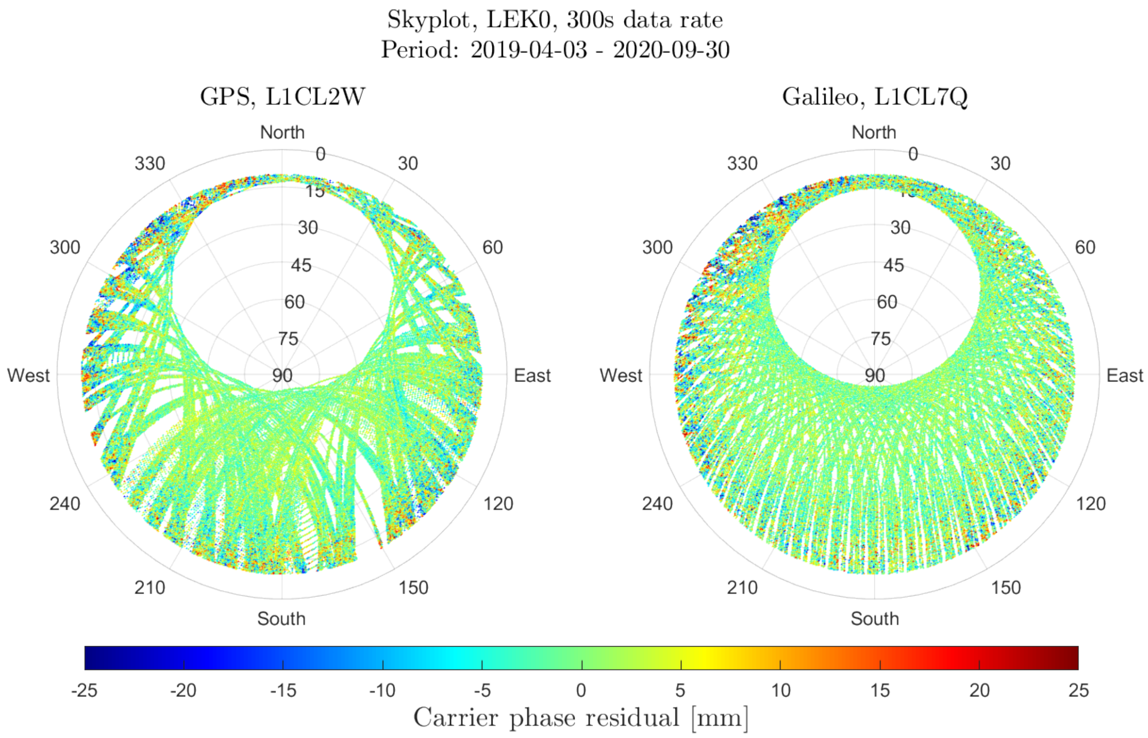

Figure A.23: Skyplot for station LEK0 for GPS (L1CL2W) and Galileo (L1CL7Q) with color coded carrier phase residuals

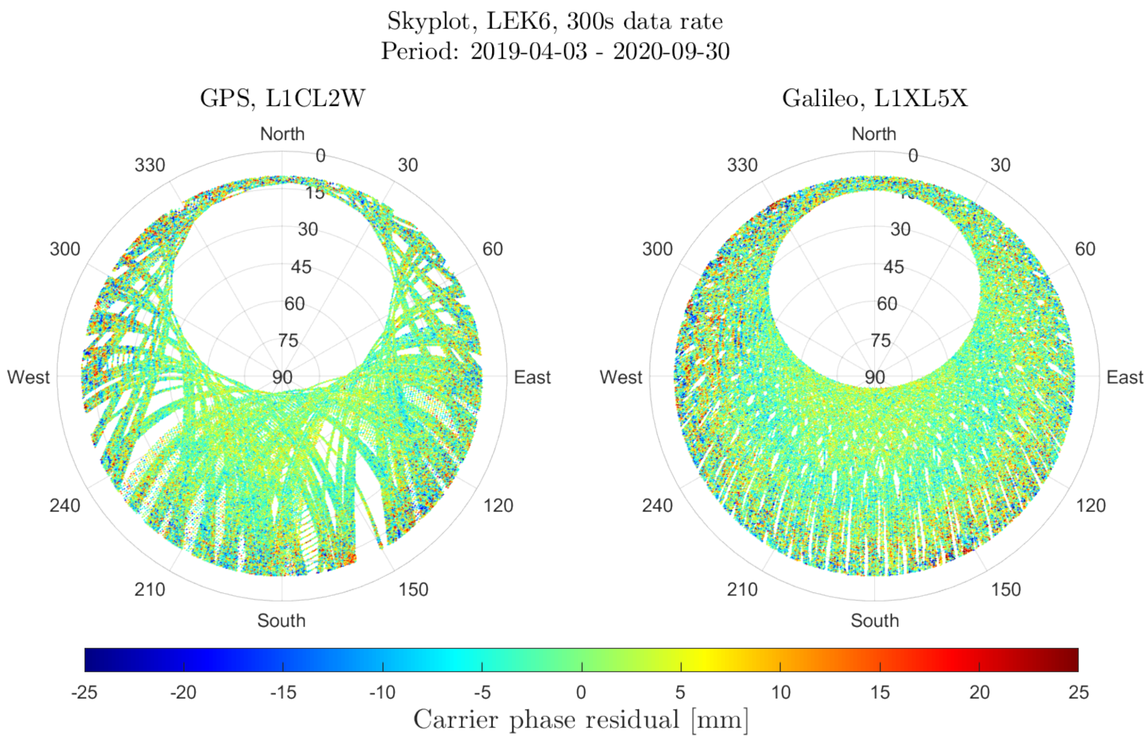

Figure A.24: Skyplot for station LEK6 for GPS (L1CL2W) and Galileo (L1XL5X) with color coded carrier phase residuals

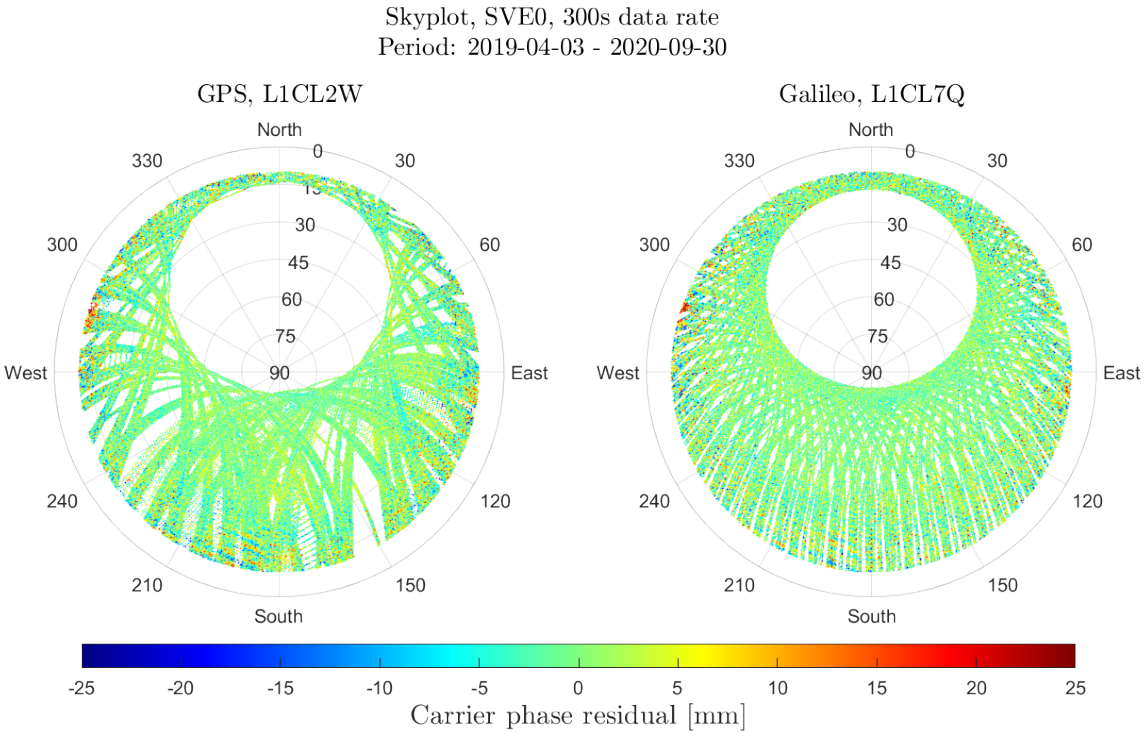

Figure A.25: Skyplot for station SVE0 for GPS (L1CL2W) and Galileo (L1CL7Q) with color coded carrier phase residuals

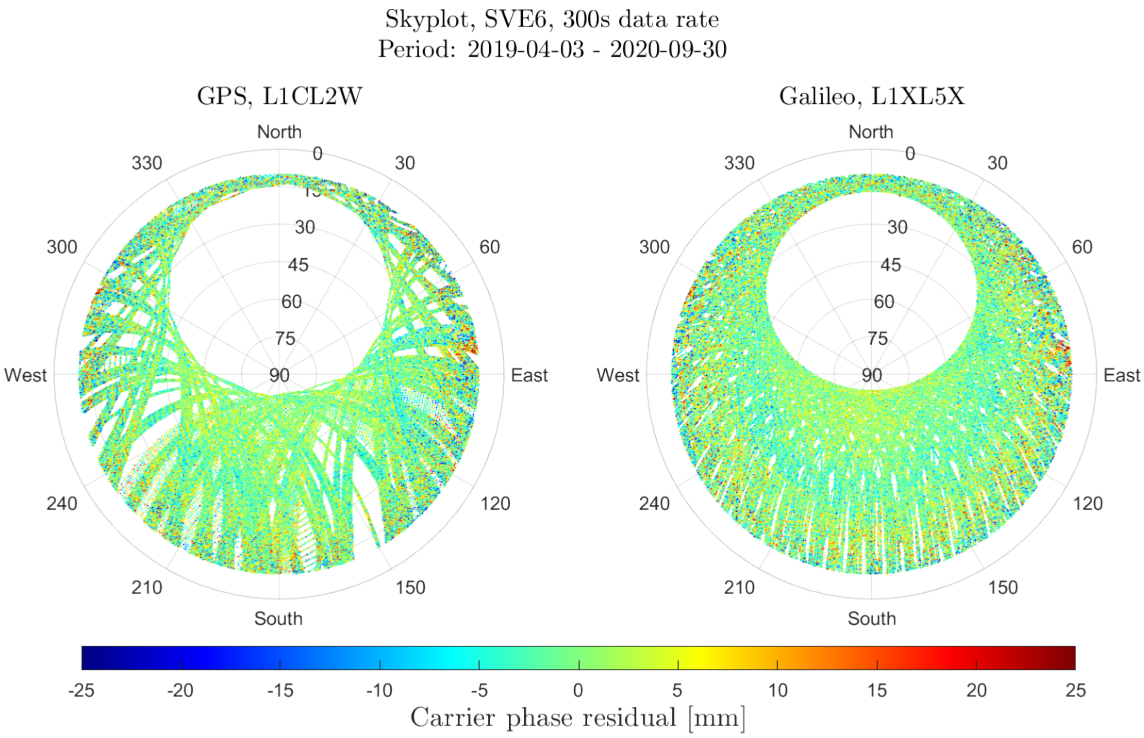

Figure A.26: Skyplot for station SVE6 for GPS (L1CL2W) and Galileo (L1XL5X) with color coded carrier phase residuals

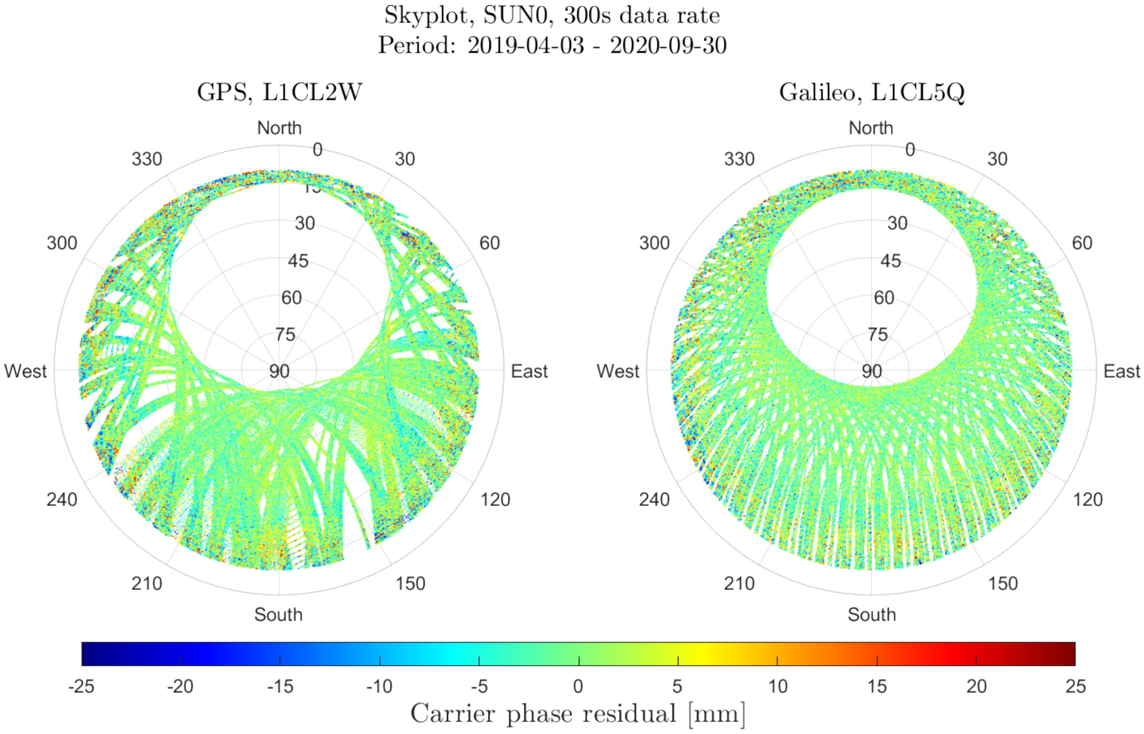

Figure A.27: Skyplot for station SUN0 for GPS (L1CL2W) and Galileo (L1CL5Q) with color coded carrier phase residuals

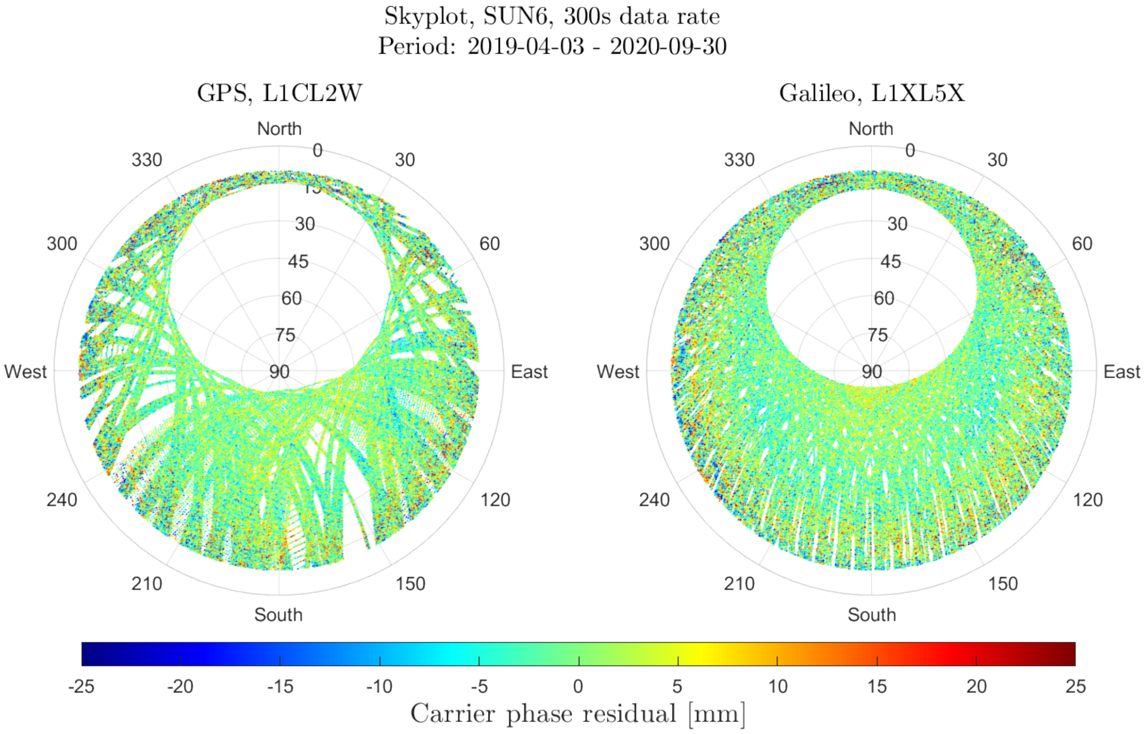

Figure A.28: Skyplot for station SUN6 for GPS (L1CL2W) and Galileo (L1XL5X) with color coded carrier phase residuals

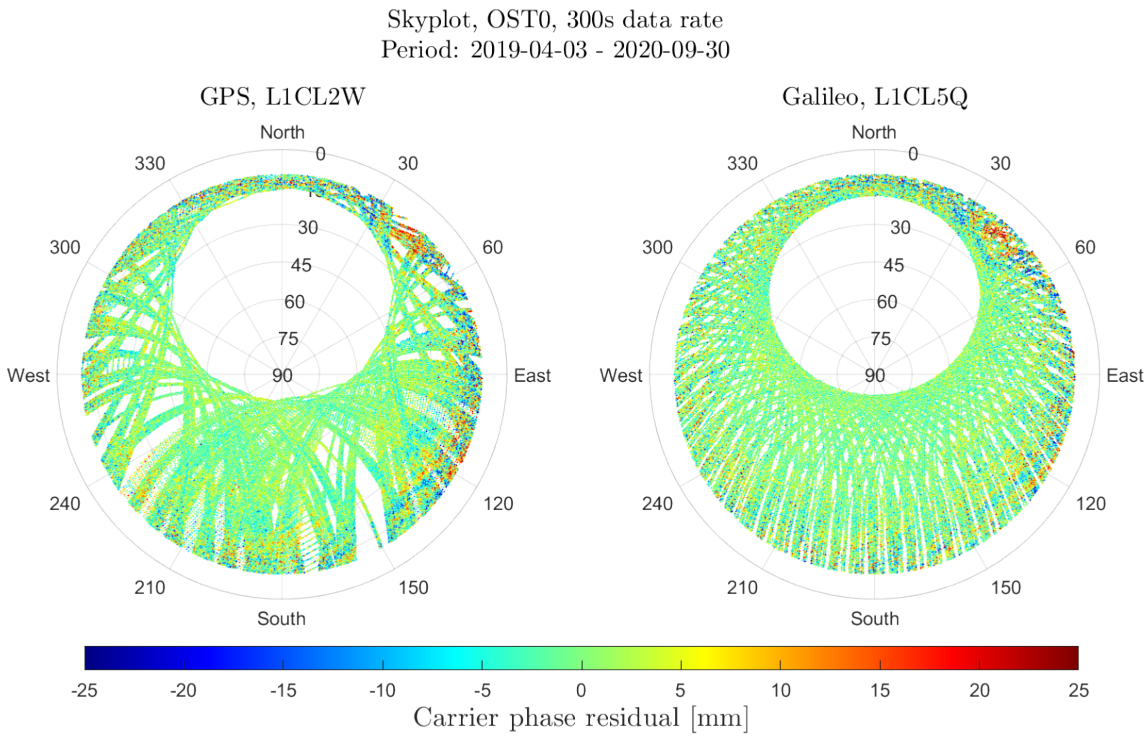

Figure A.29: Skyplot for station OST0 for GPS (L1CL2W) and Galileo (L1CL5Q) with color coded carrier phase residuals

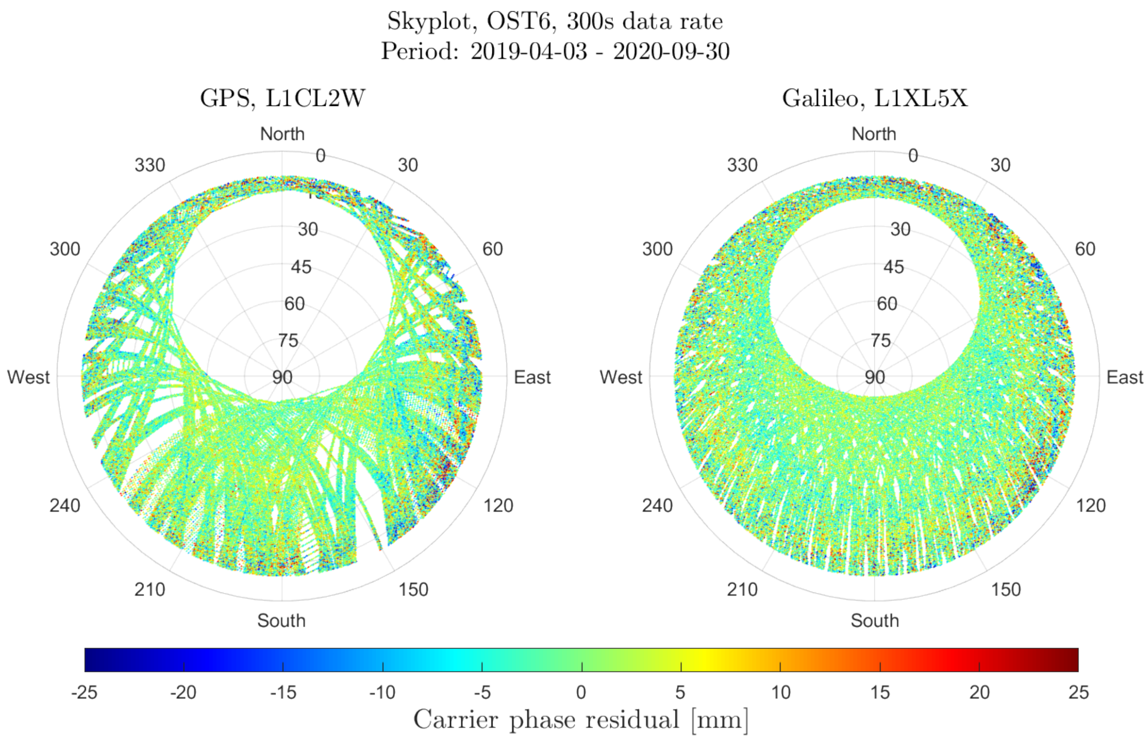

Figure A.30: Skyplot for station OST6 for GPS (L1CL2W) and Galileo (L1XL5X) with color coded carrier phase residuals

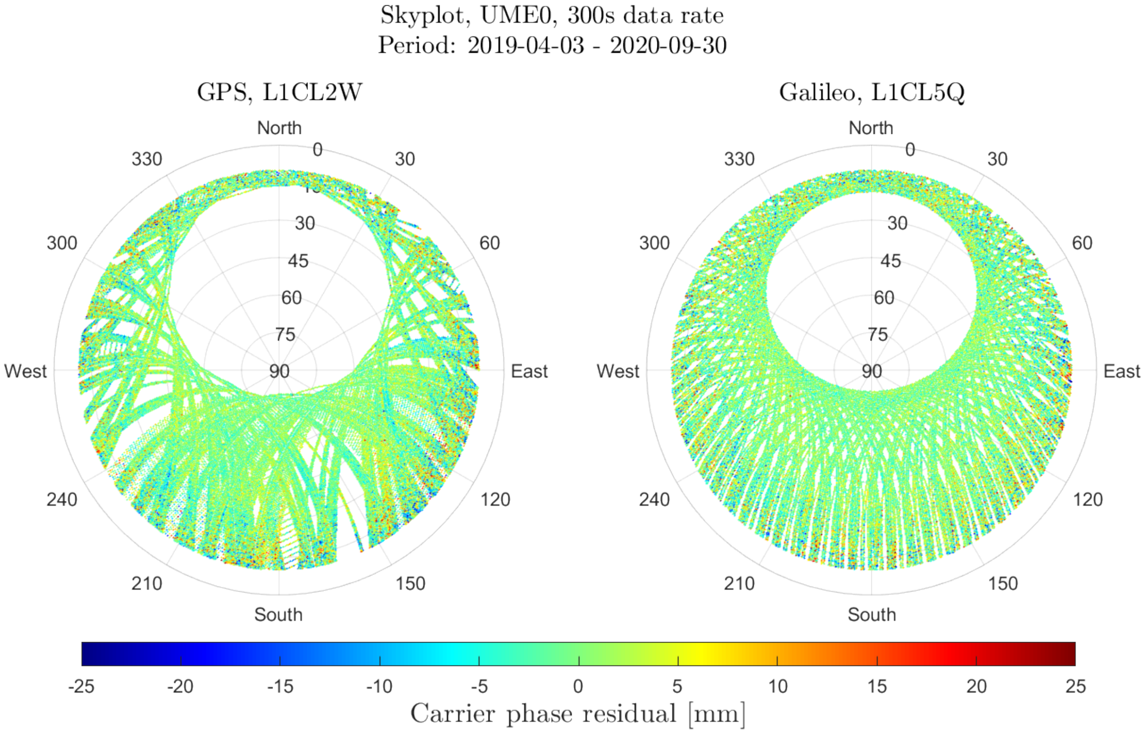

Figure A.31: Skyplot for station UME0 for GPS (L1CL2W) and Galileo (L1CL5Q) with color coded carrier phase residuals

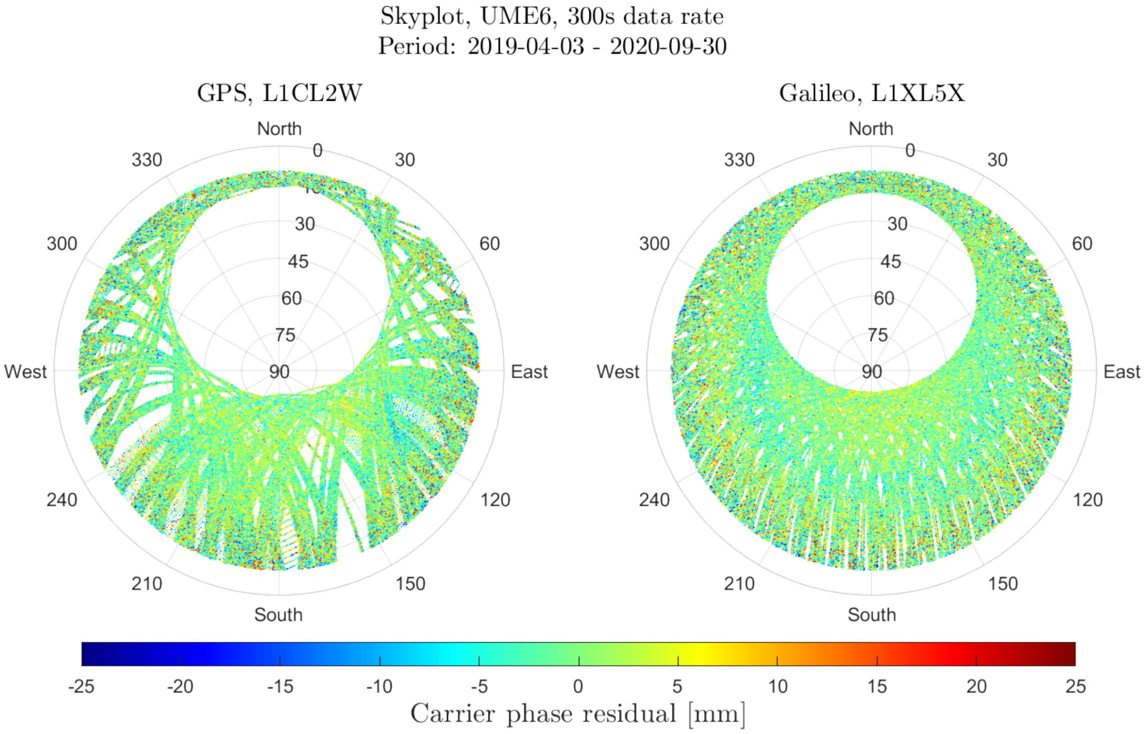

Figure A.32: Skyplot for station UME6 for GPS (L1CL2W) and Galileo (L1XL5X) with color coded carrier phase residuals

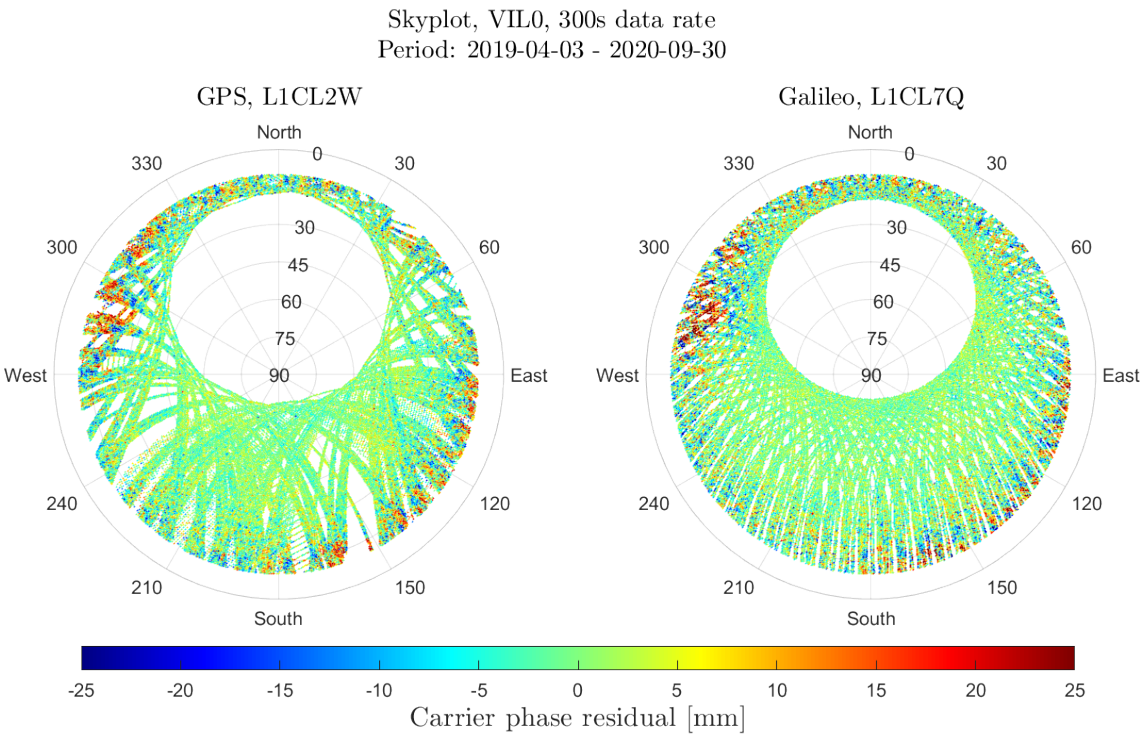

Figure A.33: Skyplot for station VIL0 for GPS (L1CL2W) and Galileo (L1CL7Q) with color coded carrier phase residuals

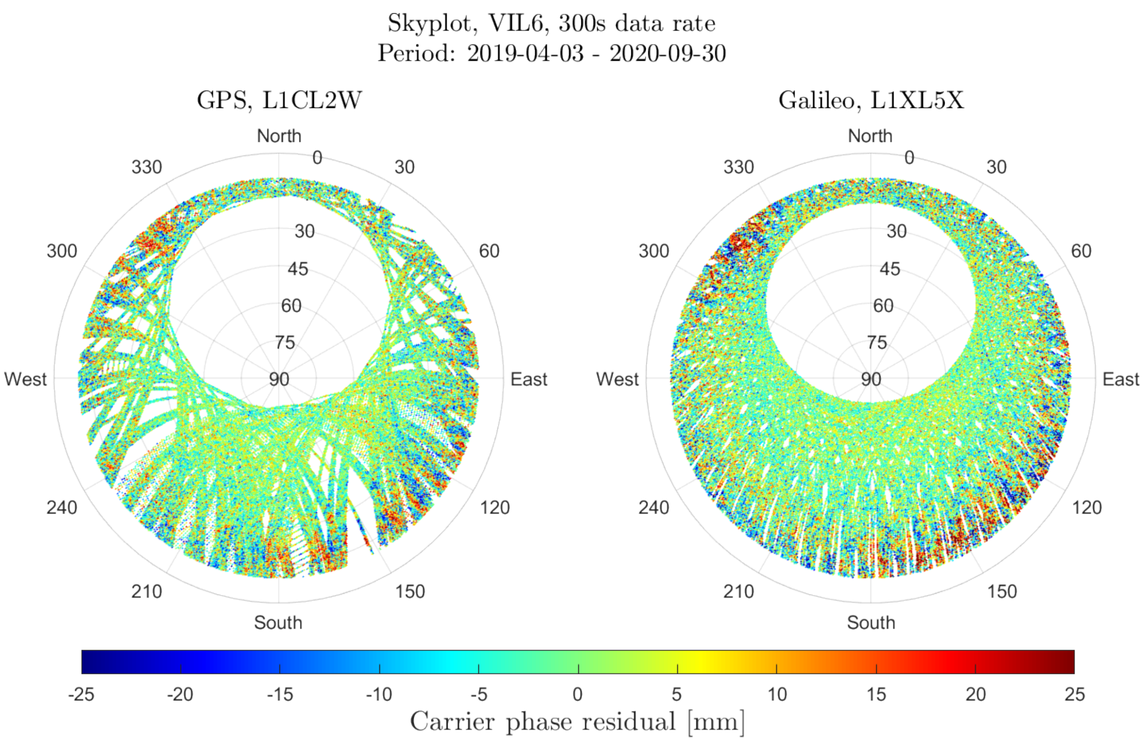

Figure A.34: Skyplot for station VIL6 for GPS (L1CL2W) and Galileo (L1XL5X) with color coded carrier phase residuals

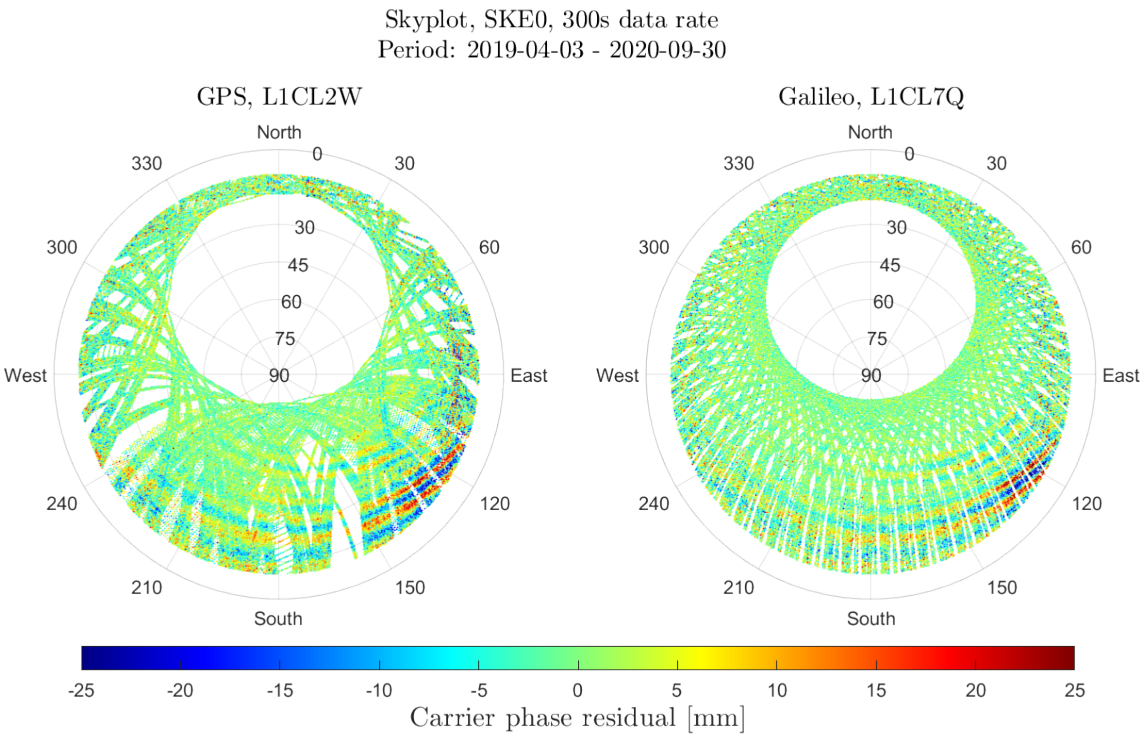

Figure A.35: Skyplot for station SKE0 for GPS (L1CL2W) and Galileo (L1CL7Q) with color coded carrier phase residuals

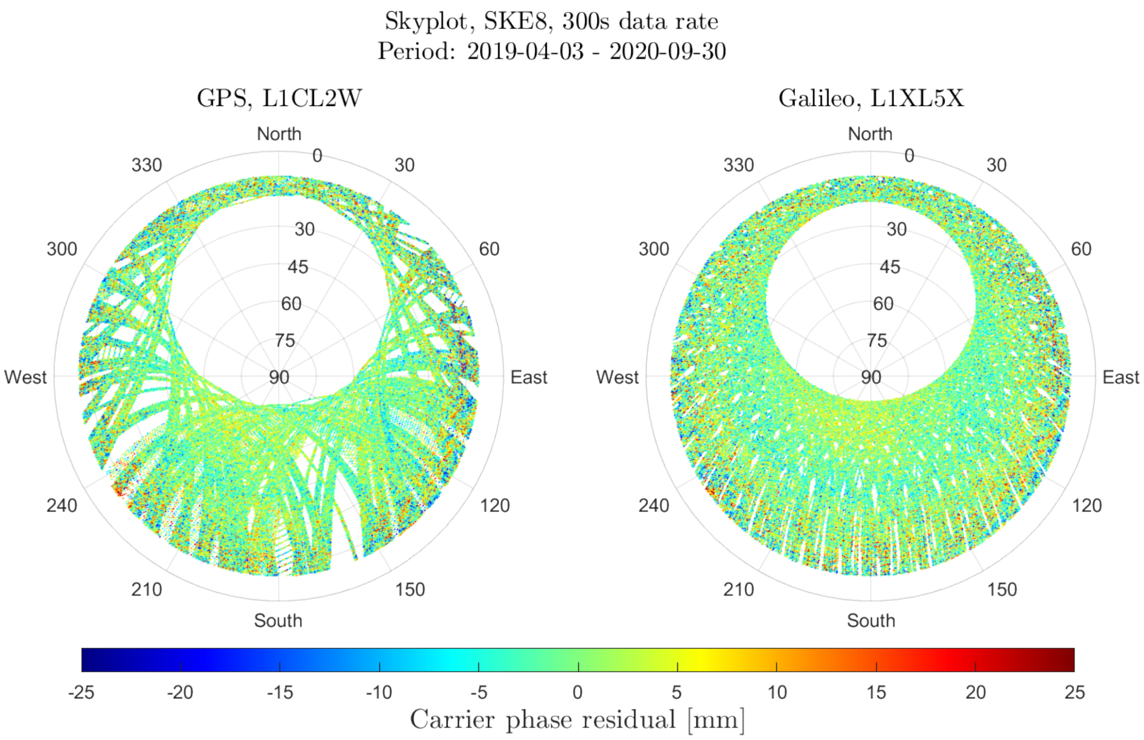

Figure A.36: Skyplot for station SKE8 for GPS (L1CL2W) and Galileo (L1XL5X) with color coded carrier phase residuals

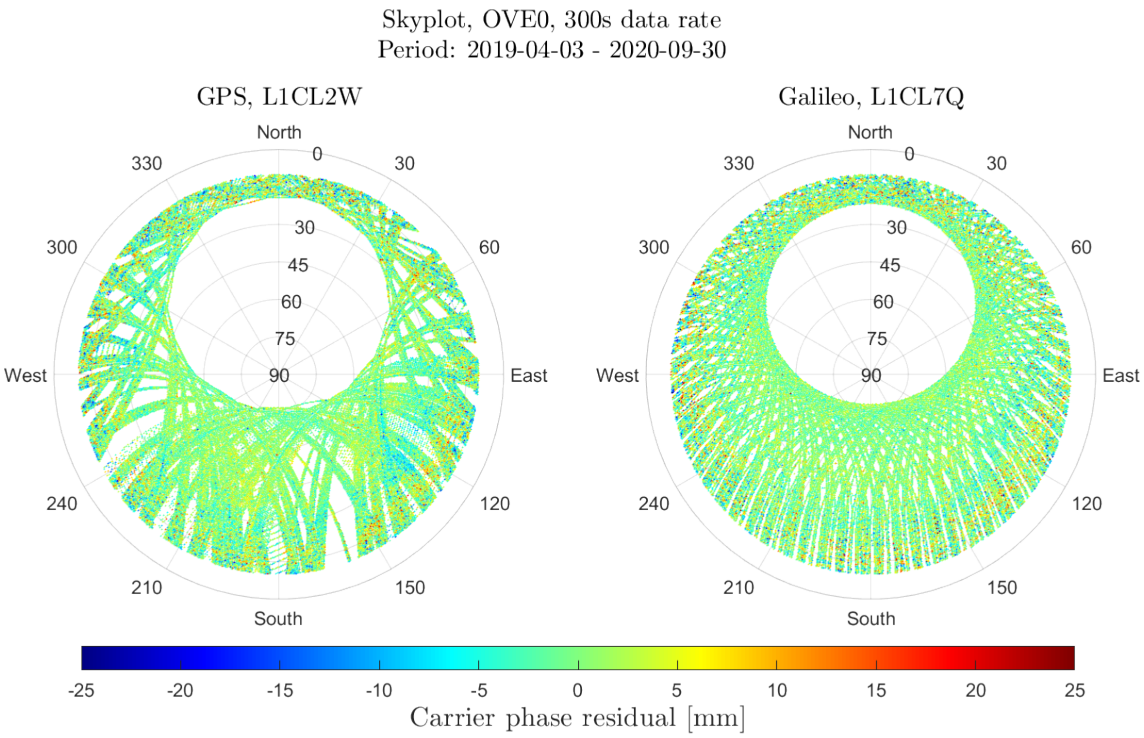

Figure A.37: Skyplot for station OVE0 for GPS (L1CL2W) and Galileo (L1CL7Q) with color coded carrier phase residuals

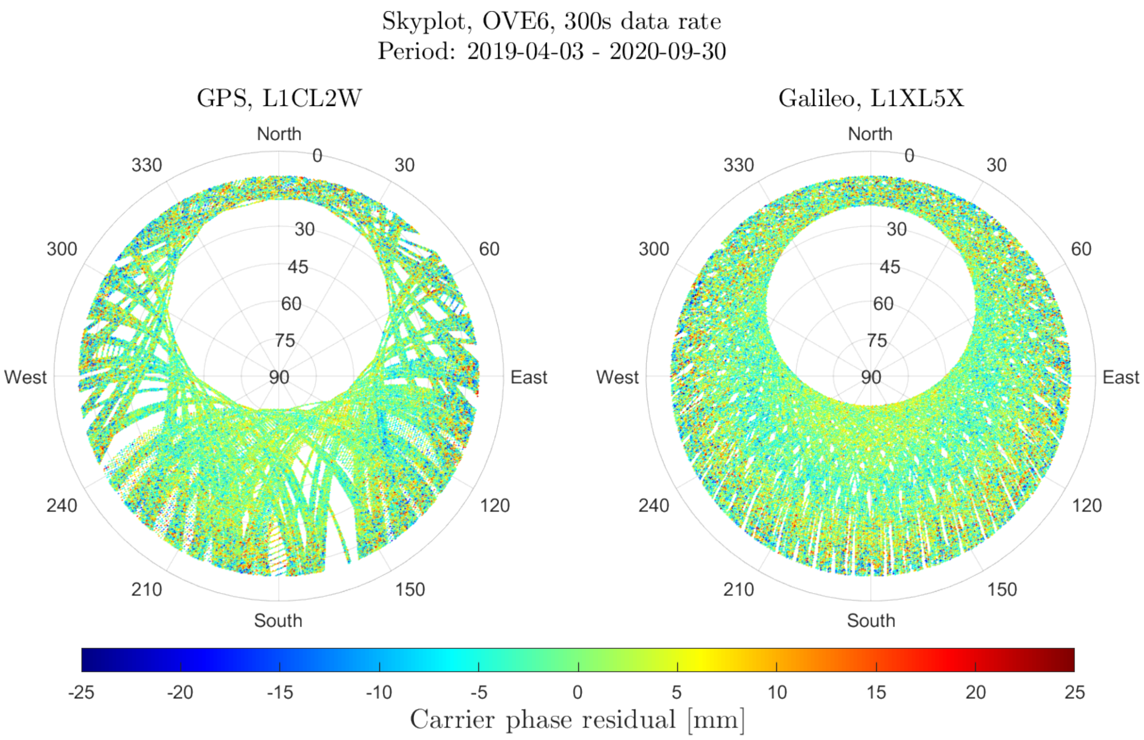

Figure A.38: Skyplot for station OVE6 for GPS (L1CL2W) and Galileo (L1XL5X) with color coded carrier phase residuals

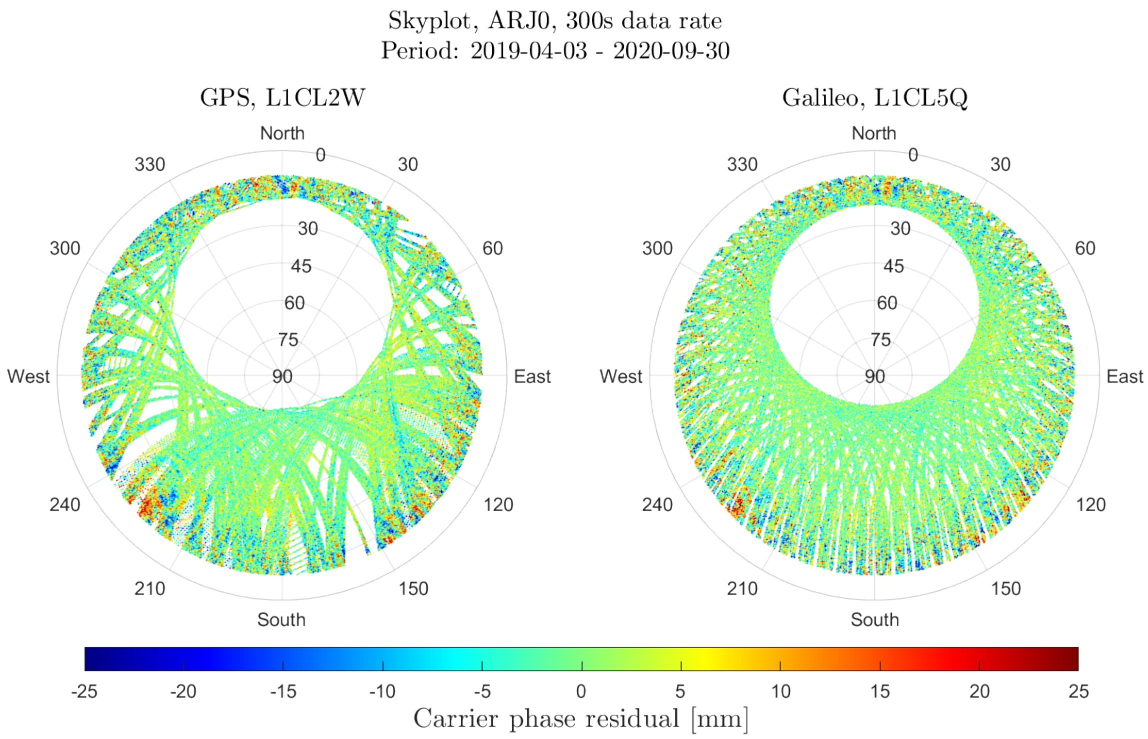

Figure A.39: Skyplot for station ARJ0 for GPS (L1CL2W) and Galileo (L1CL5Q) with color coded carrier phase residuals

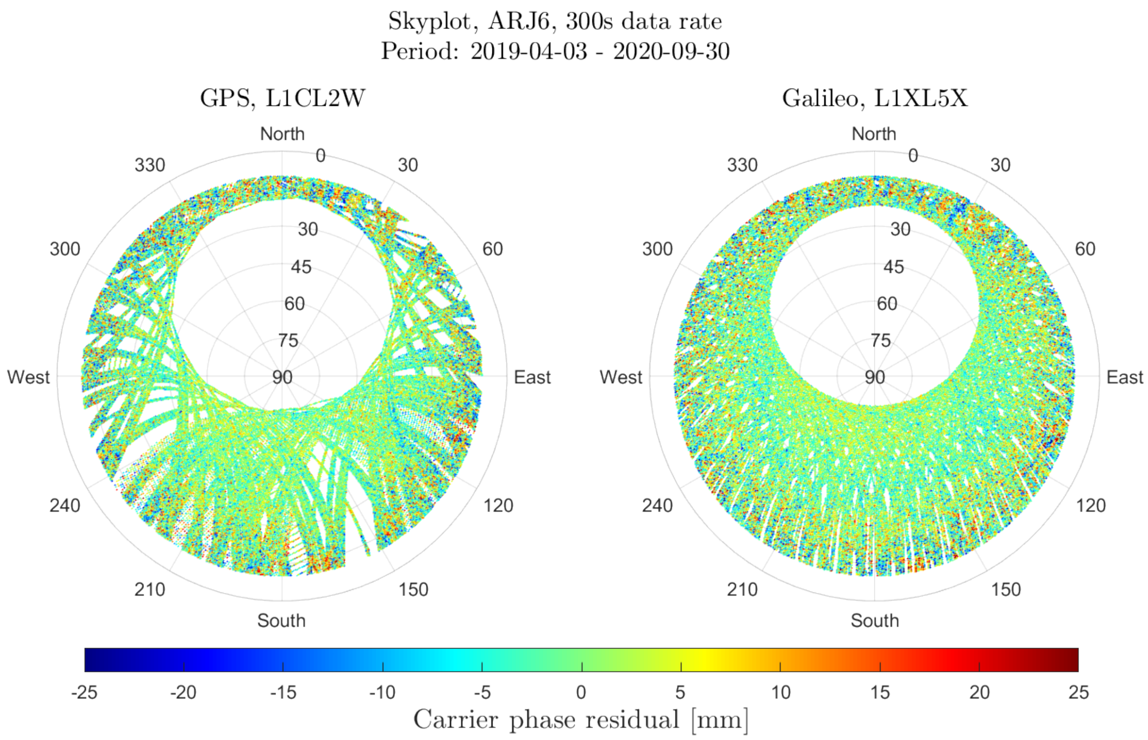

Figure A.40: Skyplot for station ARJ6 for GPS (L1CL2W) and Galileo (L1XL5X) with color coded carrier phase residuals

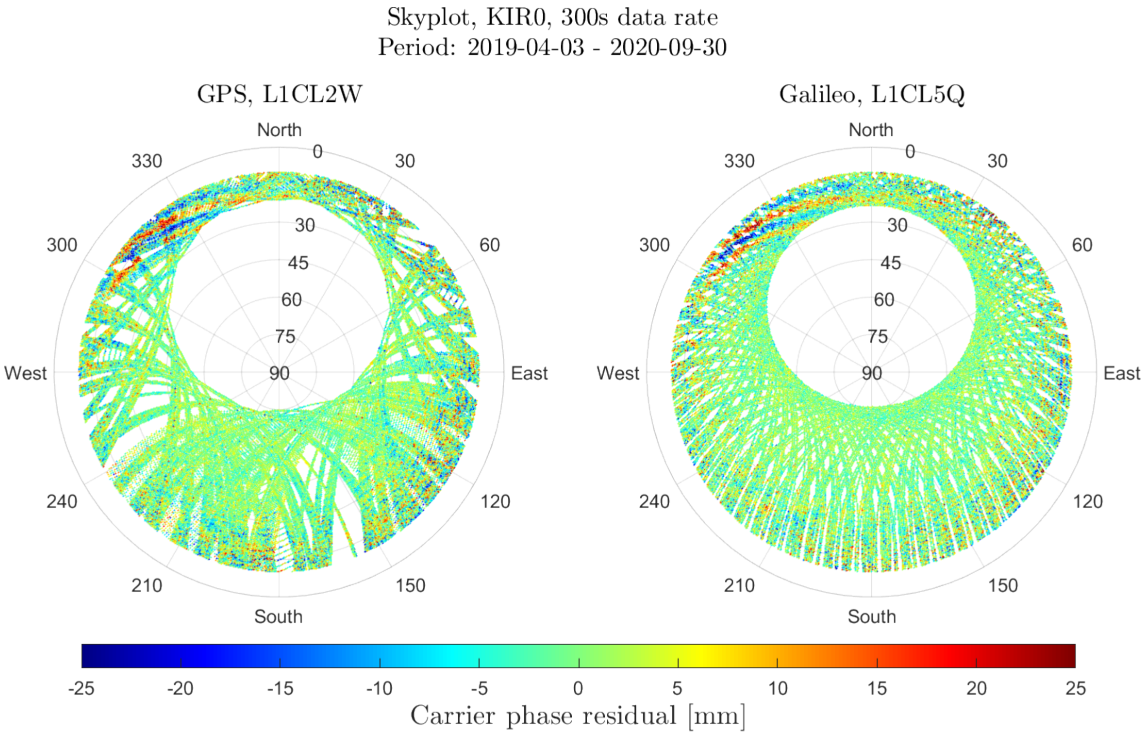

Figure A.41: Skyplot for station KIR0 for GPS (L1CL2W) and Galileo (L1CL5Q) with color coded carrier phase residuals

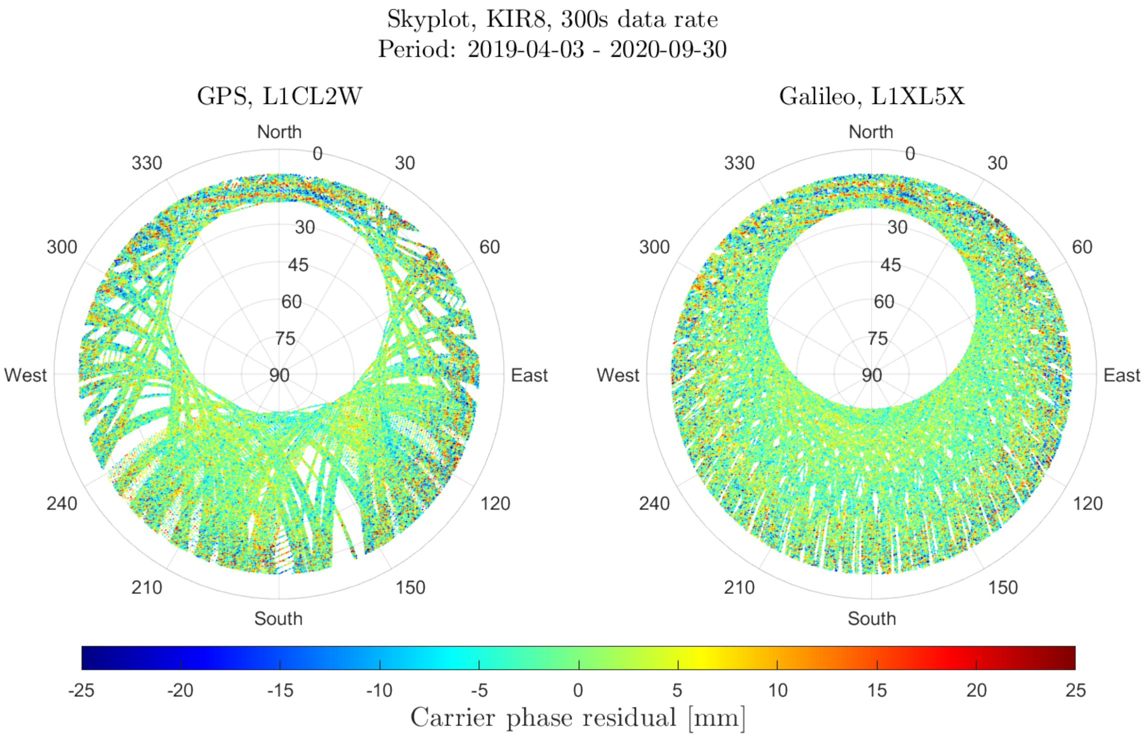

Figure A.42: Skyplot for station KIR8 for GPS (L1CL2W) and Galileo (L1XL5X) with color coded carrier phase residuals

B Monthly mean carrier phase residuals for GPS and Galileo, averaged over 1° elevation intervals for 42 SWEPOS stations

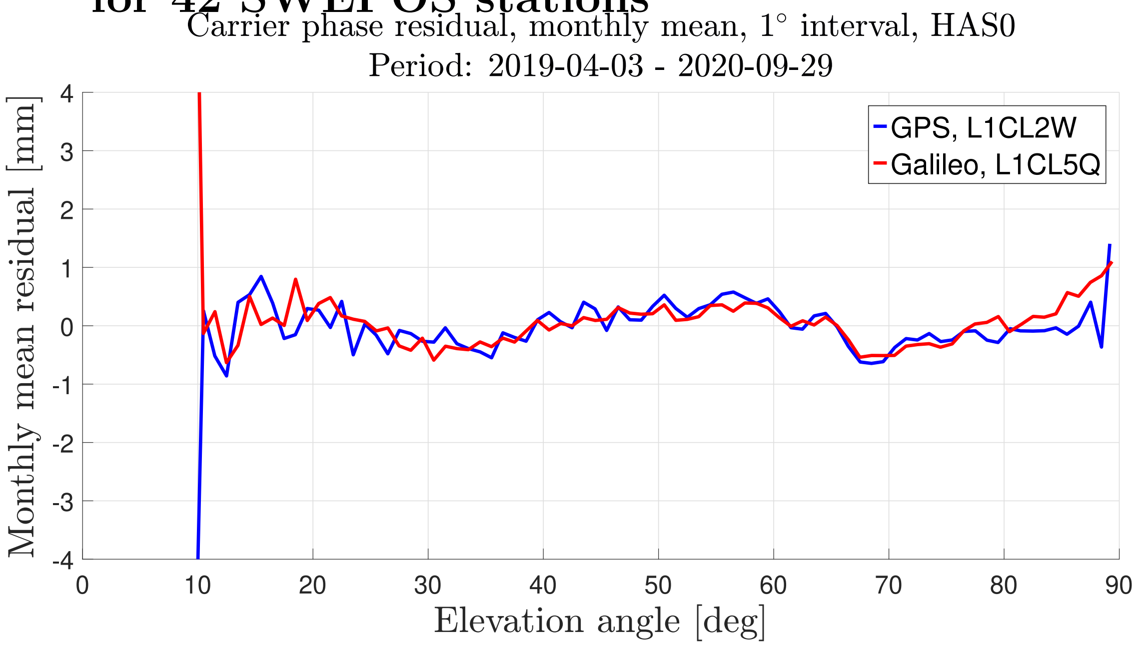

Figure B.1: Carrier phase residuals, averaged over both 1° elevation angle intervals as well as per month. Station HAS0, GPS (L1CL2W) and Galileo (L1CL5Q)

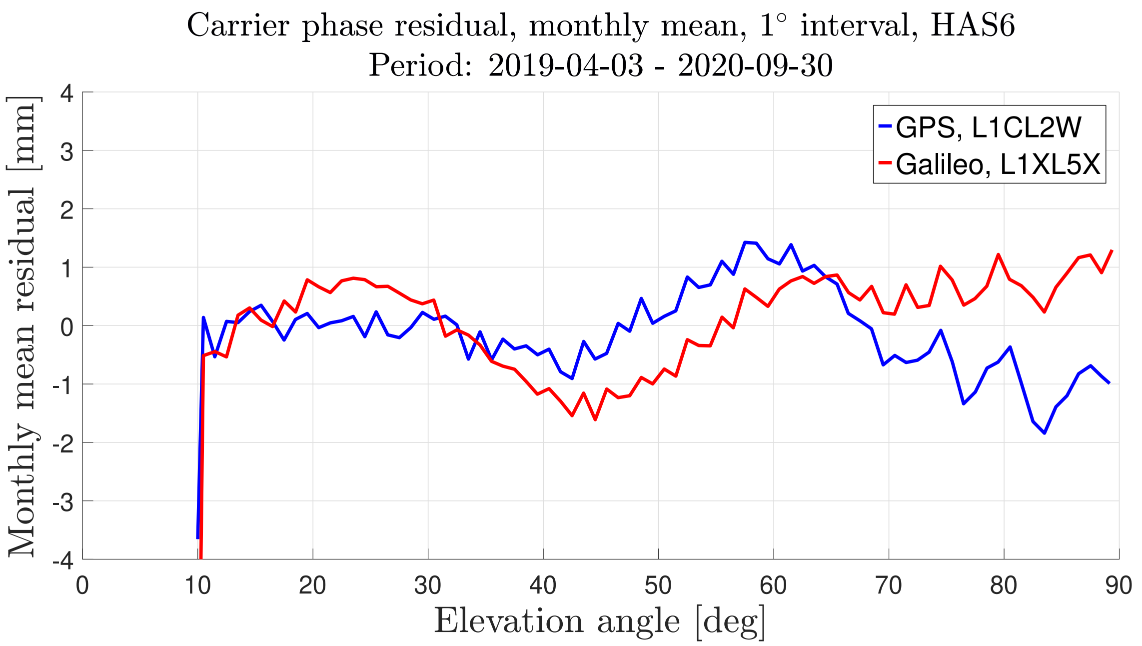

Figure B.2: Carrier phase residuals, averaged over both 1° elevation angle intervals as well as per month. Station HAS6, GPS (L1CL2W) and Galileo (L1XL5X)

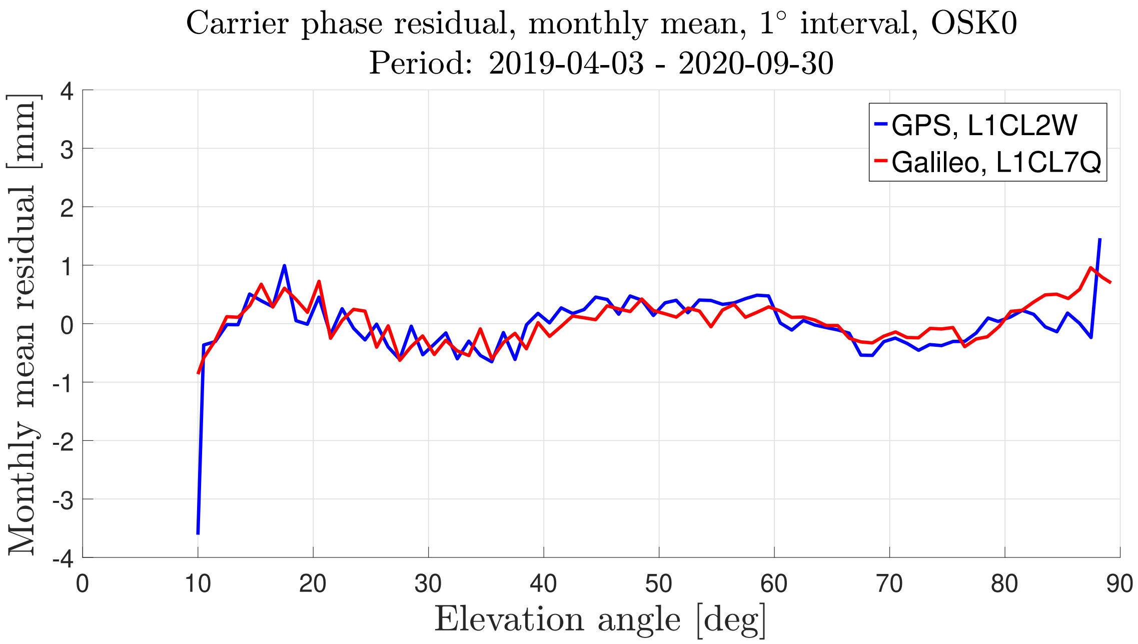

Figure B.3: Carrier phase residuals, averaged over both 1° elevation angle intervals as well as per month. Station OSK0, GPS (L1CL2W) and Galileo (L1CL7Q)

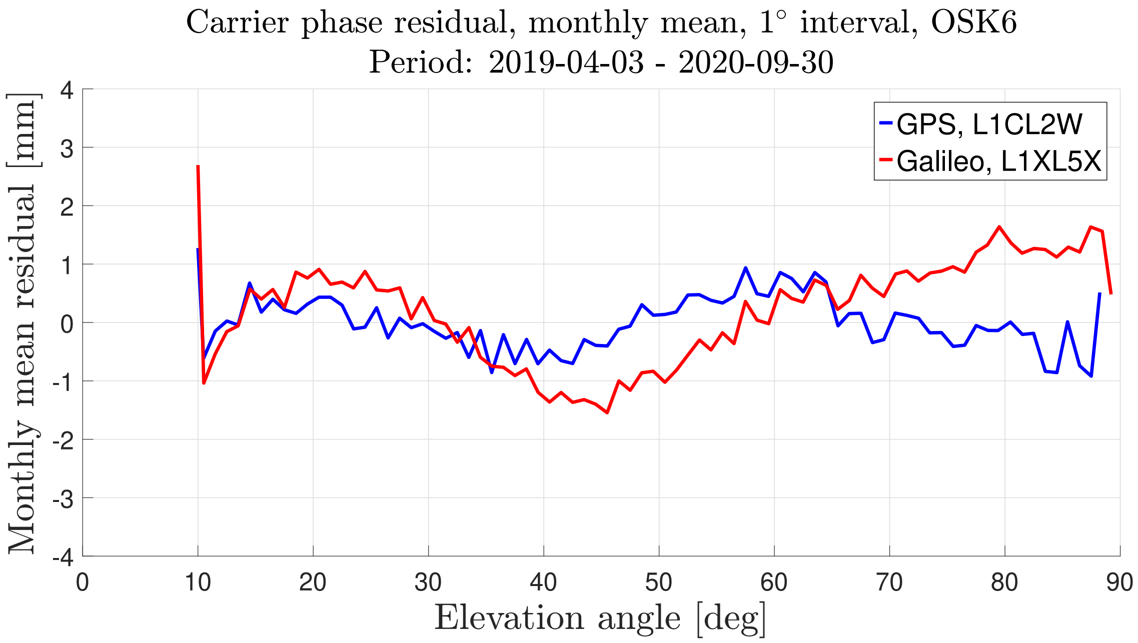

Figure B.4: Carrier phase residuals, averaged over both 1° elevation angle intervals as well as per month. Station OSK6, GPS (L1CL2W) and Galileo (L1XL5X)

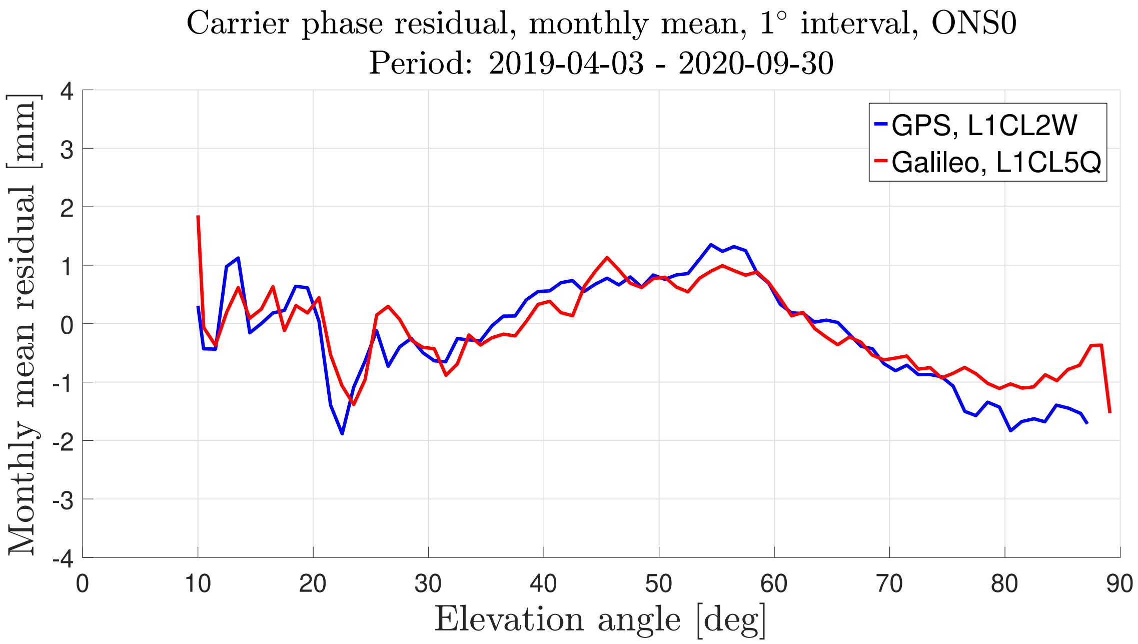

Figure B.5: Carrier phase residuals, averaged over both 1° elevation angle intervals as well as per month. Station ONS0, GPS (L1CL2W) and Galileo (L1CL5Q)

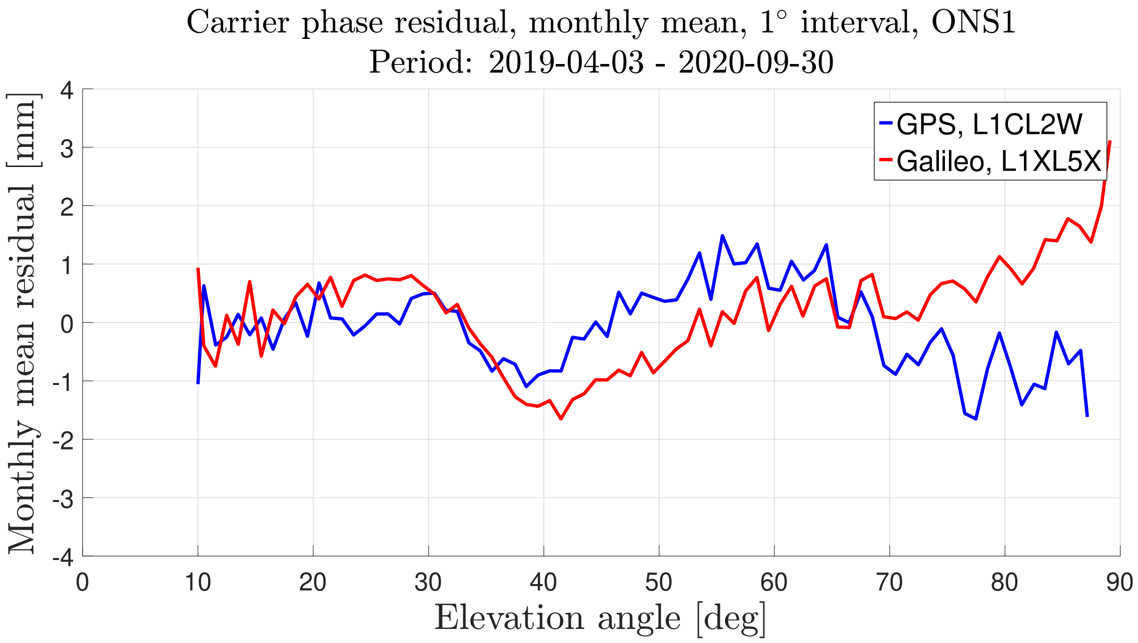

Figure B.6: Carrier phase residuals, averaged over both 1° elevation angle intervals as well as per month. Station ONS1, GPS (L1CL2W) and Galileo (L1XL5X)

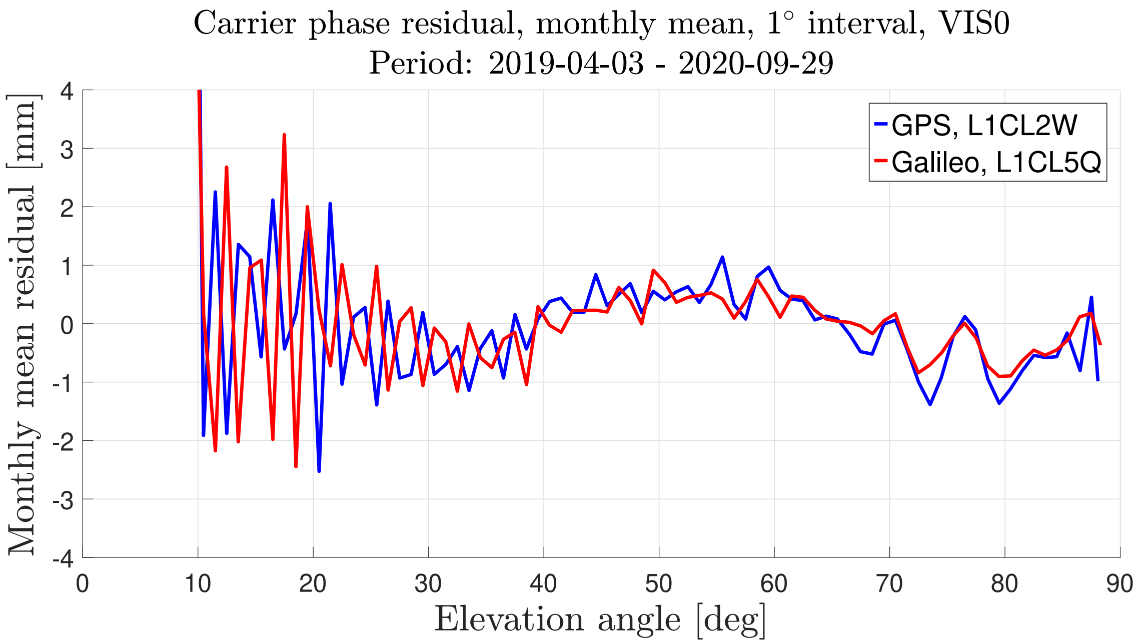

Figure B.7: Carrier phase residuals, averaged over both 1° elevation angle intervals as well as per month. Station VIS0, GPS (L1CL2W) and Galileo (L1CL5Q)

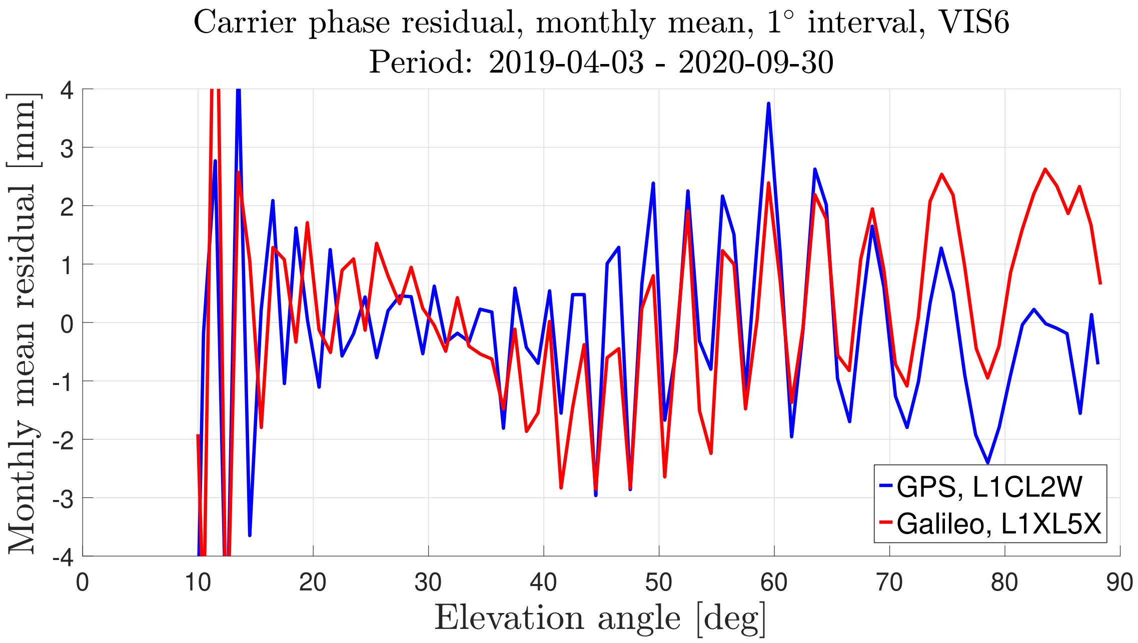

Figure B.8: Carrier phase residuals, averaged over both 1° elevation angle intervals as well as per month. Station VIS6, GPS (L1CL2W) and Galileo (L1XL5X)

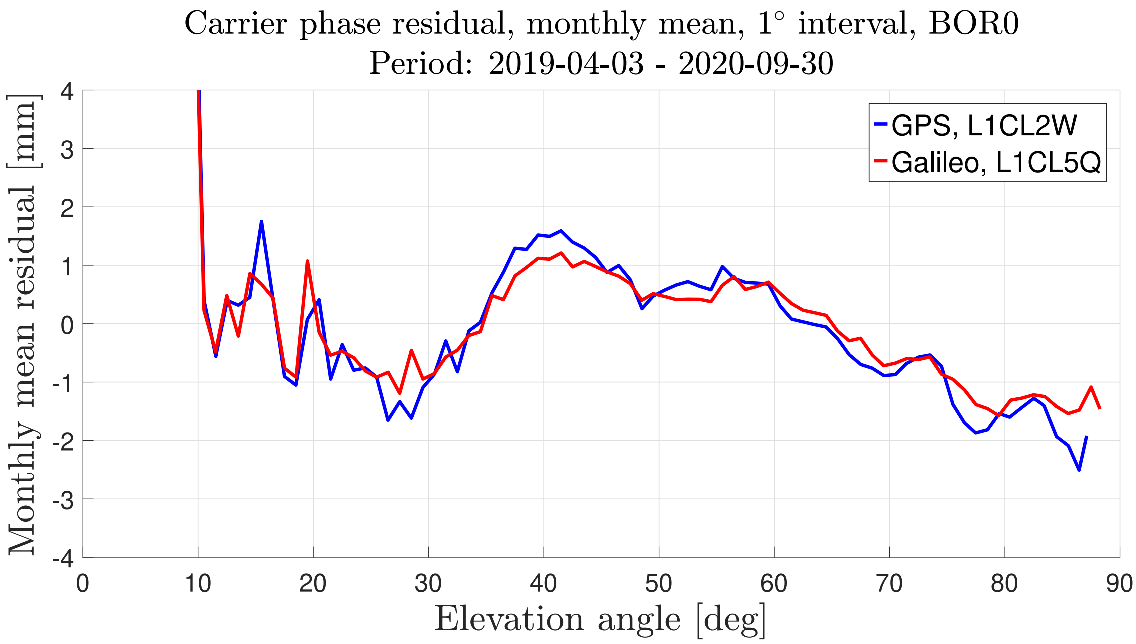

Figure B.9: Carrier phase residuals, averaged over both 1° elevation angle intervals as well as per month. Station BOR0, GPS (L1CL2W) and Galileo (L1CL5Q)

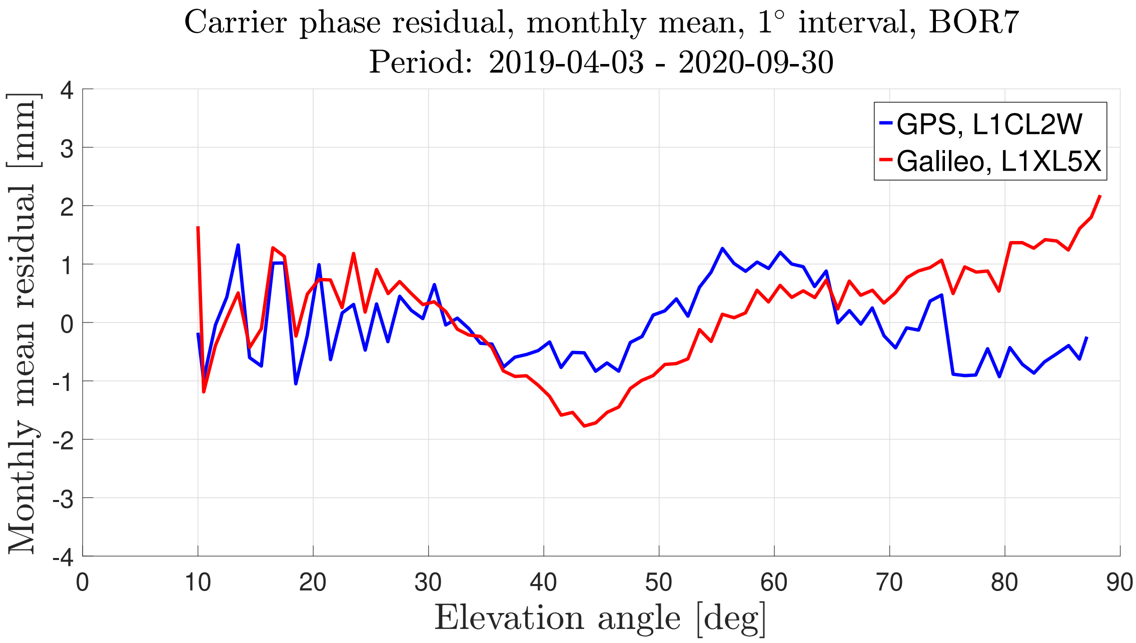

Figure B.10: Carrier phase residuals, averaged over both 1° elevation angle intervals as well as per month. Station BOR7, GPS (L1CL2W) and Galileo (L1XL5X)

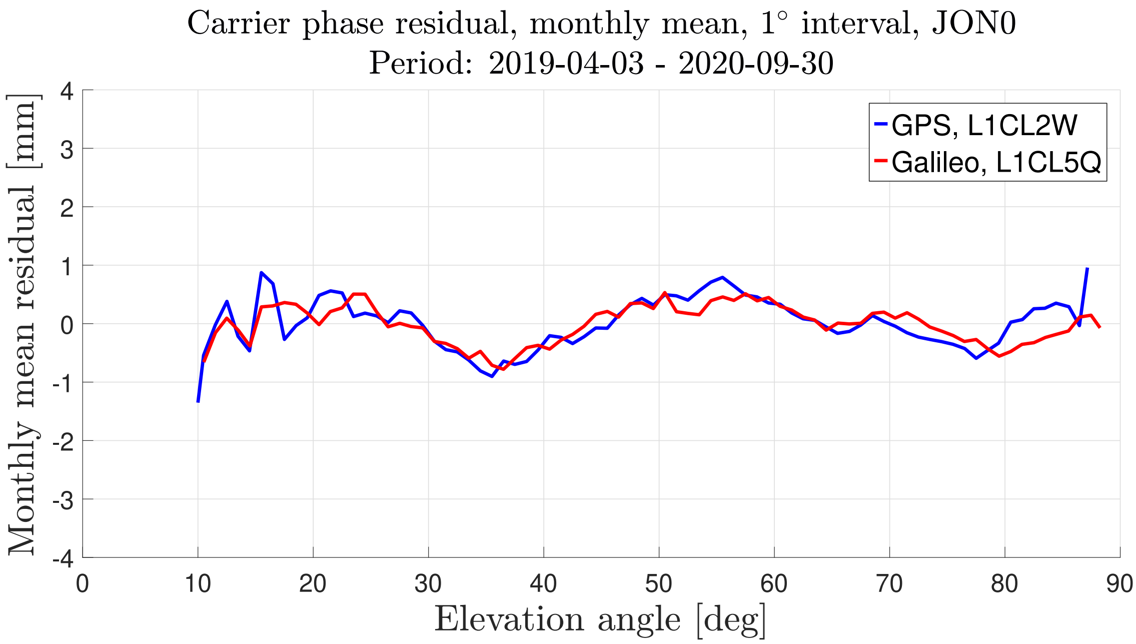

Figure B.11: Carrier phase residuals, averaged over both 1° elevation angle intervals as well as per month. Station JON0, GPS (L1CL2W) and Galileo (L1CL5Q)

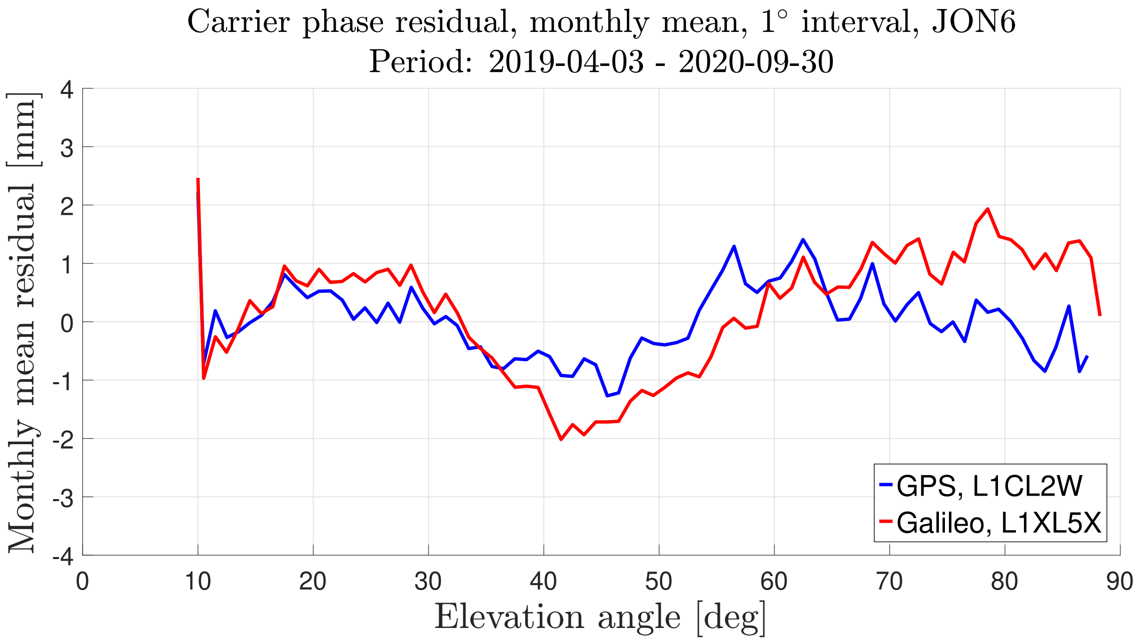

Figure B.12: Carrier phase residuals, averaged over both 1° elevation angle intervals as well as per month. Station JON6, GPS (L1CL2W) and Galileo (L1XL5X)

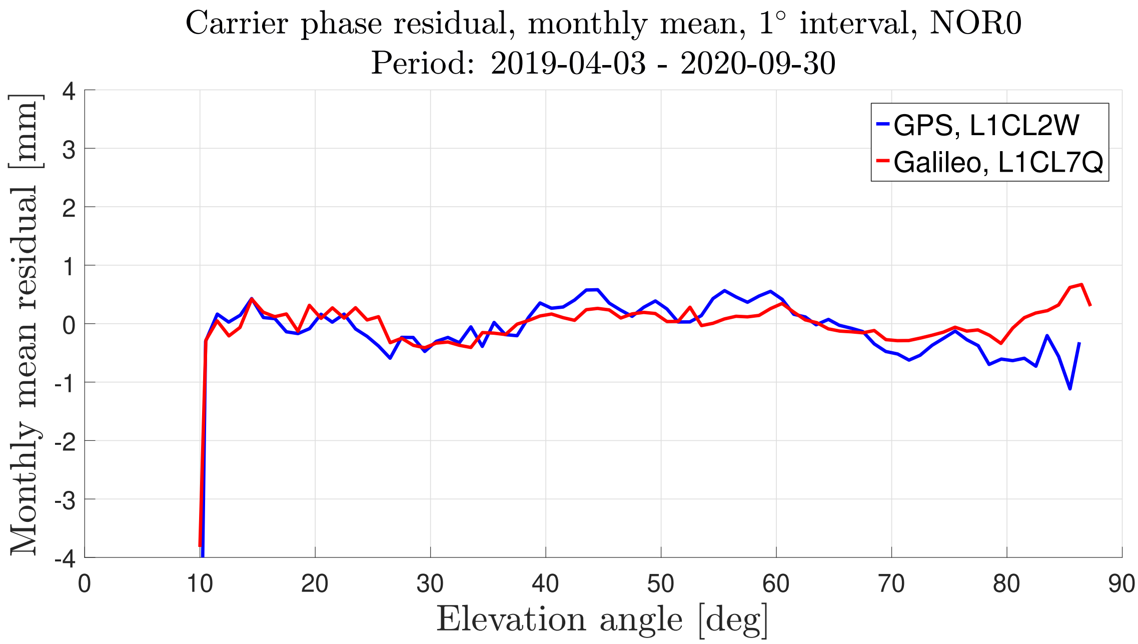

Figure B.13: Carrier phase residuals, averaged over both 1° elevation angle intervals as well as per month. Station NOR0, GPS (L1CL2W) and Galileo (L1CL7Q)

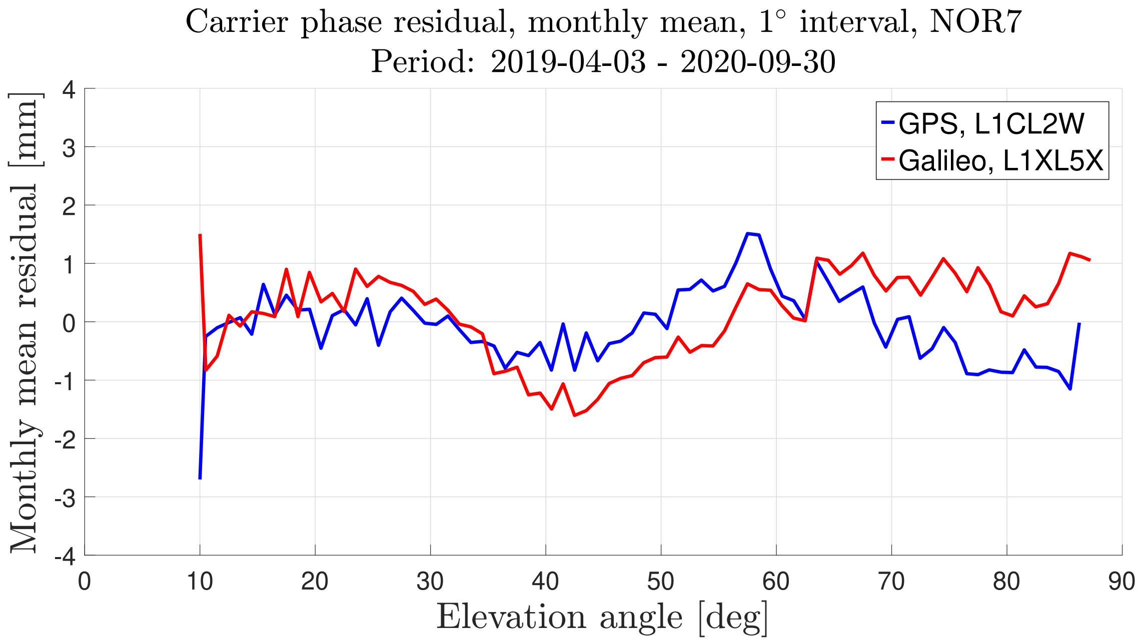

Figure B.14: Carrier phase residuals, averaged over both 1° elevation angle intervals as well as per month. Station NOR7, GPS (L1CL2W) and Galileo (L1XL5X)

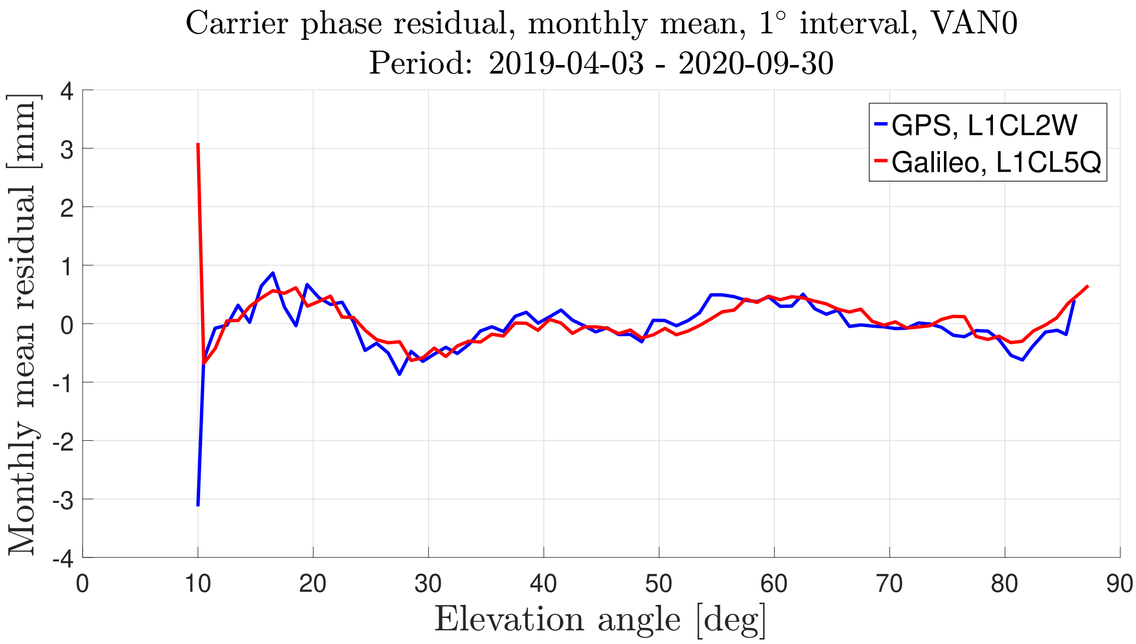

Figure B.15: Carrier phase residuals, averaged over both 1° elevation angle intervals as well as per month. Station VAN0, GPS (L1CL2W) and Galileo (L1CL5Q)

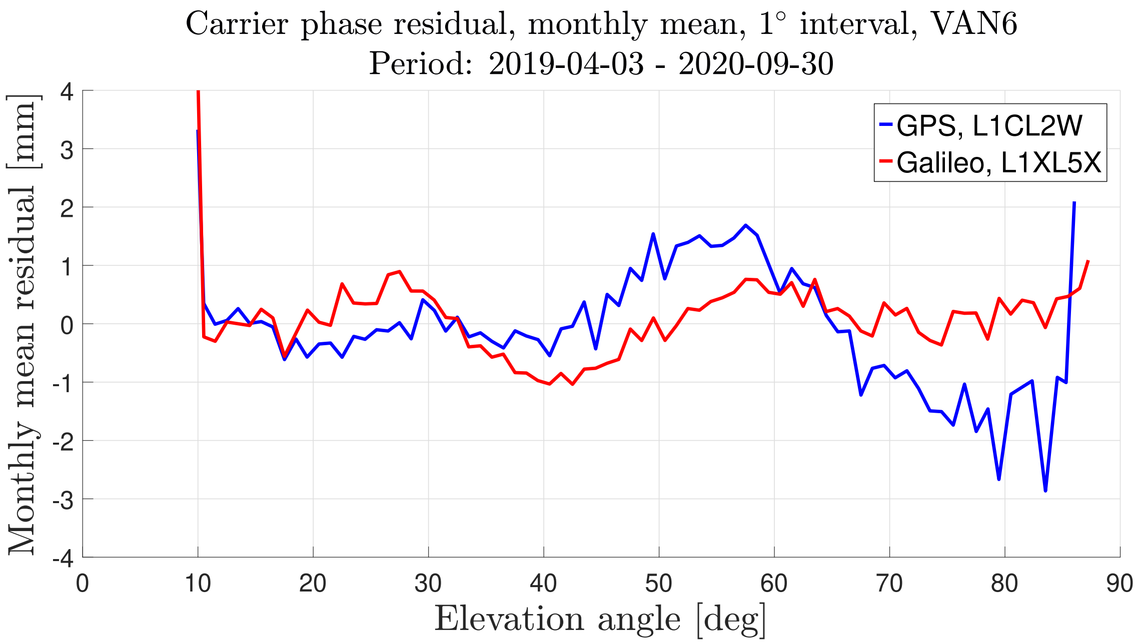

Figure B.16: Carrier phase residuals, averaged over both 1° elevation angle intervals as well as per month. Station VAN6, GPS (L1CL2W) and Galileo (L1XL5X)

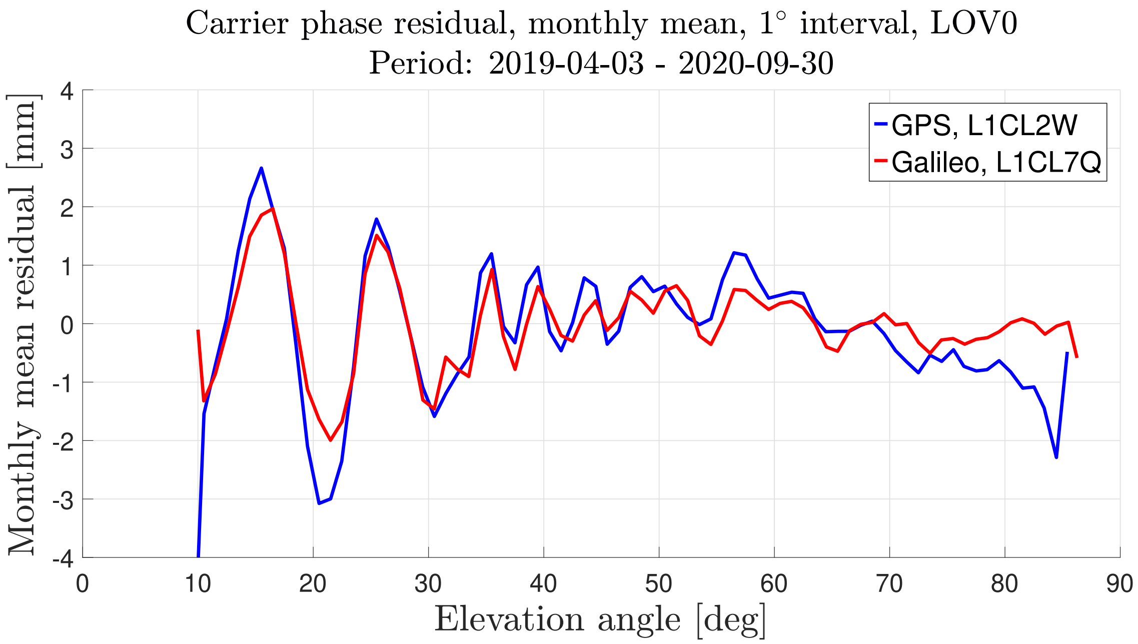

Figure B.17: Carrier phase residuals, averaged over both 1° elevation angle intervals as well as per month. Station LOV0, GPS (L1CL2W) and Galileo (L1CL7Q)

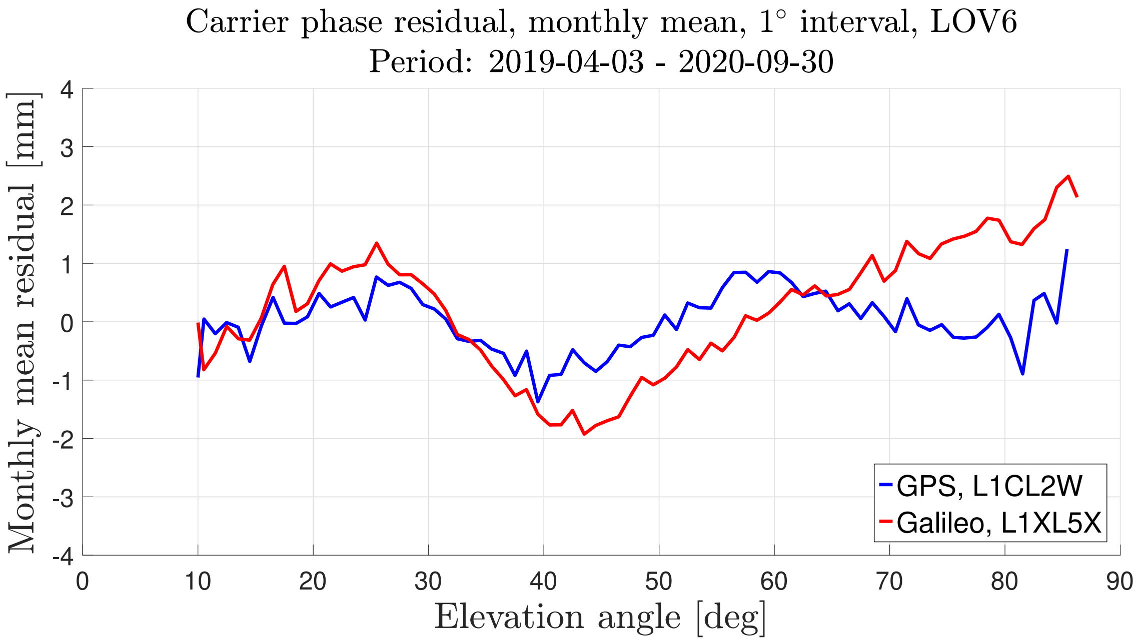

Figure B.18: Carrier phase residuals, averaged over both 1° elevation angle intervals as well as per month. Station LOV6, GPS (L1CL2W) and Galileo (L1XL5X)

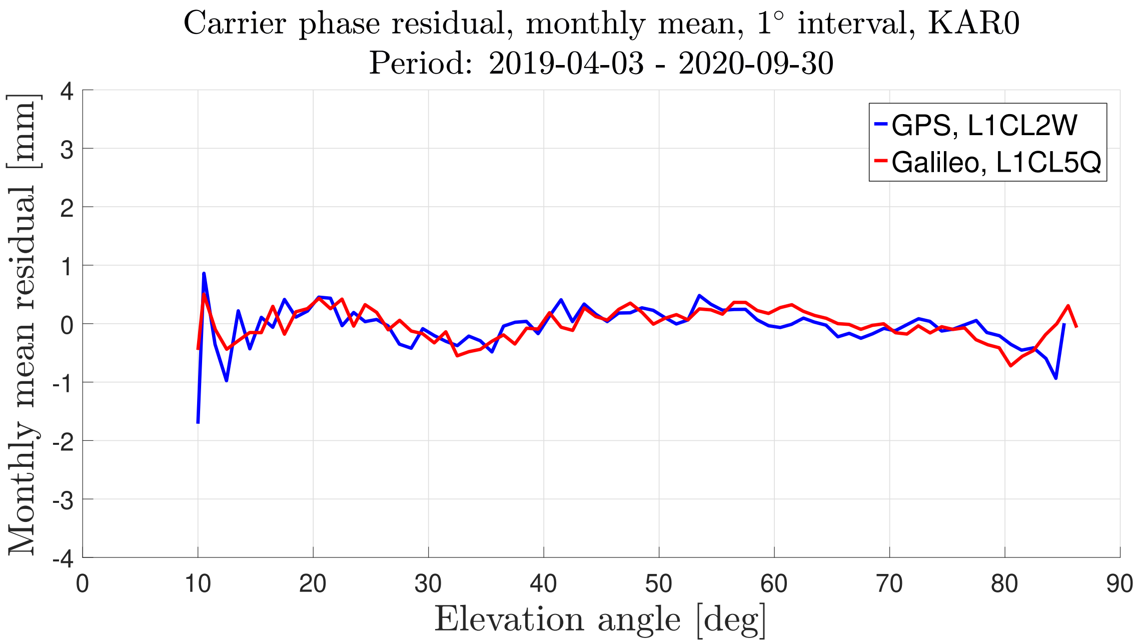

Figure B.19: Carrier phase residuals, averaged over both 1° elevation angle intervals as well as per month. Station KAR0, GPS (L1CL2W) and Galileo (L1CL5Q)

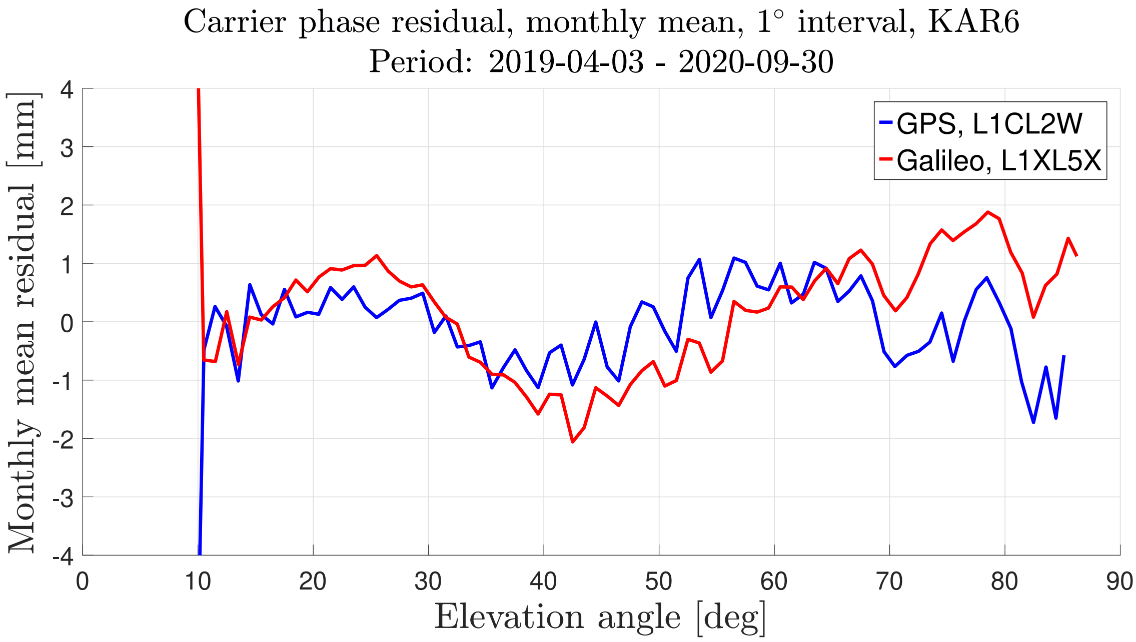

Figure B.20: Carrier phase residuals, averaged over both 1° elevation angle intervals as well as per month. Station KAR6, GPS (L1CL2W) and Galileo (L1XL5X)

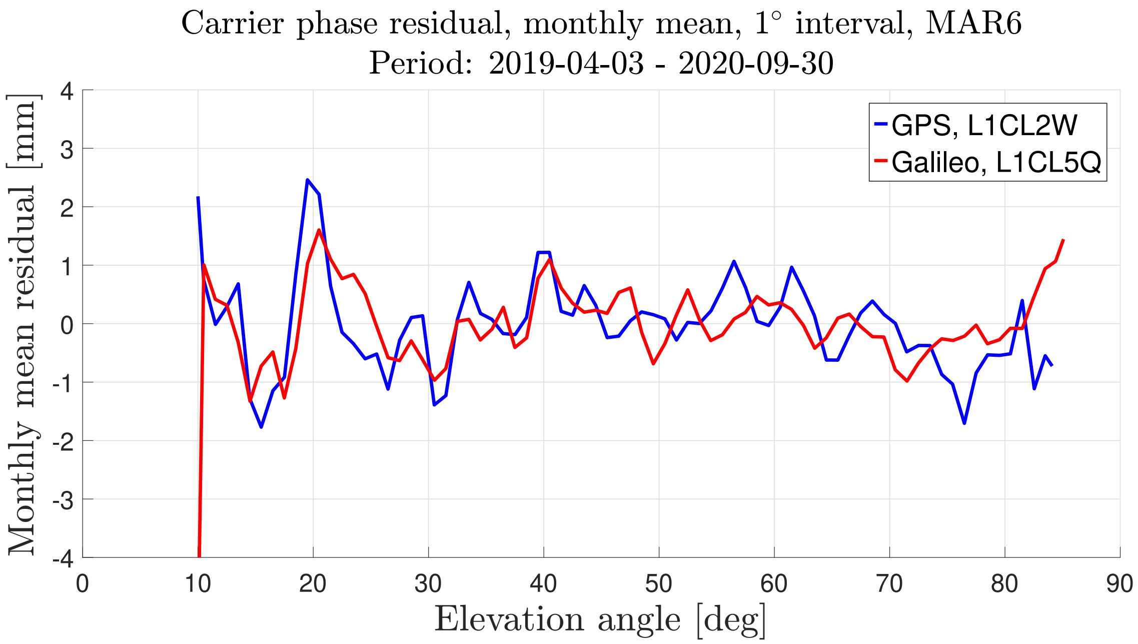

Figure B.21: Carrier phase residuals, averaged over both 1° elevation angle intervals as well as per month. Station MAR6, GPS (L1CL2W) and Galileo (L1CL5Q)

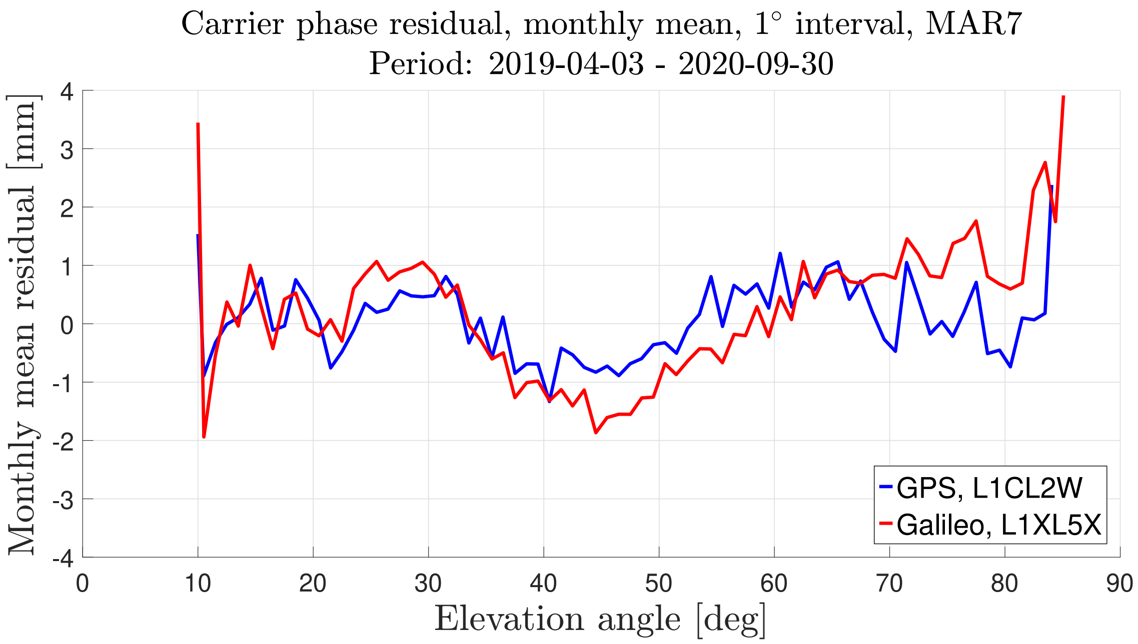

Figure B.22: Carrier phase residuals, averaged over both 1° elevation angle intervals as well as per month. Station MAR7, GPS (L1CL2W) and Galileo (L1XL5X)

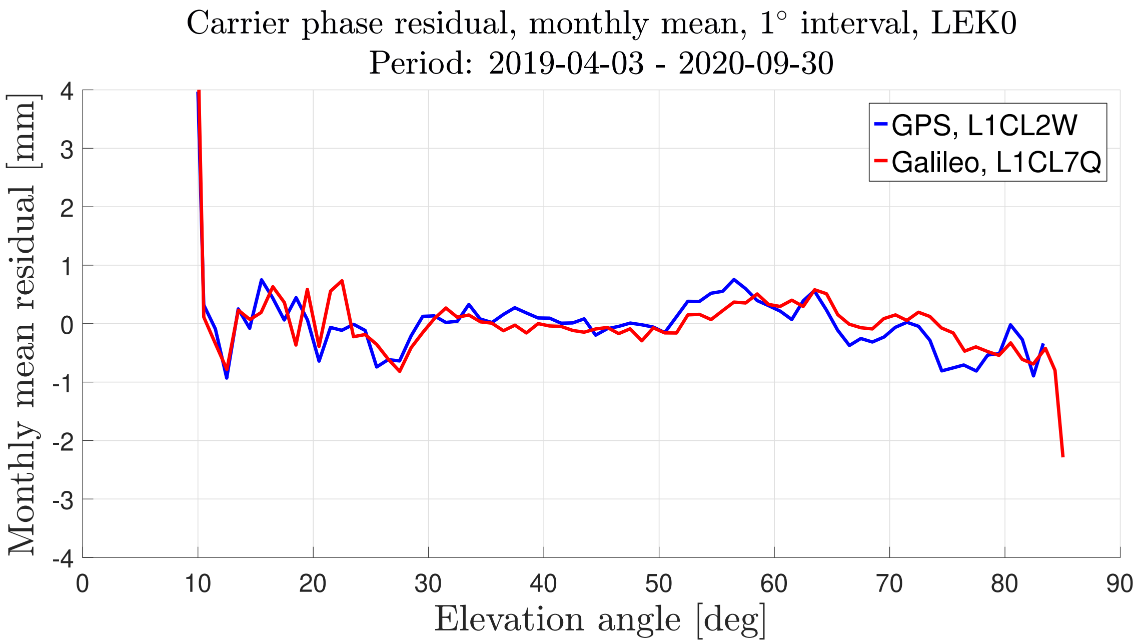

Figure B.23: Carrier phase residuals, averaged over both 1° elevation angle intervals as well as per month. Station LEK0, GPS (L1CL2W) and Galileo (L1CL7Q)

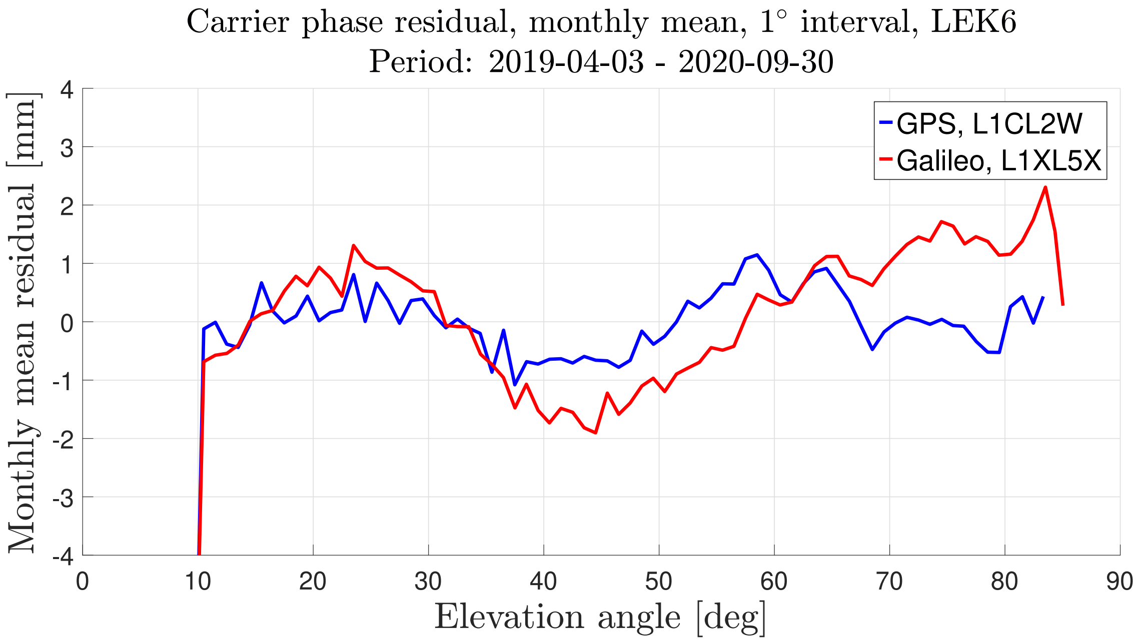

Figure B.24: Carrier phase residuals, averaged over both 1° elevation angle intervals as well as per month. Station LEK6, GPS (L1CL2W) and Galileo (L1XL5X)

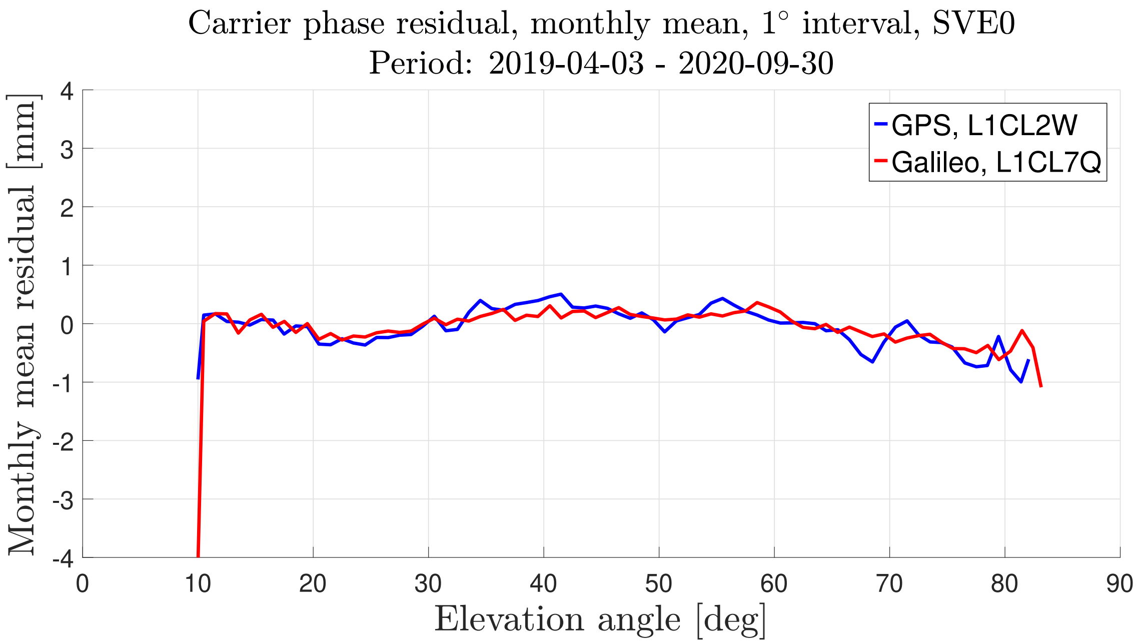

Figure B.25: Carrier phase residuals, averaged over both 1° elevation angle intervals as well as per month. Station SVE0, GPS (L1CL2W) and Galileo (L1CL7Q)

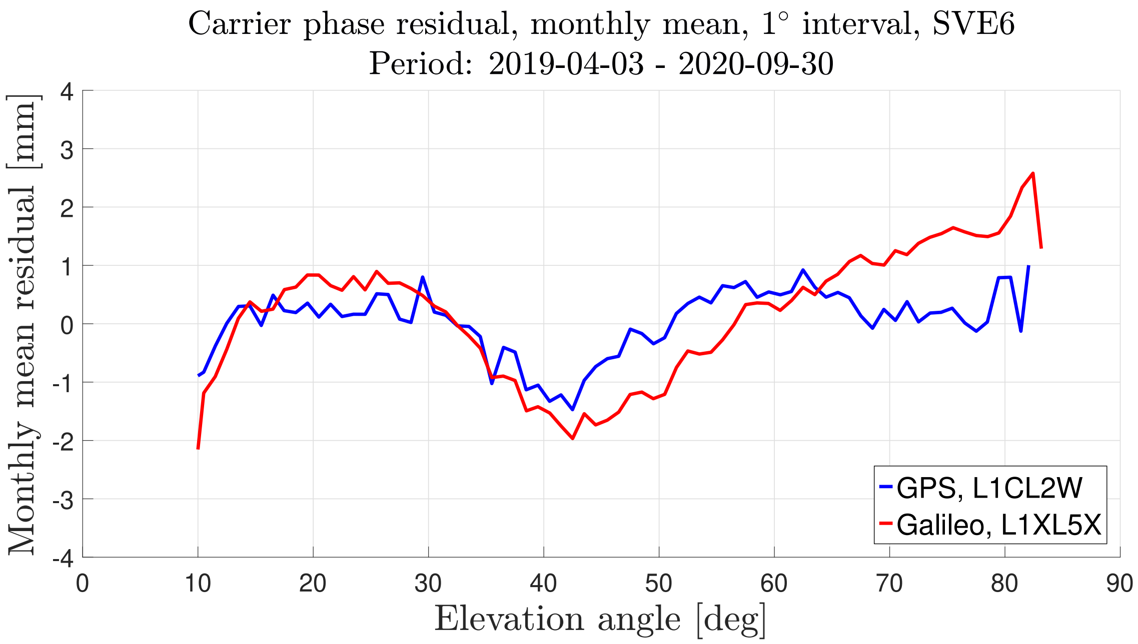

Figure B.26: Carrier phase residuals, averaged over both 1° elevation angle intervals as well as per month. Station SVE6, GPS (L1CL2W) and Galileo (L1XL5X)

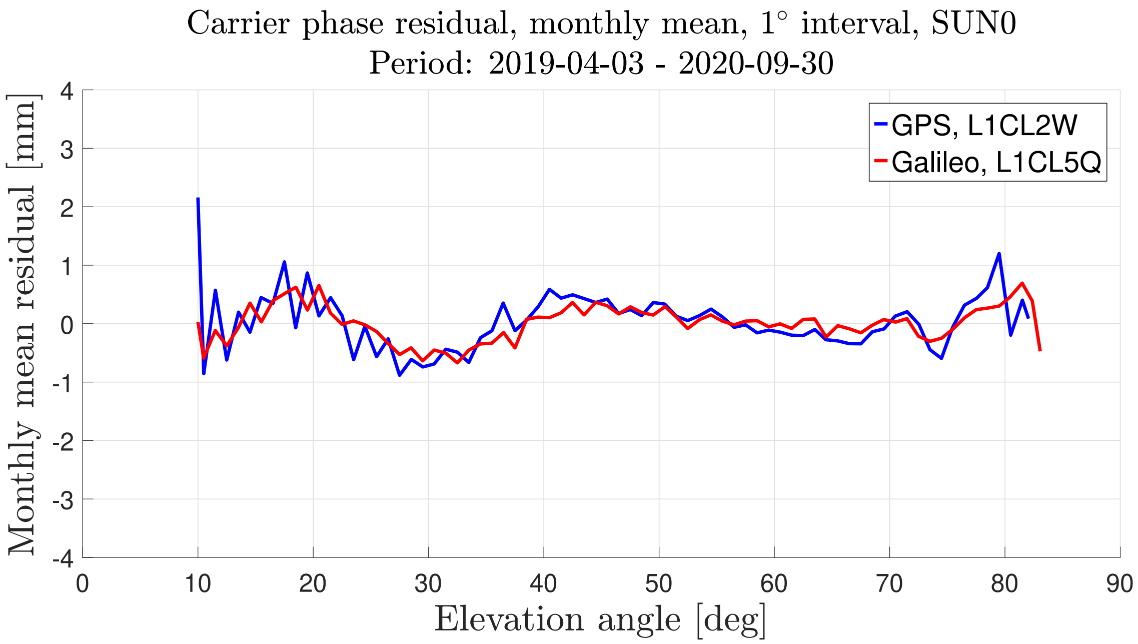

Figure B.27: Carrier phase residuals, averaged over both 1° elevation angle intervals as well as per month. Station SUN0, GPS (L1CL2W) and Galileo (L1CL5Q)

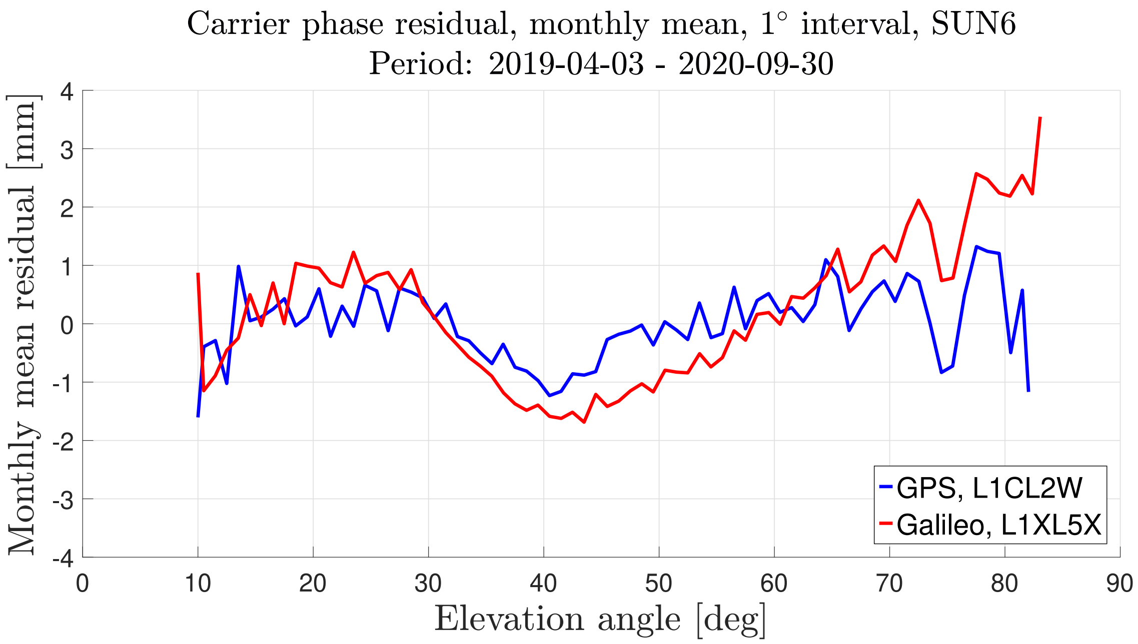

Figure B.28: Carrier phase residuals, averaged over both 1° elevation angle intervals as well as per month. Station SUN6, GPS (L1CL2W) and Galileo (L1XL5X)

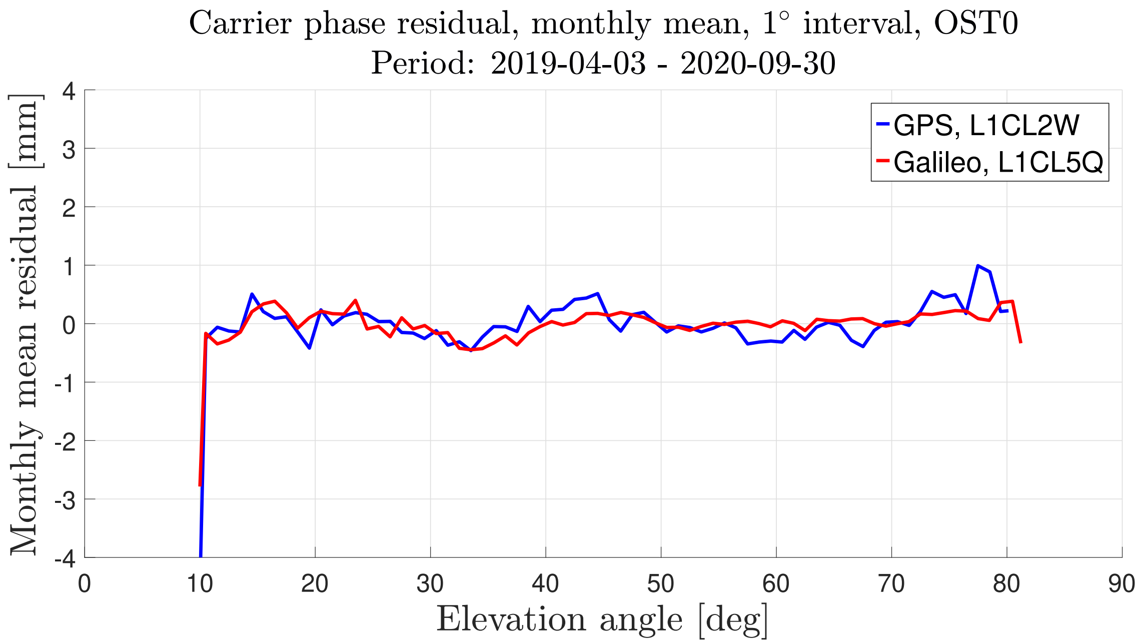

Figure B.29: Carrier phase residuals, averaged over both 1° elevation angle intervals as well as per month. Station OST0, GPS (L1CL2W) and Galileo (L1CL5Q)

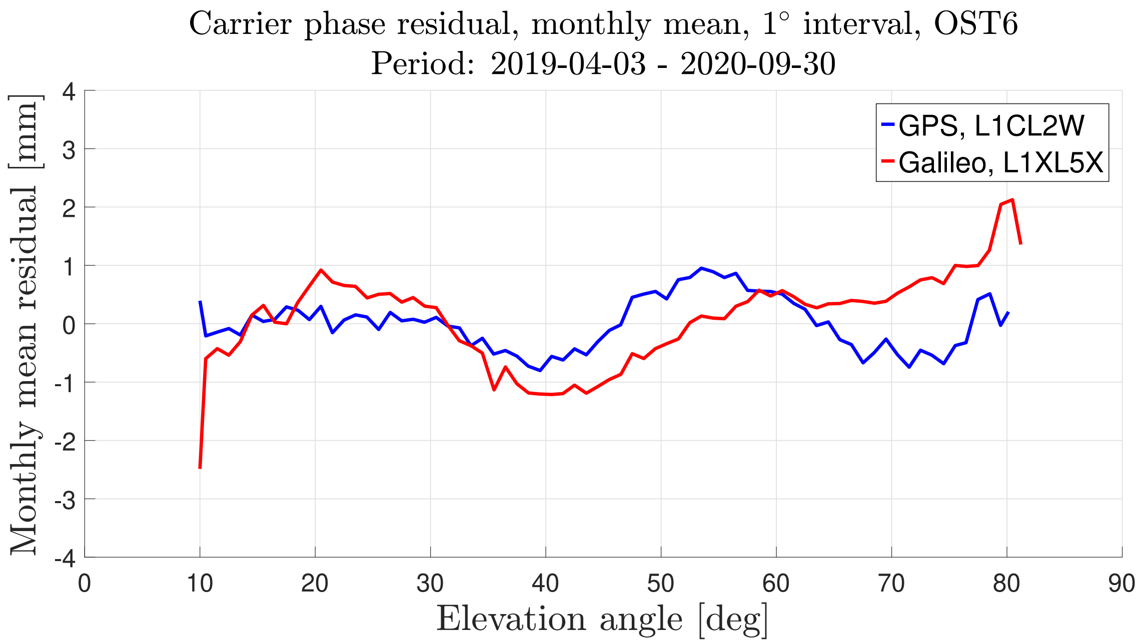

Figure B.30: Carrier phase residuals, averaged over both 1° elevation angle intervals as well as per month. Station OST6, GPS (L1CL2W) and Galileo (L1XL5X)

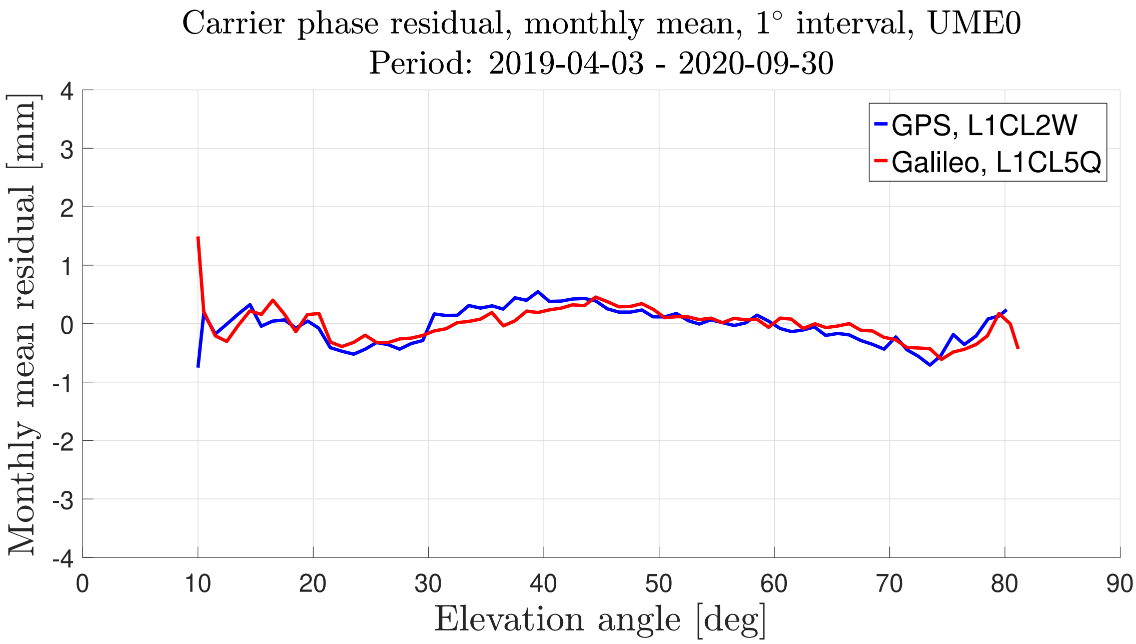

Figure B.31: Carrier phase residuals, averaged over both 1° elevation angle intervals as well as per month. Station UME0, GPS (L1CL2W) and Galileo (L1CL5Q)

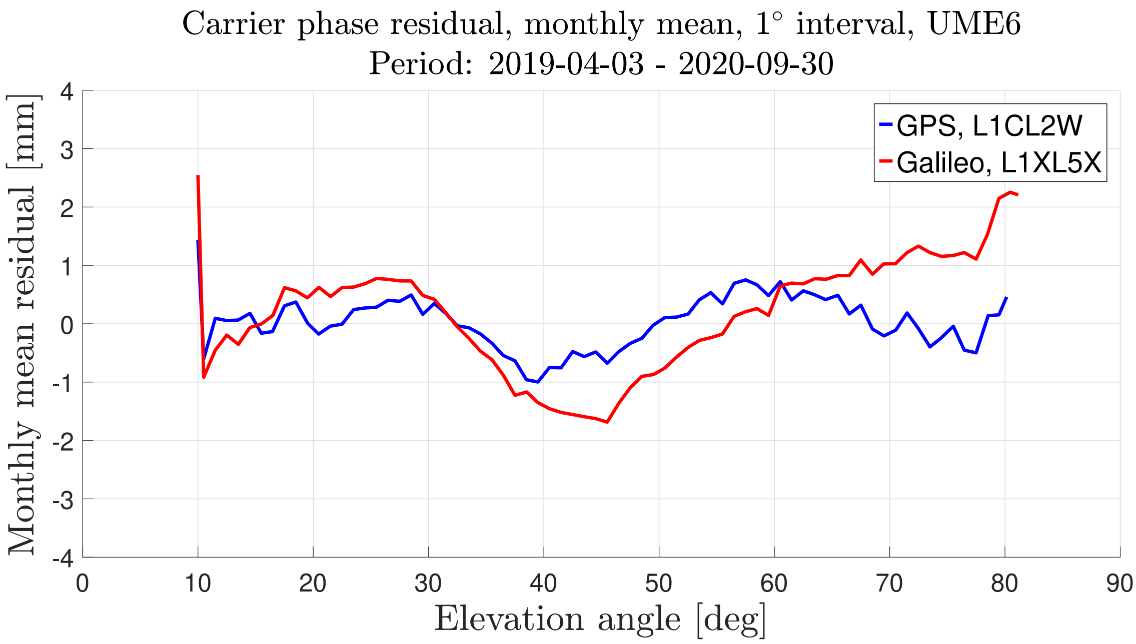

Figure B.32: Carrier phase residuals, averaged over both 1° elevation angle intervals as well as per month. Station UME6, GPS (L1CL2W) and Galileo (L1XL5X)

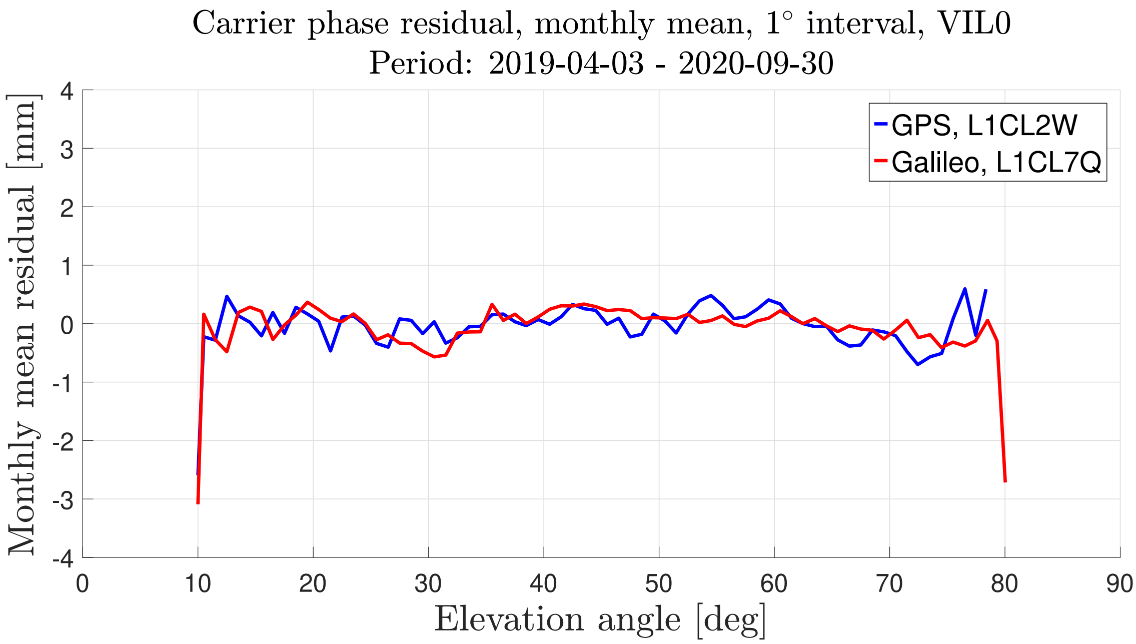

Figure B.33: Carrier phase residuals, averaged over both 1° elevation angle intervals as well as per month. Station VIL0, GPS (L1CL2W) and Galileo (L1CL7Q)

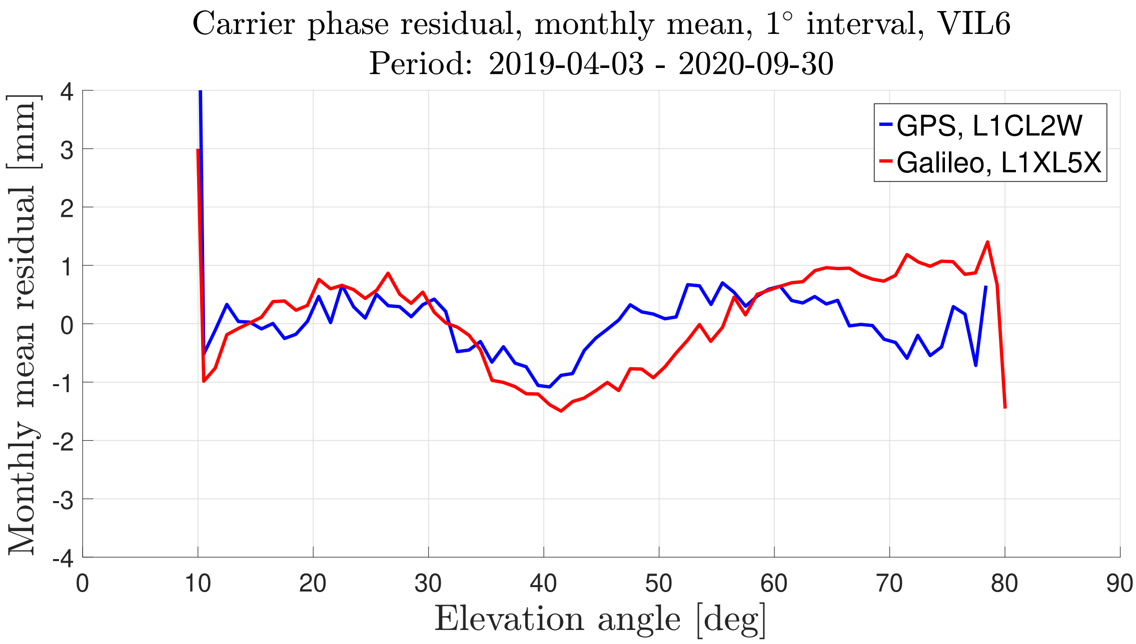

Figure B.34: Carrier phase residuals, averaged over both 1° elevation angle intervals as well as per month. Station VIL6, GPS (L1CL2W) and Galileo (L1XL5X)

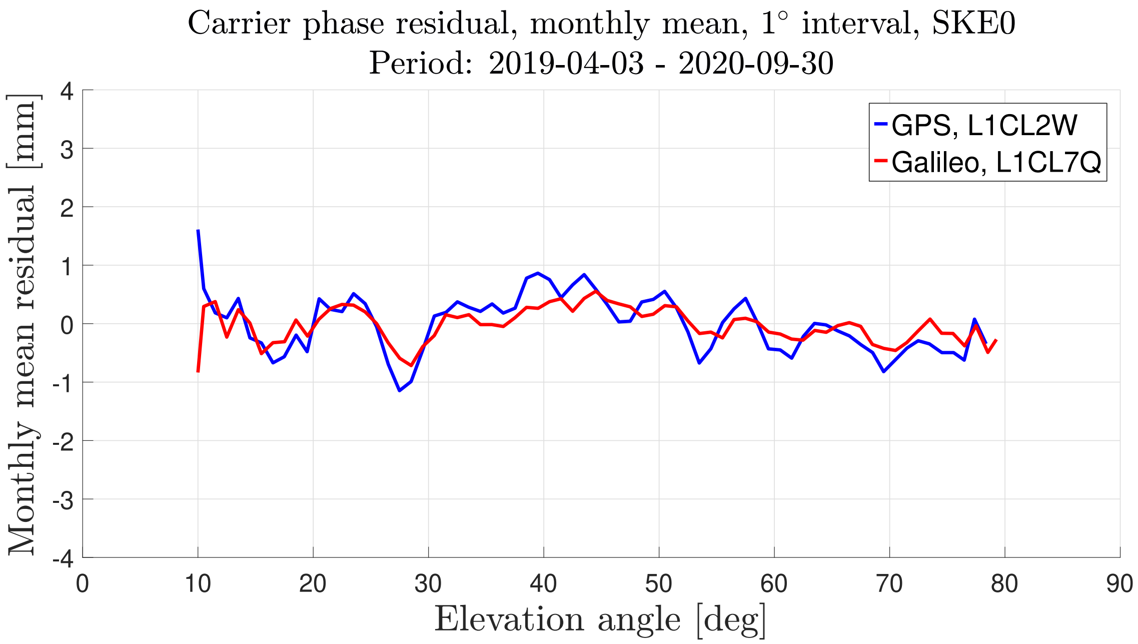

Figure B.35: Carrier phase residuals, averaged over both 1° elevation angle intervals as well as per month. Station SKE0, GPS (L1CL2W) and Galileo (L1CL7Q)

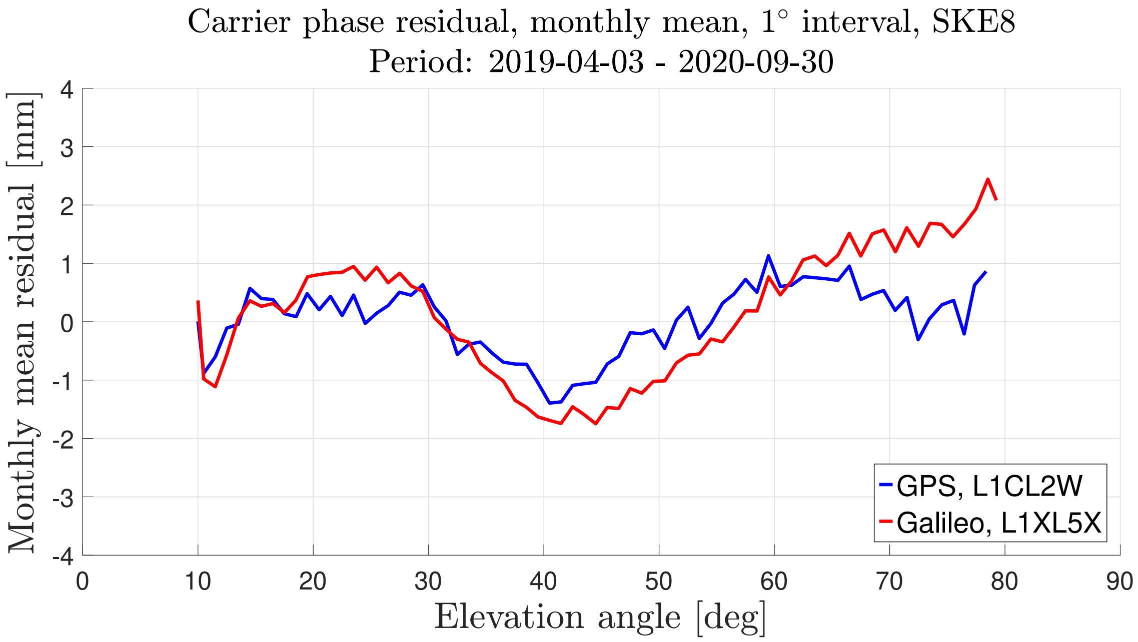

Figure B.36: Carrier phase residuals, averaged over both 1° elevation angle intervals as well as per month. Station SKE8, GPS (L1CL2W) and Galileo (L1XL5X)

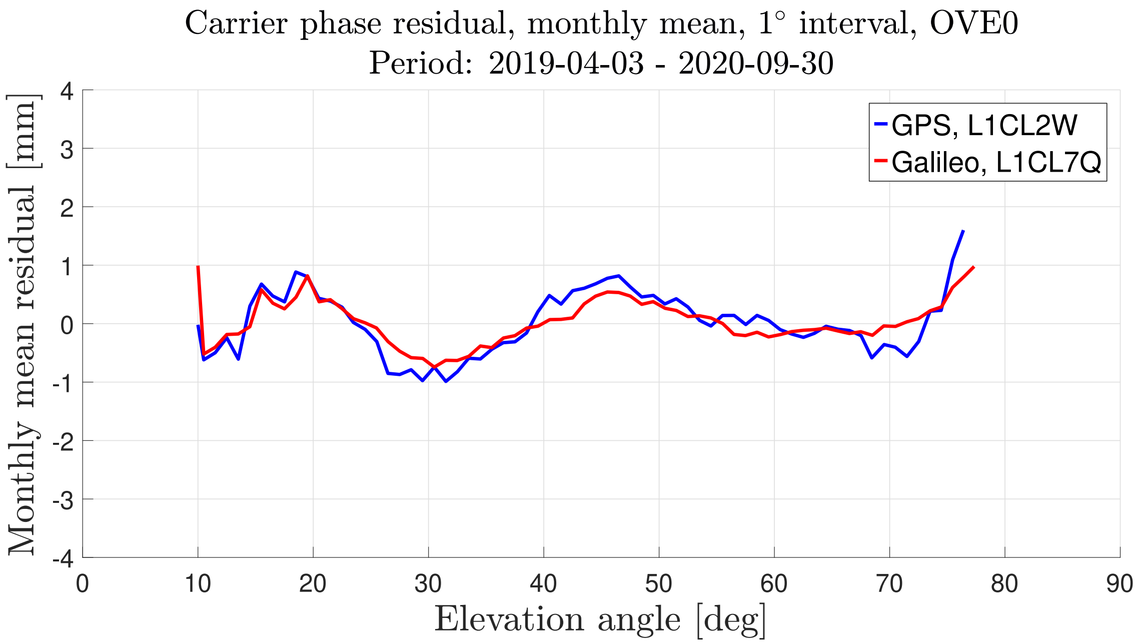

Figure B.37: Carrier phase residuals, averaged over both 1° elevation angle intervals as well as per month. Station OVE0, GPS (L1CL2W) and Galileo (L1CL7Q)

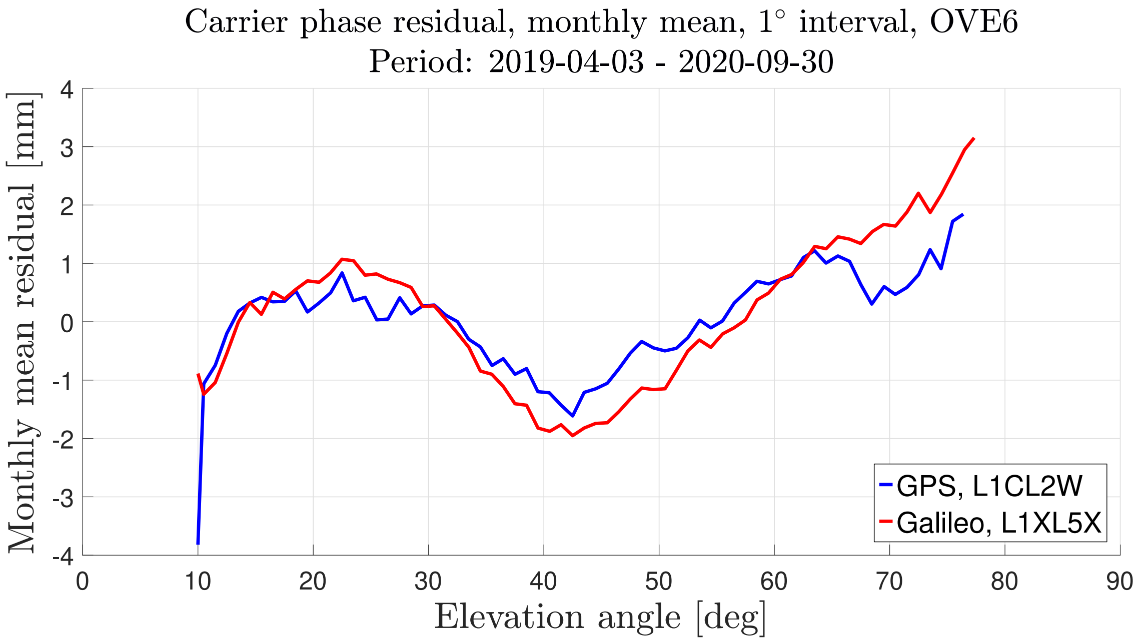

Figure B.38: Carrier phase residuals, averaged over both 1° elevation angle intervals as well as per month. Station OVE6, GPS (L1CL2W) and Galileo (L1XL5X)

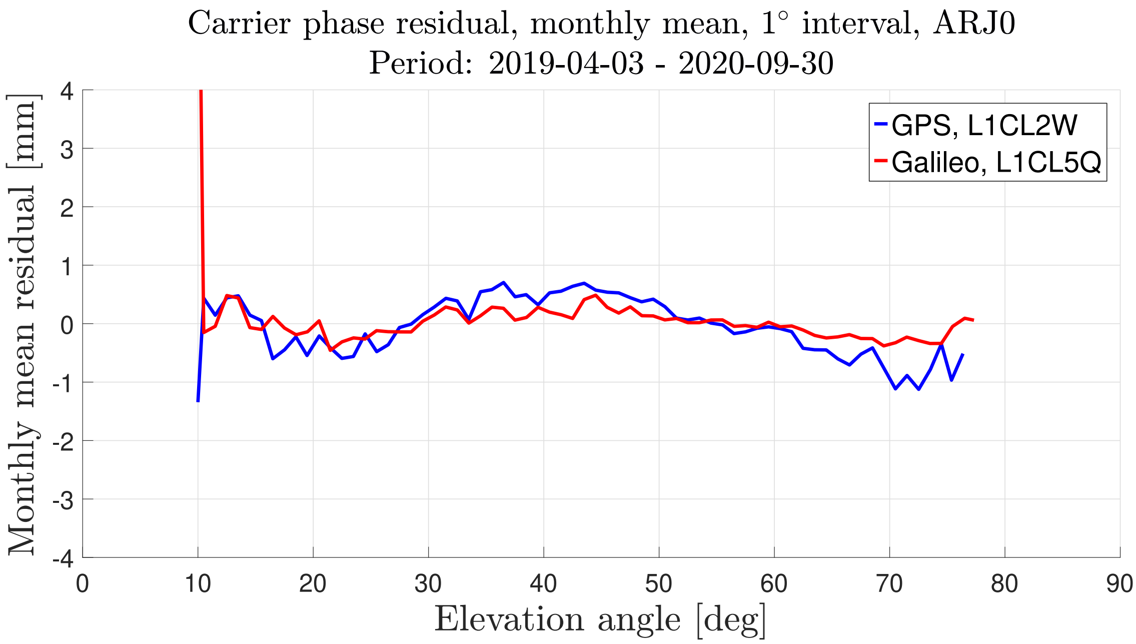

Figure B.39: Carrier phase residuals, averaged over both 1° elevation angle intervals as well as per month. Station ARJ0, GPS (L1CL2W) and Galileo (L1CL5Q)

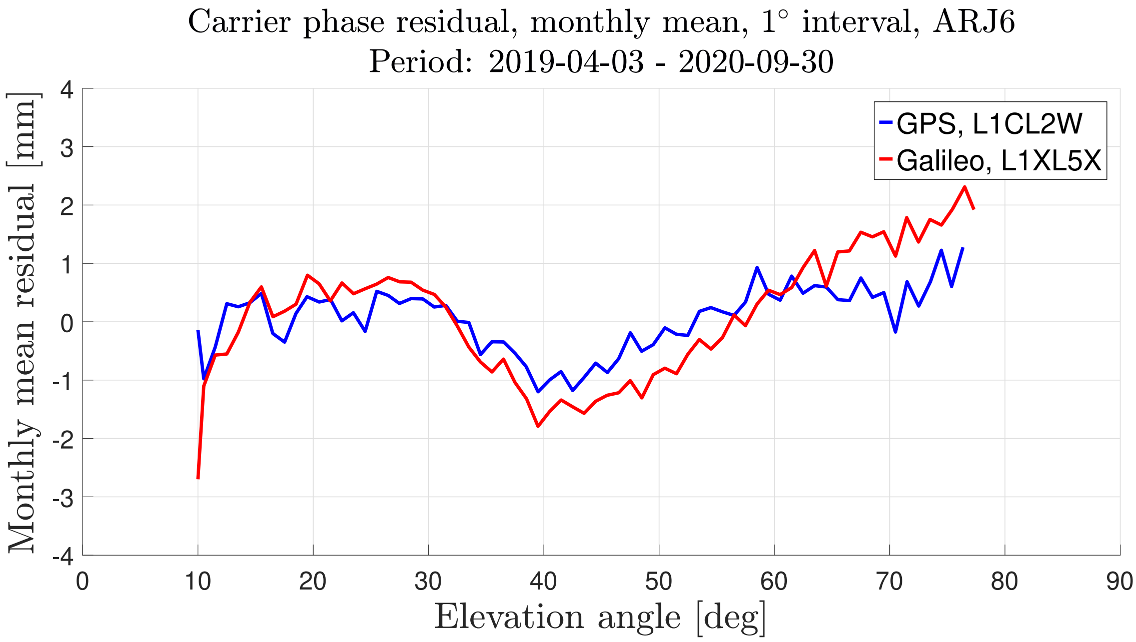

Figure B.40: Carrier phase residuals, averaged over both 1° elevation angle intervals as well as per month. Station ARJ6, GPS (L1CL2W) and Galileo (L1XL5X)

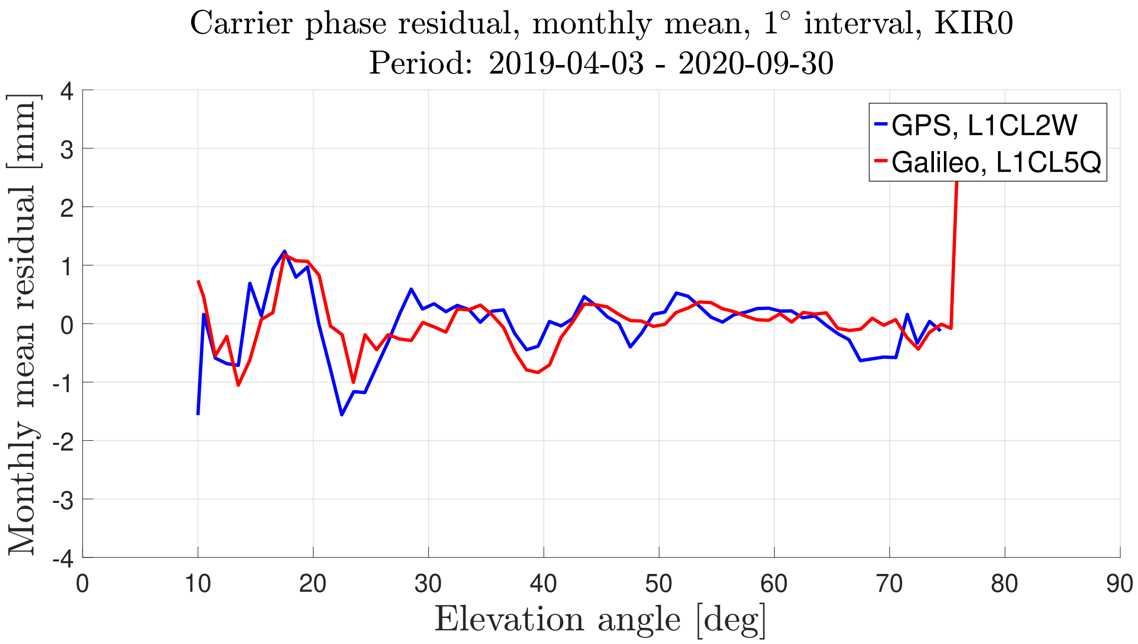

Figure B.41: Carrier phase residuals, averaged over both 1° elevation angle intervals as well as per month. Station KIR0, GPS (L1CL2W) and Galileo (L1CL5Q)

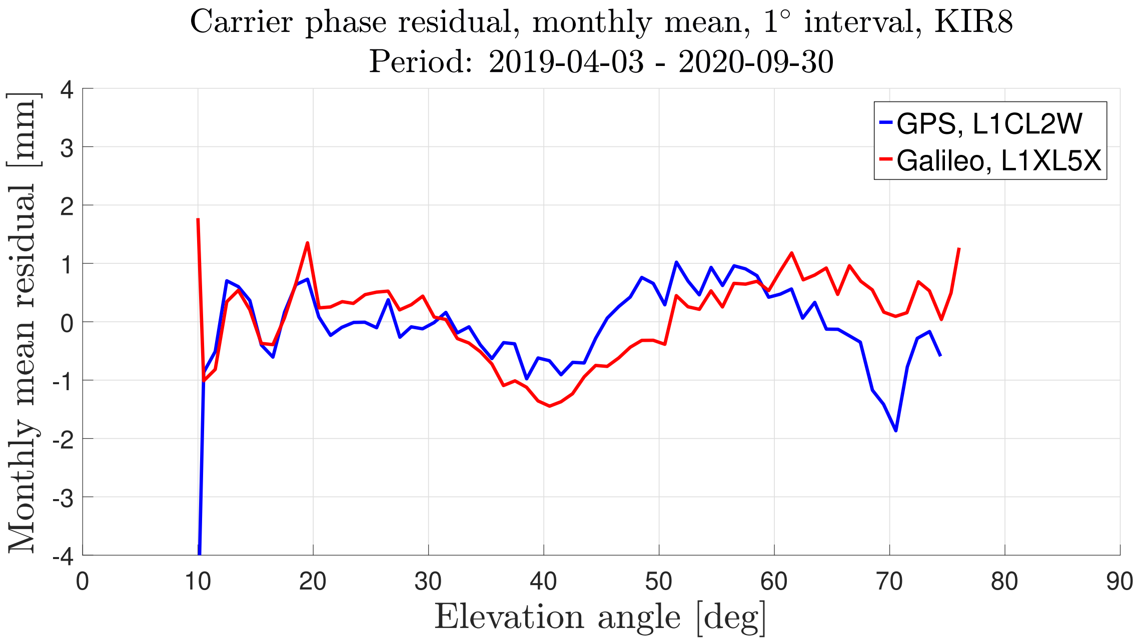

Figure B.42: Carrier phase residuals, averaged over both 1° elevation angle intervals as well as per month. Station KIR8, GPS (L1CL2W) and Galileo (L1XL5X)